ICT-619555 RESCUE

D1.2.2 Version 1.0

Theoretical Results Update of Assessment on Feasibility, Achievability, and Limits

Contractual Date of Delivery to the CEC:	08/2016 (M34)
Actual Date of Delivery to the CEC:	26/08/2016
Editor	Jiguang He
Author(s)	Jiguang He, Na Yi, Jiancao Hou, Xin He, Shen Qian, Tad Matsumoto, Albrecht Wolf
Participants	UOULU, UNIS, JAIST, TUD
Work package	WP1
Estimated person months	12
Security	**PU**
Nature	R
Version	1.0
Total number of pages	83

Abstract: Compared to the intermediate deliverable D1.2.1, additional results regarding the achievable rate region and performance limit analyses for different toy scenarios (TSs) have been achieved, which are provided in this deliverable. For TS1, we investigate the impact of the line-of-sight component on outage probability with lossy forwarding strategy. Moreover, an improved selective decode-and-forward scheme with least square based symbol level filtering is proposed in order to improve the bit error rate performance of the relaying system. Regarding TS2, the lower bound of the Hamming distortion in the binary chief executive officer (CEO) problem is derived by minimizing the distortion function subject to the inequalities between the obtained tighter outer bound and the channel capacities. An extension to an arbitrary number of sources in the CEO problem is also studied. TS3 is modeled by Slepian-Wolf coding, and we achieve the upper bound of the outage probability by reducing and relaxing the rate constraints. Regarding TS4, we extend the orthogonal transmission to its non-orthogonal counterpart and analyze the outage probability relying on the theorem of multiple access channel with a helper.

Keyword list: achievable rate region, chief executive officer (CEO), lossy forwarding, outage probability, Shannon's lossy source/channel separation theorem

Executive Summary

Compared to the intermediate deliverable D1.2.1, this deliverable presents some additional theoretical results regarding the achievable rate regions and performance limits on the links-on-the-fly concept introduced in "Links-on-the-fly Technology for Robust, Efficient, and Smart Communication in Unpredictable Environments" (RESCUE) project. As in D1.2.1, all the theoretical results are obtained based on the simplified four toy scenarios (TSs), where the relays always forward their decoded information sequence to the destination ignoring whether it contains error or not. The advantages of the links-on-the-fly concept over its baseline schemes have been extensively studied and investigated in D1.2.1. Therefore, in this deliverable we mainly focus on the theoretical results of the links-on-the-fly concept by making some scenario extensions and generalizations.

Toy Scenario 1 (TS1) is a typical three-node one-way relay network. The achievable rate region of TS1 was studied in D1.2.1 based on the theorem of source coding with a helper and approximated by the Slepian-Wolf theorem. All the links are supposed to be independent and identically distributed (i.i.d) Rayleigh block fading without considering line-of-sight component. We further extend the wireless channels to i.i.d Rician and Nakagami-*m* fading and calculate the theoretical outage probability of TS1. In addition, the Kullback-Leibler distance between the Rician and Nakagami-*m* fading distributions is studied, which in turn provides the guideline for the analysis of diversity and coding gains shown in the theoretical outage probability. A more advanced lossy forwarding[1] scheme with least square based symbol level filtering is investigated over TS1, which guarantees better bit error rate (BER) performance compared to the baselines.

Toy scenario 2 (TS2) is a single-source multiple-relays and single-destination system without direct link between the source and the destination. As in D1.2.1, we mainly focus on the chief executive officer (CEO) problem, which results from the special case where all the source-to-relay links are lossy. We first reduce the binary CEO problem to a binary multiterminal source coding problem. Then, we derive the tighter outer bound on the rate distortion region for the binary multiterminal source coding problem based on the converse proof of the bound. Furthermore, a lower bound on the Hamming distortion for the CEO problem is obtained by minimizing the distortion function subject to the inequalities between the derived outer bound and the channel capacities. Finally, an extension of the binary CEO problem to an arbitrary number of terminals is investigated. The correctness/accuracy of the derivations is also verified through practical simulations using accumulator (ACC) aided turbo codes.

Toy scenario 3 (TS3) is an extension of TS2 with direct link between the source and the destination. In the D1.2.1, the selective DF was intensively investigated. Here, we analyze the upper bound of the outage probability by reducing and relaxing the rate constraints based on Slepian-Wolf theorem. Closed form expression for the outage probability is derived for the high signal to noise ratio (SNR) regime with up to four relays. Comparison between the cases with different number of relays is carried out to show the improved diversity order when the number of relays increases.

Toy scenario 4 (TS4) is a multiple access relay channel (MARC) with two sources, single relay and a common destination. The achievable rate region and outage probability was intensively studied in D1.2.1 under the constraint of perfect or imperfect source-to-relay links and orthogonal transmission. We relax the restriction on the assumption of orthogonal transmission and apply the non-orthogonal transmission to MARC. A virtual channel between the source-to-relay links is established for the purpose of simplifying the analysis. The achievable rate region is further obtained by the theorem of multiple access channel with a helper, which determines the outage probability. The outage probability of non-orthogonal MARC is slightly worse than orthogonal MARC, but the time slot consumption for the data transmission between sources and destination is reduced considerably.

[1] This term is exchangeable with lossy decode-and-forward (DF) throughout the deliverable.

Authors

Partner	Name	Phone/Fax/e-mail
University of Oulu (UOULU)	Jiguang He	Phone: +358 46 8439798 Fax: – e-mail: jhe@ee.oulu.fi
	Valtteri Tervo	Phone: +358 40 4167991 Fax: – e-mail: valtteri.tervo@ee.oulu.fi
University of Surrey (UNIS)	Na Yi	Phone: +44 1483 684703 Fax: +44 1483 686011 e-mail: n.yi@surrey.ac.uk
	Jiancao Hou	Phone: +44 1483 682229 Fax: – e-mail: j.hou@surrey.ac.uk
Japan Advanced Institute of Science and Technology (JAIST)	Tad Matsumoto	Phone: +81 761 51 1408 Fax: +81 761 51 1149 e-mail: matumoto@jaist.ac.jp
	Shen Qian	Phone: – Fax: – e-mail: shen.qian@jaist.ac.jp
	Xin He	Phone: – Fax: – e-mail: xin.he@jaist.ac.jp
Technical University Dresden (TUD)	Albrecht Wolf	Phone: +49 351 463 41 047 Fax: – e-mail: albrecht.wolf@ifn.et.tu-dresden.de

Table of Contents

List of Acronyms and Abbreviations

Term	Description
ACC	Accumulator
AF	Amplify-and-forward
AWGN	Additive white Gaussian noise
BCJR	Bahl-Cocke-Jelinek-Raviv
BEP	Bit error probability
BER	Bit error rate
BMTSC	Binary multiterminal source coding
BPSK	Binary phase-shift keying
BSC	Binary symmetric channel
CEO	Chief executive officer
CRC	Cyclic redundancy check
CSI	Channel state information
D	Destination
DACC	Doped-accumulator
DF	Decode-and-forward
DF-IE	Decode-and-forward relaying allowing intra-link errors
FER	Frame error rate
GI	Global iteration
i.i.d.	Indepentely and identically distributed
JSC	Joint source channel
KLD	Kullback-Leibler Distance
KPI	Key performance indicator
LI	Local iteration
LLR	Log-likelihood ratio
LOS	Line-of-sight
LS	Lease-square
MAC	Multiple access channel
MARC	Multiple access relay channel
MRC	Maximum-ratio combine
NLOS	Non line-of-sight
PDF	Probability density function
PHY	Physical
PMF	Probability mass function
QPSK	Quadrature phase shift Keying
R	Relay
R-D	Relay-to-destination
S	Source
S-D	Source-to-destination
SDF	Selective decode-and-forward
SNCC	Separate network-and-channel coding
SNR	Signal-to-noise ratio
SNRCC	Systematic non-recursive convolution code
S-R	Source-to-relay
SRCC	Systematic recursive convolutional code
TDMA	Time division multiple access
TS	Toy scenario
V2V	Vehicle-to-vehicle
XOR	Exclusive-OR

1. Introduction

The RESCUE project mainly focuses on two use cases. One is related to public safety, and the other to vehicle-to-vehicle (V2V) communications. We apply the links-on-the-fly concept to the situation for the former use case when the infrastructure is not available due to some natural disasters. For the V2V communications, safety related information is exchanged among vehicles with the help of roadside units or the other vehicles. The key technique lies in the links-on-the-fly concept is lossy decode-and-forward (DF) relaying strategy. Unlike conventional selective DF (SDF), the relay nodes always forward their decoded data to the destination, where it is ignored that whether it contains error or not. Even though the decoded data contains some errors, it is correlated with the original data sent from the sources. It is a waste of resource (e.g., time slot, energy and etc.) if we discard the erroneous data at the relay, since it could help to recover the original data at the destination. As shown in our previous deliverable [ICT15], significant performance gain regarding outage probability can be achieved compared to the conventional SDF scheme.

The deliverable focuses on the theoretical results update of assessment on feasibility, achievability, and limits. It is extremely challenging to analyze the theoretical performance limits from the perspective of the whole large network, especially when we take into account the dynamic topology change. Therefore, we divide the complicated network into four independent simplified toy scenarios (TSs). TS1 is a three-node one-way relay network consisting of one source, one relay, and one destination. TS2 is so called diamond network, composed of one source, two or multiple relays, and one destination, without direct link between the source and the destination. TS3 can be considered as an extension of TS1 and/or TS2. It adds more relays between the source and the destination compared to TS1 while direct link is included which differentiates the scenario from TS2. TS4 is multiple access relay channel (MARC). Unlike previous three TSs, multiple sources are introduced in TS4.

In the intermediate deliverable [ICT15], some preliminary results were obtained. We calculated the outage probability of TS1 over Rayleigh block fading channels based on source coding with a helper. The approximated outage probability was obtained using Slepian-Wolf theorem [Zho+14]. Optimal relay position was found to be the exact midpoint between the source and the destination. Regarding TS2, we investigated the special case when all the source-to-relay links are lossy, which results in the chief executive officer (CEO) problem [Xin13CL; XinISITA]. Berger-Tung outer bound based bit error rate (BER) was calculated. For TS3, we could not analyze the achievable rate region and its corresponding outage probability. However, we proposed a SDF based relaying strategy and studied the BER performance over Rayleigh fading channel. In TS4, the outage probabilities of orthogonal MARC were studied for both the perfect intra links and imperfect intra links [Xiaobo2014; Lu+14].

Main Contribution of D1.2.2

In reality, wireless channels may contain line-of-sight (LoS) component, especially when the transmitter and receiver are geometrically closely located. We extend the wireless Rayleigh fading channel assumption to Rician and Nakagami-*m* fading and calculate the theoretical outage probability of TS1. The Kullback-Leibler distance between the Rician and Nakagami-*m* fading distributions is studied to provide the guideline for the analysis of diversity and coding gains, shown in the theoretical outage probability. A more advanced lossy forwarding technique with least square based symbol level filtering is investigated for TS1, which presents better BER performance compared to the baselines.

We reduce the binary CEO problem to a binary multiterminal source coding problem and derive the tighter outer bound on the rate distortion region for the binary multiterminal source coding problem. We obtain a lower bound on the Hamming distortion for the CEO problem by solving a convex optimization problem. Finally, an extension of the binary CEO problem to an arbitrary number of terminals is also investigated. Practical simulations using an accumulator (ACC) aided turbo code for each link are provided to verify the accuracy of the derived lower bound of Hamming distortion.

The upper bound of the outage probability of TS3 is achieved by reducing and relaxing the rate constraints based on Slepian-Wolf theorem. We derived the closed form expressions for the outage probabilities for the high signal to noise ratio (SNR) regime with up to four relays. Theoretical analyses are verified by both Monte-Carlo simulation results and practical results using ACC aided turbo codes. Comparison between the cases with different numbers of relays is also conducted to show the improved diversity order when the number of relays increases.

We relax the restriction on the assumption of orthogonal transmission and apply the non-orthogonal transmission to MARC. A virtual channel between the source-to-relay links is established in a heuristic manner for the purpose of simplifying the outage analysis. The achievable rate region is further obtained based on the theorem of multiple access channel with a helper. It is found that the outage probability of non-orthogonal MARC is slightly worse than orthogonal MARC, but the network throughput can be significantly improved instead.

2. Performance Analysis of TS1

2.1 System Model

We consider a simple relaying system with three nodes as shown in Fig. 2.1. A source S communicates with a destination D with help of one relay R. In the first time slot, the original binary information sequences b_{S} broadcast from S. R attempts to recover b_{S}. However, because of the fading of the S-R link, b_{R} is obtained as the decoding result at R may contain errors. Nevertheless, R re-interleaves, re-encodes and forwards b_{R} to D during the second time slot. At D, the S-R link error probabilities are estimated from log-likelihood ratios (LLRs), and used as the correlation knowledge between the information sent from S and R. The LLRs of the information bits are exchanged between two decoders during an iterative decoding process.

Specifically, the S-R link is modeled by a binary symmetric channel (BSC) [GFZ05] with a crossover probability p_f, where p_f represents the bit flipping probability of b_{R}. Hence, $b_{\mathrm{R}} = b_{\mathrm{S}} \oplus e$, where $\oplus$ denotes the modulo-2 addition and e is a binary error variable with $\Pr(e=1) = p_f$ fixed within each block. The error probability p_f changes block-by-block assuming block fading of the S-R link.

The S-D link is assumed to experience frequency non-selective block Rayleigh fading which only has non LOS (NLOS) components. The probability density function (PDF) of the instantaneous signal-to-noise ratio (SNR) of the S-D link (i.e., γ_{SD}) is given by

$$p(\gamma_{\mathrm{SD}}) = \frac{1}{\overline{\gamma}_{\mathrm{SD}}} \exp(-\frac{\gamma_{\mathrm{SD}}}{\overline{\gamma}_{\mathrm{SD}}}), \tag{2.1}$$

where $\overline{\gamma}_{\mathrm{SD}}$ represents the average SNR of the S-D link.

Both S-R and R-D links are assumed to suffer from block fading variation having LOS component, following either Rician or Nakagami-*m* distributions. The PDF of the instantaneous SNR γ_{ij} $(ij = \mathrm{SR}, \mathrm{RD})$ following Rician distribution is

$$p^{\mathrm{Rici}}(\gamma_{ij}) = \left(\frac{(1+K_{ij})\, e^{-K_{ij}}}{\overline{\gamma}_{ij}} \right) \exp\left(-\frac{(1+K_{ij})\gamma_{ij}}{\overline{\gamma}_{ij}} \right) \cdot I_0\left(2\sqrt{\frac{K_{ij}(1+K_{ij})\,\gamma_{ij}}{\overline{\gamma}_{ij}}} \right), \tag{2.2}$$

where $I_0(\cdot)$ is the zero-*th* order modified Bessel function of the first kind. Average SNR of the corresponding link is denoted as $\overline{\gamma}_{ij}$, and the ratio of the LOS component power-to-NLOS component average power is denoted as K_{ij}.

The PDF of the instantaneous SNR γ_{ij} $(ij = \mathrm{SR}, \mathrm{RD})$ following the Nakagami-*m* distribution is given by

$$p^{\mathrm{Naka}}(\gamma_{ij}) = \frac{m_{ij}^{m_{ij}} (\gamma_{ij})^{m_{ij}-1}}{\left(\overline{\gamma}_{ij}\right)^{m_{ij}} \Gamma(m_{ij})} \exp\left(-\frac{m_{ij}\gamma_{ij}}{\overline{\gamma}_{ij}} \right), m_{ij} > 0.5, \tag{2.3}$$

where $\Gamma(\cdot)$ is the complete Gamma function, and shape factor m_{ij} represents the severity of the fading variation of the corresponding link. The Nakagami-*m* fading with factor *m* is approximated by Rician fading with factor *K* [Gol05], [SA05], as

$$m = \frac{(K+1)^2}{2K+1}. \tag{2.4}$$

2.2 Outage Probability Derivation

According to the theorem of source coding with side information [GK11], b_{S} can be reconstructed losslessly at D if the source coding rates of b_{S} and b_{R}, R_{S} and R_{R} respectively, satisfy the following inequalities:

$$\begin{cases} R_{\mathrm{S}} & \geq H(b_{\mathrm{S}}|\hat{b}_{\mathrm{R}}), \\ R_{\mathrm{R}} & \geq I(b_{\mathrm{R}};\hat{b}_{\mathrm{R}}), \end{cases} \tag{2.5}$$

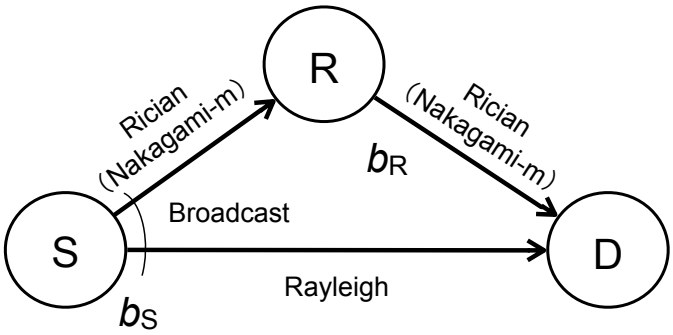

Figure 2.1: Single relay lossy-forward relaying network.

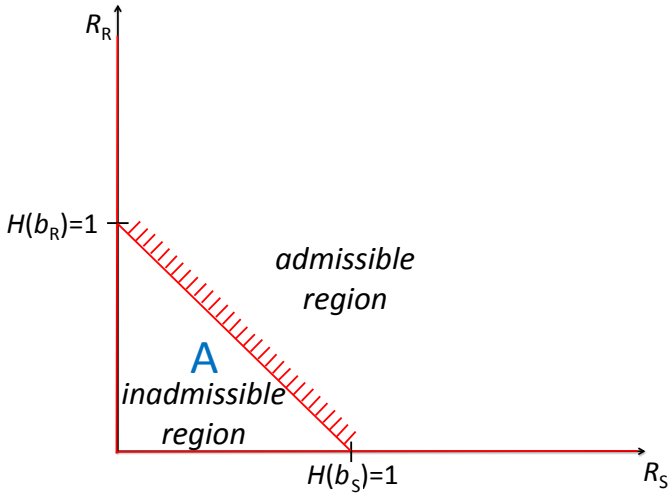

Figure 2.2: Rate region for S and R when $p_f = 0$. The red solid lines separate the admissible and inadmissible regions.

where $\hat{b}_R$ is the estimate of b_R at D, and $H(\cdot|\cdot)$ and $I(\cdot;\cdot)$ denote the conditional entropy and the mutual information between the arguments, respectively.

When $p_f = 0$, which indicates perfect decoding at R, we have $H(b_S|b_R) = H(b_R|b_S) = 0$. Hence, the inadmissible rate region becomes the triangle area A as shown in Fig. 2.2. When $0 < p_f \leq 0.5$, the inadmissible region is shown in Fig. 2.3 which can be divided into two areas, B and C.

The rate region defined in (2.5) indicates that, even b_R containing errors, with $0 \leq R_R \leq H(b_R)$, it can serve as the side information for losslessly recovering b_S. In the case $R_R > H(b_R)$, the condition becomes to $R_S \geq H(p_f)$.

If the rate pair (R_S, R_R) falls into the inadmissible region, the outage event occurs, and D cannot reconstruct b_S with an arbitrarily small error probability. Since $p_f = 0$ and $0 < p_f \leq 0.5$ are distinctive, the outage probability of the LF relaying can be expressed as

$$P_{\text{out}} = P_A + P_B + P_C, \tag{2.6}$$

where P_A, P_B, and P_C denote the probabilities that (R_S, R_R) falls into the inadmissible areas A, B, and C, respectively. Taking into account the impact of p_f, P_A, P_B, and P_C can further be expressed as

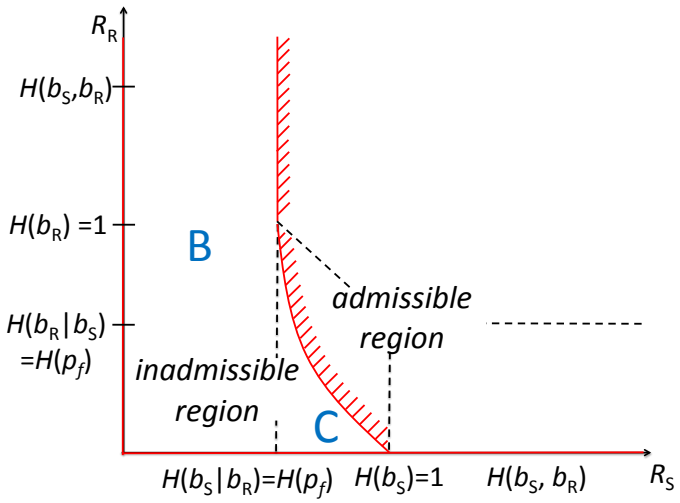

Figure 2.3: Rate region for S and R when $p_f \neq 0$. The red solid lines separate the admissible and inadmissible regions.

$$P_A = \Pr[p_f = 0, 0 \leq R_S < 1, 0 \leq R_R < H(p_f * p'_f)], \tag{2.7}$$

$$P_B = \Pr[0 < p_f \leq 0.5, 0 \leq R_S < H(p_f), R_R \geq 0], \tag{2.8}$$

$$P_C = \Pr[0 < p_f \leq 0.5, H(p_f) \leq R_S < 1, 0 \leq R_R < H(p_f * p'_f)], \tag{2.9}$$

where a BSC model is also used to represent the R-D link (helper channel) with flipping probability p'_f, with $p_f * p'_f = (1-p_f)p'_f + (1-p'_f)p_f$.

Based on the Shannon's lossless source channel separation theorem, the relationship between the instantaneous channel SNR $\gamma_{ij}\,(ij = \mathrm{SD}, \mathrm{RD})$ and its corresponding rate R_k is given by[1]

$$R_k \leq \Theta(\gamma_{ij}) = \log_2(1+\gamma_{ij}), \tag{2.10}$$

with its inverse function

$$\gamma_{ij} \geq \Theta^{-1}(R_k) = \left(2^{R_k} - 1\right), (k = \mathrm{S}, \mathrm{R}). \tag{2.11}$$

Based on the Shannon's lossy source channel separation theorem, the relationship between p_f and the instantaneous channel SNR γ_{SR} is given as

$$p_f = \Lambda(\gamma_{\mathrm{SR}}) = H_2^{-1}(1 - \log_2(1+\gamma_{\mathrm{SR}})), \tag{2.12}$$

with $H_2^{-1}(\cdot)$ denoting the inverse function of the binary entropy. The minimum distortion is equivalent to p_f [GK11].

Solving (2.7), (2.8) and (2.9) based on the PDFs of the instantaneous SNR of the corresponding channels, the outage probabilities of the LF relaying with the fading variations of the S-R and R-D links following the Rician distribution can be expressed as

$$\begin{aligned} P_A^{\mathrm{Rici}} &= \int_{\gamma_{\mathrm{SR}}=\Theta^{-1}(1)}^{\Theta^{-1}(\infty)} \int_{\gamma_{\mathrm{SD}}=\Theta^{-1}(0)}^{\Theta^{-1}(1)} \int_{\gamma_{\mathrm{RD}}=\Theta^{-1}(0)}^{\Theta^{-1}(1-\Theta(\gamma_{\mathrm{SD}}))} p^{\mathrm{Rici}}(\gamma_{\mathrm{SR}}) p(\gamma_{\mathrm{SD}}) p^{\mathrm{Rici}}(\gamma_{\mathrm{RD}}) d\gamma_{\mathrm{SR}} d\gamma_{\mathrm{SD}} d\gamma_{\mathrm{RD}} \\ &= \frac{1}{\overline{\gamma}_{\mathrm{SD}}} Q_1\left(\sqrt{2K_{\mathrm{SR}}}, \sqrt{\frac{2(1+K_{\mathrm{SR}})}{\overline{\gamma}_{\mathrm{SR}}}}\right) \cdot \int_{\gamma_{\mathrm{SD}}=\Theta^{-1}(0)}^{\Theta^{-1}(1)} \exp\left(-\frac{\gamma_{\mathrm{SD}}}{\overline{\gamma}_{\mathrm{SD}}}\right) \left[1 - Q_1\left(\sqrt{2K_{\mathrm{RD}}}, \sqrt{2(1+K_{\mathrm{RD}})\frac{\Theta^{-1}(1-\Theta(\gamma_{\mathrm{SD}}))}{\overline{\gamma}_{\mathrm{RD}}}}\right)\right] d\gamma_{\mathrm{SD}}, \end{aligned} \tag{2.13}$$

[1]The spectrum efficiency of the transmission chain, including the channel coding scheme and modulation multiplicity in all of the links are set to the unity.

$$P_{\mathrm{B}}^{\mathrm{Rici}} = \int_{\gamma_{\mathrm{SR}}=\Theta^{-1}(0)}^{\Theta^{-1}(1)} \int_{\gamma_{\mathrm{SD}}=\Theta^{-1}(0)}^{\Theta^{-1}(1-\Lambda(\gamma_{\mathrm{SR}}))} \int_{\gamma_{\mathrm{RD}}=\Theta^{-1}(0)}^{\Theta^{-1}(\infty)} p^{\mathrm{Rici}}(\gamma_{\mathrm{SR}}) p(\gamma_{\mathrm{SD}}) p^{\mathrm{Rici}}(\gamma_{\mathrm{RD}}) d\gamma_{\mathrm{SR}} d\gamma_{\mathrm{SD}} d\gamma_{\mathrm{RD}}$$
$$= \int_{\gamma_{\mathrm{SR}}=\Theta^{-1}(0)}^{\Theta^{-1}(1)} \exp\left(-\frac{(1+K_{\mathrm{SR}})\gamma_{\mathrm{SR}}}{\overline{\gamma}_{\mathrm{SR}}}\right) \cdot \left(\frac{(1+K_{\mathrm{SR}})e^{-K_{\mathrm{SR}}}}{\overline{\gamma}_{\mathrm{SR}}}\right) I_0\left(2\sqrt{\frac{K_{\mathrm{SR}}(1+K_{\mathrm{SR}})\gamma_{\mathrm{SR}}}{\overline{\gamma}_{\mathrm{SR}}}}\right) \cdot \left[1-\exp\left(-\frac{\Theta^{-1}(1-\Lambda(\gamma_{\mathrm{SR}}))}{\overline{\gamma}_{\mathrm{SD}}}\right)\right] d\gamma_{\mathrm{SR}} \tag{2.14}$$

and

$$P_{\mathrm{C}}^{\mathrm{Rici}} = \int_{\gamma_{\mathrm{SR}}=\Theta^{-1}(0)}^{\Theta^{-1}(1)} \int_{\gamma_{\mathrm{SD}}=\Theta^{-1}(1-\Lambda(\gamma_{\mathrm{SR}}))}^{\Theta^{-1}(1)} \int_{\gamma_{\mathrm{RD}}=\Theta^{-1}(0)}^{\Theta^{-1}[\xi(\gamma_{\mathrm{SD}},\gamma_{\mathrm{SR}})]} p^{\mathrm{Rici}}(\gamma_{\mathrm{SR}}) p(\gamma_{\mathrm{SD}}) p^{\mathrm{Rici}}(\gamma_{\mathrm{RD}}) d\gamma_{\mathrm{SR}} d\gamma_{\mathrm{SD}} d\gamma_{\mathrm{RD}}$$
$$= \frac{1}{\overline{\gamma}_{\mathrm{SD}}} \left(\frac{(1+K_{\mathrm{SR}})e^{-K_{\mathrm{SR}}}}{\overline{\gamma}_{\mathrm{SR}}}\right) \int_{\gamma_{\mathrm{SD}}=\Theta^{-1}(1-\Lambda(\gamma_{\mathrm{SR}}))}^{\Theta^{-1}(1)} \cdot \int_{\gamma_{\mathrm{SR}}=\Theta^{-1}(0)}^{\Theta^{-1}(1)} \exp\left(\frac{-\gamma_{\mathrm{SD}}}{\overline{\gamma}_{\mathrm{SD}}}\right) \exp\left(-\frac{(1+K_{SR})\gamma_{\mathrm{SR}}}{\overline{\gamma}_{\mathrm{SR}}}\right)$$
$$\cdot I_0\left(2\sqrt{\frac{K_{\mathrm{SR}}(1+K_{\mathrm{SR}})\gamma_{\mathrm{SR}}}{\overline{\gamma}_{\mathrm{SR}}}}\right) \left[1-Q_1\left(\sqrt{2K_{\mathrm{RD}}}, \sqrt{2(1+K_{\mathrm{RD}})\frac{\Theta^{-1}[\xi(\gamma_{\mathrm{SD}},\gamma_{\mathrm{SR}})]}{\overline{\gamma}_{\mathrm{RD}}}}\right)\right] d\gamma_{\mathrm{SD}} d\gamma_{\mathrm{SR}}, \tag{2.15}$$

where $\xi(\gamma_{\mathrm{SD}},\gamma_{\mathrm{SR}}) = H\{H^{-1}[1-\Theta(\gamma_{\mathrm{SD}})] * H^{-1}[1-\Lambda(\gamma_{\mathrm{SR}})]\}$ and $Q_1(\cdot,\cdot)$ is the Marcum Q-Function.

The outage probability of the LF relaying with S-R and R-D links following Nakagami-m fading can be derived in the same way as for the Rician case, as

$$P_{\mathrm{A}}^{\mathrm{Naka}} = \frac{1}{\overline{\gamma}_{\mathrm{SD}}} \left(1-\left[\frac{\gamma\left(m_{\mathrm{SR}}, m_{\mathrm{SR}}\frac{1}{\overline{\gamma}_{\mathrm{SR}}}\right)}{\Gamma(m_{\mathrm{SR}})}\right]\right) \cdot \int_{\gamma_{\mathrm{SD}}=\Theta^{-1}(0)}^{\Theta^{-1}(1)} \exp\left(-\frac{\gamma_{\mathrm{SD}}}{\overline{\gamma}_{\mathrm{SD}}}\right) \cdot \left[\frac{\gamma\left(m_{\mathrm{RD}}, m_{\mathrm{RD}}\frac{\Theta^{-1}(1-\Theta(\gamma_{\mathrm{SD}}))}{\overline{\gamma}_{\mathrm{RD}}}\right)}{\Gamma(m_{\mathrm{RD}})}\right] d\gamma_{\mathrm{SD}}, \tag{2.16}$$

$$P_{\mathrm{B}}^{\mathrm{Naka}} = \int_{\gamma_{\mathrm{SR}}=\Theta^{-1}(0)}^{\Theta^{-1}(1)} \frac{m_{\mathrm{SR}}^{m_{\mathrm{SR}}}(\gamma_{\mathrm{SR}})^{m_{\mathrm{SR}}-1}}{(\overline{\gamma}_{\mathrm{SR}})^{m_{\mathrm{SR}}}\Gamma(m_{\mathrm{SR}})} \exp\left(-\frac{m_{\mathrm{SR}}\gamma_{\mathrm{SR}}}{\overline{\gamma}_{\mathrm{SR}}}\right) \cdot \left[1-\exp\left(-\frac{\Theta^{-1}(1-\Lambda(\gamma_{\mathrm{SR}}))}{\overline{\gamma}_{\mathrm{SD}}}\right)\right] d\gamma_{\mathrm{SR}}, \tag{2.17}$$

and

$$P_{\mathrm{C}}^{\mathrm{Naka}} = \frac{1}{\overline{\gamma}_{\mathrm{SD}}} \int_{\gamma_{\mathrm{SR}}=\Theta^{-1}(0)}^{\Theta^{-1}(1)} \int_{\gamma_{\mathrm{SD}}=\Theta^{-1}(1-\Lambda(\gamma_{\mathrm{SR}}))}^{\Theta^{-1}(1)} \exp\left(\frac{-\gamma_{\mathrm{SD}}}{\overline{\gamma}_{\mathrm{SD}}}\right) \frac{m_{\mathrm{SR}}^{m_{\mathrm{SR}}}(\gamma_{\mathrm{SR}})^{m_{\mathrm{SR}}-1}}{(\overline{\gamma}_{\mathrm{SR}})^{m_{\mathrm{SR}}}\Gamma(m_{\mathrm{SR}})} \exp\left(-\frac{m_{\mathrm{SR}}\gamma_{\mathrm{SR}}}{\overline{\gamma}_{\mathrm{SR}}}\right)$$
$$\cdot \left[\frac{\gamma\left(m_{\mathrm{RD}}, m_{\mathrm{RD}}\frac{\xi(\gamma_{\mathrm{SD}},\gamma_{\mathrm{SR}})}{\overline{\gamma}_{\mathrm{RD}}}\right)}{\Gamma(m_{\mathrm{RD}})}\right] d\gamma_{\mathrm{SD}} d\gamma_{\mathrm{SR}}, \tag{2.18}$$

where $\gamma(\cdot,\cdot)$ is the lower incomplete gamma function. Note that the factor K of Rician fading is connected to the factor m of Nakagami-m fading by (2.4), the impact of the difference in the statistical characteristics between the Rician and Nakagami-m fading on the outage performance can be evaluated by adjusting the factor K in Rician fading and the factor m in Nakagami-m fading.

2.2.1 Kullback-Leibler Distance (KLD)

The Kullback-Leibler distance (KLD) is used to measure the difference between probability distributions. Based on (2.2) and (2.3), the KLD of Rician relative to Nakagami-m distribution is given as [CT06]

$$D_{\mathrm{KL}}(p^{\mathrm{Rici}}(\gamma)\,||\,p^{\mathrm{Naka}}(\gamma)) = \int_{\gamma} p^{\mathrm{Rici}}(\gamma) \ln \frac{p^{\mathrm{Rici}}(\gamma)}{p^{\mathrm{Naka}}(\gamma)} d\gamma. \tag{2.19}$$

Relatively, the KLD of Nakagami-m relative to Rician distribution is defined as

$$D_{\mathrm{KL}}(p^{\mathrm{Naka}}(\gamma)\,||\,p^{\mathrm{Rici}}(\gamma)) = \int_{\gamma} p^{\mathrm{Naka}}(\gamma) \ln \frac{p^{\mathrm{Naka}}(\gamma)}{p^{\mathrm{Rici}}(\gamma)} d\gamma. \tag{2.20}$$

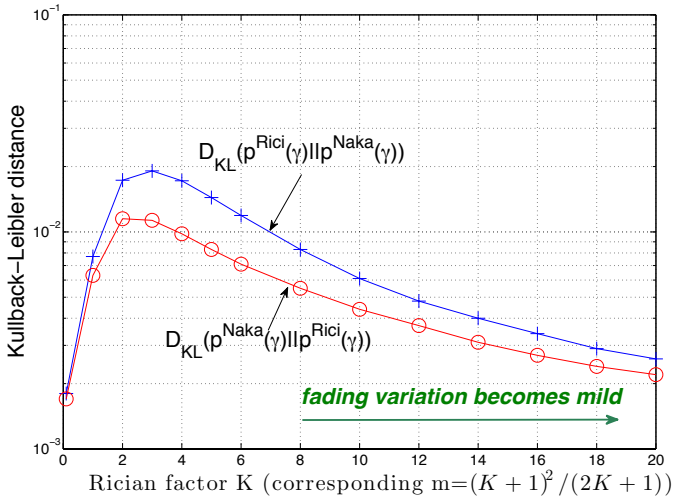

Figure 2.4: KLD between Rician and Nakagami-m distributions

When $K = 0$ and $m = 1$, $D_{\mathrm{KL}}(p^{\mathrm{Rici}}(\gamma)||p^{\mathrm{Naka}}(\gamma)) = 0, D_{\mathrm{KL}}(p^{\mathrm{Naka}}(\gamma)||p^{\mathrm{Rici}}(\gamma)) = 0$, which indicates that the Rician and Nakagami-m distributions converge to the identical Rayleigh distribution. Fig. 2.4 shows the KLD curves, $D_{\mathrm{KL}}\left(p^{\mathrm{Rici}}(\gamma)||p^{\mathrm{Naka}}(\gamma)\right)$, as well as the $D_{\mathrm{KL}}(p^{\mathrm{Naka}}(\gamma)||p^{\mathrm{Rici}}(\gamma))$, as a function of the factor K (its corresponding m value follows (2.4)). We can easily find that $D_{\mathrm{KL}}\left(p^{\mathrm{Rici}}(\gamma)||p^{\mathrm{Naka}}(\gamma)\right)$ and $D_{\mathrm{KL}}(p^{\mathrm{Naka}}(\gamma)||p^{\mathrm{Rici}}(\gamma))$ are not identical to each other, because of the asymmetricity of KLD. We can also see from Fig. 2.4 that $D_{\mathrm{KL}}\left(p^{\mathrm{Rici}}(\gamma)||p^{\mathrm{Naka}}(\gamma)\right)$ and $D_{\mathrm{KL}}(p^{\mathrm{Naka}}(\gamma)||p^{\mathrm{Rici}}(\gamma))$ increase as K (m) increase until a point between 2 and 3 for K (between 1.8 and 2.3 for m). After that, the KLDs gradually reduce as K (and hence m) further increases.

2.2.2 Diversity and Coding Gains

The derivation of the explicit expression of (2.16), (2.17), and (2.18) may be excessively complex. However, the diversity and coding gains can be obtained by approximating (2.16), (2.17), and (2.18) at high SNR region.

Invoking the series representation of incomplete gamma function $\gamma(a,x) = \sum_{n=0}^{\infty} \frac{(-1)^n x^{a+n}}{n!(a+n)}$ [GR07, equation 8.354.1] and together with the approximation [WG03]

$$p^{\mathrm{Naka}}(\gamma_{ij}) \approx \frac{m_{ij}^{m_{ij}} (\gamma_{ij})^{m_{ij}-1}}{\left(\overline{\gamma}_{ij}\right)^{m_{ij}} \Gamma(m_{ij})}, \tag{2.21}$$

the outage probability of the LF relaying over Nakagami-m fading channel can be approximated as

$$P_{\mathrm{A}}^{\mathrm{Naka}} \approx A \cdot A' \cdot \left(\frac{E_s}{N_0}\right)^{-(m_{\mathrm{SD}}+m_{\mathrm{RD}})}, \tag{2.22}$$

$$P_{\mathrm{B}}^{\mathrm{Naka}} \approx B \cdot \left(\frac{E_s}{N_0}\right)^{-(m_{\mathrm{SD}}+m_{\mathrm{SR}})}, \tag{2.23}$$

$$P_{\mathrm{C}}^{\mathrm{Naka}} \approx C \cdot \left(\frac{E_s}{N_0}\right)^{-(m_{\mathrm{SD}}+m_{\mathrm{RD}}+m_{\mathrm{SR}})}, \tag{2.24}$$

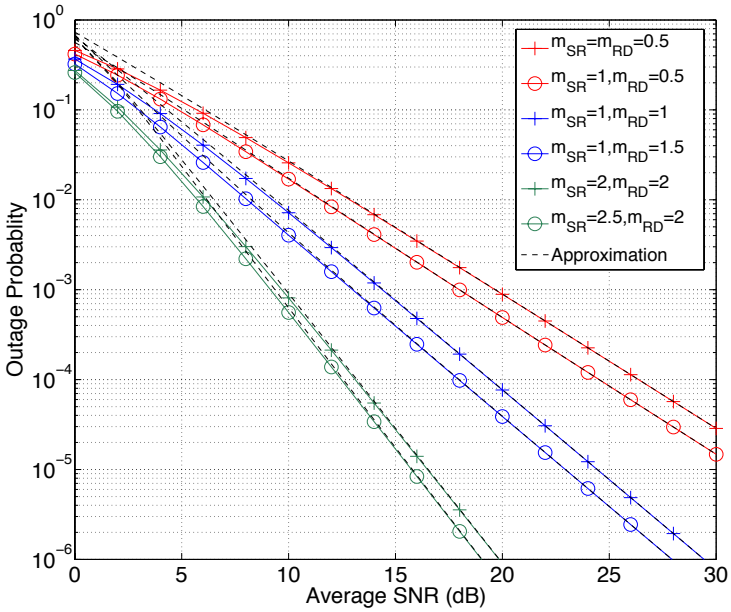

Figure 2.5: Comparison of outage curves obtained by using the numerical calculation (2.16)**,** (2.17)**, and** (2.18) **and approximation method** (2.22)**,** (2.23)**, and** (2.24)**,** $m_{\mathrm{SD}} = 1$**.**

where

$$A = \frac{m_{\mathrm{SD}}^{m_{\mathrm{SD}}} m_{\mathrm{RD}}^{m_{\mathrm{RD}}-1}}{G_{\mathrm{SD}}^{m_{\mathrm{SD}}} G_{\mathrm{RD}}^{m_{\mathrm{RD}}} \Gamma(m_{\mathrm{SD}})\Gamma(m_{\mathrm{RD}})} \int_{\gamma_{\mathrm{SD}}=\Theta^{-1}(0)}^{\Theta^{-1}(1)} \frac{\left(\frac{2}{1+\gamma_{\mathrm{SD}}}-1\right)^{m_{\mathrm{RD}}}}{\gamma_{\mathrm{SD}}^{1-m_{\mathrm{SD}}}} d\gamma_{\mathrm{SD}}, \tag{2.25}$$

$$B = \frac{m_{\mathrm{SR}}^{m_{\mathrm{SR}}} m_{\mathrm{SD}}^{m_{\mathrm{SD}}-1}}{G_{\mathrm{SD}}^{m_{\mathrm{SD}}} G_{\mathrm{SR}}^{m_{\mathrm{SR}}} \Gamma(m_{\mathrm{SD}})\Gamma(m_{\mathrm{SR}})} \int_{\gamma_{\mathrm{SR}}=\Theta^{-1}(0)}^{\Theta^{-1}(1)} \frac{\left(\frac{2}{1+\gamma_{\mathrm{SR}}}-1\right)^{m_{\mathrm{SD}}}}{\gamma_{\mathrm{SR}}^{m_{\mathrm{SR}}-1}} d\gamma_{\mathrm{SR}}, \tag{2.26}$$

$$C = \frac{m_{\mathrm{SR}}^{m_{\mathrm{SR}}} m_{\mathrm{SD}}^{m_{\mathrm{SD}}} m_{\mathrm{RD}}^{m_{\mathrm{RD}}-1}}{G_{\mathrm{SD}}^{m_{\mathrm{SD}}} G_{\mathrm{RD}}^{m_{\mathrm{RD}}} G_{\mathrm{SR}}^{m_{\mathrm{SR}}} \Gamma(m_{\mathrm{SD}})\Gamma(m_{\mathrm{RD}})\Gamma(m_{\mathrm{SR}})} \int_{\gamma_{\mathrm{SR}}=\Theta^{-1}(0)}^{\Theta^{-1}(1)} \cdot \int_{\gamma_{\mathrm{SD}}=\Theta^{-1}(1-\Lambda(\gamma_{\mathrm{SR}}))}^{\Theta^{-1}(1)} \gamma_{\mathrm{SD}}^{m_{\mathrm{SD}}-1} \gamma_{\mathrm{SR}}^{m_{\mathrm{SR}}-1} \xi^{m_{\mathrm{SD}}}(\gamma_{\mathrm{SD}}, \gamma_{\mathrm{SR}}) d\gamma_{\mathrm{SR}} d\gamma_{\mathrm{SD}}. \tag{2.27}$$

$G_{\mathrm{SD}}^{m_{\mathrm{SD}}}$, $G_{\mathrm{RD}}^{m_{\mathrm{RD}}}$, and $G_{\mathrm{SR}}^{m_{\mathrm{SR}}}$ are the geometric gains of S-D, R-D, and S-R links, respectively. $A' = 1 - \frac{\gamma\left(m_{\mathrm{SR}}, m_{\mathrm{SR}} \frac{1}{\Gamma_{\mathrm{SR}}}\right)}{\Gamma(m_{\mathrm{SR}})}$ indicates the probability of $p_f = 0$ (i.e., decoding error can be arbitrarily small at R). One can easily see that the value of A' asymptotically equal to one at high SNR regime.

Fig. 2.5 shows that, at high SNR region the approximated outage curves obtained from (2.22), (2.23), and (2.24) well match the numerically calculated curves from (2.16), (2.17), and (2.18), which indicates that the approximation is accurate.

Furthermore, it can be observed from (2.22), (2.23), and (2.24) that, $\left(\frac{E_s}{N_0}\right)^{-(m_{\mathrm{SD}}+m_{\mathrm{RD}}+m_{\mathrm{SR}})}$ is higher-order infinitesimal of $\left(\frac{E_s}{N_0}\right)^{-(m_{\mathrm{SD}}+m_{\mathrm{RD}})}$ and $\left(\frac{E_s}{N_0}\right)^{-(m_{\mathrm{SD}}+m_{\mathrm{SR}})}$ when $\frac{E_s}{N_0}$ goes to infinity. Therefore, the overall outage probability of the LF relaying with Nakagami-m fading can be formulated as

$$P_{\mathrm{out}}^{\mathrm{Naka}} = \left(G_c \cdot \frac{E_s}{N_0}\right)^{(-G_d)}, \tag{2.28}$$

where

$$G_d = m_{\mathrm{SD}} + \min(m_{\mathrm{SR}}, m_{\mathrm{RD}}) \tag{2.29}$$

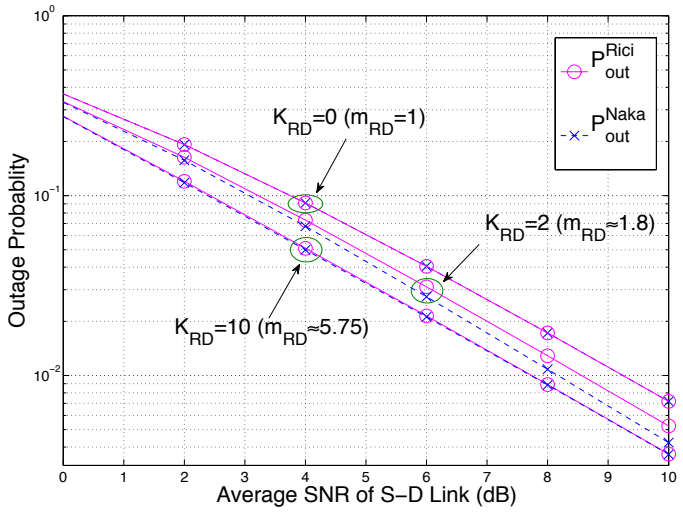

Figure 2.6: Outage probability with Rician and Nakagami-m fading in the R-D link. The S-R link is Rayleigh fading: $K_{\mathrm{SR}} = 0$ ($m_{\mathrm{SR}} = 1$).

and

$$G_c = \begin{cases} \frac{1}{(G_d\sqrt[4]{B})}, & m_{\mathrm{SR}} < m_{\mathrm{RD}} \\ \frac{1}{(G_d\sqrt[4]{A+B})}, & m_{\mathrm{SR}} = m_{\mathrm{RD}} \\ \frac{1}{(G_d\sqrt[4]{A})}, & m_{\mathrm{SR}} > m_{\mathrm{RD}} \end{cases} \tag{2.30}$$

are the diversity and coding gains [WG03] of the LF relaying. We can see from (2.30) that, the system diversity order of the LF relaying is restricted by the less reliable channel among the S-R and R-D links. The outage curves shown in Fig. 2.5 also illustrate that the diversity gain cannot be obtained by only increase m of either the S-R or the R-D link. As the values of m_{SR} or m_{RD} increase, the lower outage probability can be achieved. However, the decay of outage curves always remains the same. The outage curves can achieve sharper decay (higher diversity order) only when m of both the S-R and R-D links increase simultaneously, which confirms the conclusion shown in (2.29) regarding diversity order.

2.2.3 Theoretical Results

The theoretical outage probabilities of the LF relaying system with R-D link suffering from Rician fading are presented in Fig. 2.6, where the outage probability is denoted as $P_{\mathrm{out}}^{\mathrm{Rici}}$. Also, the theoretical outage probabilities with the R-D link undergoing Nakagami-m fading, denoted as $P_{\mathrm{out}}^{\mathrm{Naka}}$, are shown in Fig. 2.6. Both the S-D and S-R links suffer from Rayleigh fading ($K_{\mathrm{SR}} = 0$ for $P_{\mathrm{out}}^{\mathrm{Rici}}$, $m_{\mathrm{SR}} = 1$ for $P_{\mathrm{out}}^{\mathrm{Naka}}$). We can see that the $P_{\mathrm{out}}^{\mathrm{Rici}}$ and $P_{\mathrm{out}}^{\mathrm{Naka}}$ curves have similar tendency: the larger the K_{RD} (m_{RD}) values are, the smaller the outage probability is, for a given average SNR value. This indicates that as the channel variation of the R-D link becomes milder, lower outage probability can be achieved. This is due to the contribution of the increased LOS component power in the R-D link. However, as shown in Fig. 2.6, the diversity order remains with a higher ratio of the R-D link LOS component. This is because the S-R and S-D link variations follow Rayleigh distribution and can only achieve 1st order diversity. Even though higher order diversity can be achieved over the R-D link with the increased LOS component power, it is obvious that the whole relaying system cannot 2nd order diversity according to max-flow min-cut theorem, which is widely used for network performance evaluation.

Fig. 2.7 shows the theoretical outage probability $P_{\mathrm{out}}^{\mathrm{Rici}}$ and $P_{\mathrm{out}}^{\mathrm{Naka}}$ versus the average SNR, where $K_{\mathrm{SR}} = K_{\mathrm{RD}}$ ($m_{\mathrm{SR}} = m_{\mathrm{RD}}$). It is found that the outage curves can achieve sharper decay than that with 2nd order diversity, when the LOS component ratio of the both the S-R and R-D links increases simultaneously. It is reasonable since the bottleneck of S-R and R-D links magnifies as the LOS component getting stronger, according to the max-flow min-cut theorem.

From Fig. 2.6 and 2.7 we found that, when $K_{\mathrm{RD}} = 0$ ($m_{\mathrm{RD}} = 1$), $P_{\mathrm{out}}^{\mathrm{Rici}}$ and $P_{\mathrm{out}}^{\mathrm{Naka}}$ show the same performance. This is because obviously, with $K_{\mathrm{RD}} = 0$ ($m_{\mathrm{RD}} = 1$), Rician (Nakagami-m) fading with R-D link reduces to Rayleigh

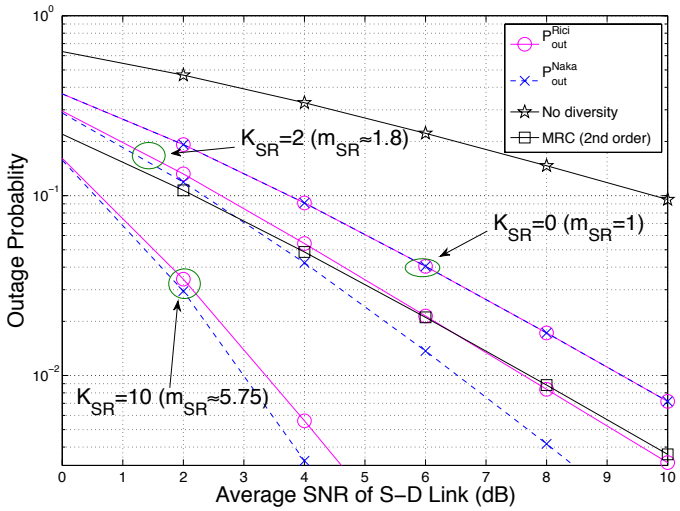

Figure 2.7: Outage probability with Rician and Nakagami-m fading in both S-R and R-D links. $K_{\mathrm{SR}} = K_{\mathrm{RD}}$, $m_{\mathrm{SR}} = m_{\mathrm{RD}}$.

fading. However, when the K_{RD} (m_{RD}) values increase, e.g., $K_{\mathrm{RD}} = 2$ ($m_{\mathrm{RD}} \approx 1.8$), the outage curves exhibit different tendencies. Again, the difference diminishes when K_{RD} (m_{RD}) becomes larger, e.g., $K_{\mathrm{RD}} = 10$ ($m_{\mathrm{RD}} \approx 5.76$). This observation can be verified by the KLD analysis given in section 2.2.1.

2.3 Lossy Decode and Forward with Symbol-Level Filtering

In this section, a lossy decode and forward with symbol-level filtering technique will be considered in TS1.

Cooperative relaying has been intensively investigated in the last decade with various aspects. Recently, it has been reconsidered as one of the solutions to explore the nature of densely deployed wireless networks. As one of the widely accepted relay protocols, DF relaying faces the problem of decoding errors propagation particularly in the case of relatively weak source-relay (SR) link. Forwarding erroneous symbols to destination has effect to the overall system and can cause error floor in bit error rate as discussed in [Li+06].

To solve this problem, selective DF (SDF) relaying has been proposed and approached the goal through the cost of increasing system complexity [YMT08]-[Nos06]. For example, cyclic redundancy code (CRC) based SDF has been proposed in [Nos06]. Authors proposed to use CRC check at relay and prevent it from forwarding if CRC fails. However, a single error in a coded frame will trigger a CRC failure at the relay and hinder a significant number of correctly decoded symbols to be forwarded to destination. This results the diversity gain loss. To improve the performance, threshold-based SDF approaches have been proposed, which allows relay node to calculate a reliability measure of the receive symbols and forward it to destination in the case the measure passes a pre-set value. For example, authors use the receive SNR as the measure at relay in [MYT08] and log-likelihood ratio (LLR) has also been proposed to be used as the measure in [PAR08]. The authors in [Voj06] proposed that the relay can operate in the DF mode when the SNR exceeds a pre-set value and in the amplify-and-forward (AF) mode when below such a value. Consequently, having a properly designed threshold is very important to the performance of the threshold based SDF. The optimum threshold is normally difficult to find and especially with multiple relay nodes. It also worth to notice, these threshold-SDF schemes are still frame level based selection.

To compensate the diversity gain loss through discarding whole frame, symbol-level selection approach has been proposed. A LLR-based selection approach has been investigated for demodulation-forward relaying in [Kwo+10]. The magnitude of the LLR for each symbol is calculated at relay and compared with a pre-defined threshold. If the LLR magnitude is equal to or larger than the threshold, the symbols are included in the frame to retransmit. Otherwise, the reserved slot for this symbol remains empty in the frame. A similar approach is also proposed in [AHGAD11], where authors proposed only the bits with associated LLR that exceed the pre-set threshold will be forwarded in coded cooperation. The relay then keeps silent (transmit zero energy) in the places of the blocked bits. It is noticed here, both approaches need to have the knowledge of noise variance of source-relay (SR) link to

calculate LLR, and all three links to calculate the pre-defined threshold. However, it is not practical to have noise variance, especially for the forward link. These limit the application of symbol-level selection in SDF.

This motivated us to propose an improved SDF, which relay can forward the reliable symbols to destination to compensate the spatial-domain channel diversity. Meanwhile, no pre-set threshold and noise variance is needed at relay. To approach this goal, we propose a novel approach named lease-square (LS) based symbol level filtering, which employs absolute value to filter out the unreliable symbols after signal regeneration at relay.

Consider a classical three-node relaying model accommodating one source (S), one destination (D), and a half-duplex relay (R). The relaying protocol is orthogonal DF to prevent interference from transmitting concurrently. Hence, each transmission is divided into two phases. In phase I, source broadcasts signals to relay and destination, the discrete-time equivalent form of mth receive symbol at relay as well at the destination are described by

$$\text{SD Link} : y_m^{\text{sd}} = \sqrt{P_m^{\text{s}}} h^{\text{sd}} x_m^s + v_m^{\text{sd}}, \tag{2.31}$$

$$\text{SR Link} : y_m^{\text{sr}} = \sqrt{P_m^{\text{s}}} h^{\text{sr}} x_m^s + v_m^{\text{sr}}, \tag{2.32}$$

where y_m^{sd}, y_m^{sr} denotes the m th receive symbol through the SD channel, h^{sd} and SR channel, h^{sr} respectively, which is considered here as block fading; P_m^{s} the source transmit power; x_m^{s} the coded m th symbol sent by source; v_m denotes the noise of corresponding links with the variance $\mathscr{N}_o$. Then relay node demodulates and decodes the receive coded symbols into uncoded ones for all symbols in the frame. If CRC does not report error for this frame, then relay will re-encode and modulate the information bits and send whole frame to destination through relay-destination (RD) channel, h^{rd}, for diversity combining. In this case, there is no difference between our proposed one and the CRC-based SDF. The discrete-time equivalent form of received mth symbol at destination is expressed as

$$\text{RD Link} : y_m^{\text{rd}} = \sqrt{P_m^{\text{r}}} h^{\text{rd}} x_m^r + v_m^{\text{rd}}, \tag{2.33}$$

where P_m^{r} denotes the relay transmit power for m th symbol. Linear combining is employed at destination to enjoy the diversity gain.

Once CRC reports frame error, if the relay discards the receive frame and sends signalling to source node, a frame will be re-sent through SD link. Then, receive SNR at destination for such repetition-coded DF can be expressed as

$$\gamma^{\text{baseline}} = \frac{2P^{\text{s}}}{\mathscr{N}_o} |h^{\text{sd}}|^2 \delta^2, \tag{2.34}$$

where P^{s} denotes the frame transmit power per frame and δ^2 the signal variance.

In our proposed approach, relay does not simply discard the whole frame although CRC reports decoding error. To help to select trust-able symbols, we define the decoding error for mth symbol at relay node as ε_m. The error probability per frame is given as $\mathscr{P}_\varepsilon$, which varies in each frame due to the channel fading. Ideally, only correctly decoded symbols should be selected and forwarded, and relay should transmit zero energy in the places for the rest symbols. An utility function is defined here as

$$\Theta_m = \begin{cases} 1, \ m\text{th symbol is selected} \\ 0, \ m\text{th symbol is not selected} \end{cases} \tag{2.35}$$

Therefore, the mth transmit symbol at relay is given as

$$x_m^{\text{r}} = \Theta_m \hat{x}_m^{\text{r}}, \tag{2.36}$$

where $\hat{x}_m^{\text{r}}$ denotes the mth coded symbol after reconstruction at relay. For every frame, a selection mask is given as $\blacksquare = [\Theta_1, \ldots, \Theta_M]$.

At destination, a linear combining is employed to enjoy the diversity gain. Then, the destination can perform the combination of y_m^{sd} with y_m^{rd} or y_m^{sd} as

$$y_m^{(\text{r})} = w^{(\text{sd})} y_m^{(\text{sd})} + w^{(\text{rd})} y_m^{(\text{rd})}, \tag{2.37}$$

where $w^{(\text{sd})}$, $w^{(\text{rd})}$ are the weighting coefficient. Single-tap equalizers, e.g., zero-forcing, can be employed for the channel equalization. These equalizers do not affect the SNR of the receive symbols. In the case, relay forwards the frame to destination, the receive SNR at destination is given as

$$\gamma^{(\text{r})} = \frac{P^{\text{s}}}{\mathscr{N}_o} |h^{\text{sd}}|^2 \delta^2 + (1 - \mathscr{P}_\varepsilon) \frac{P^{\text{r}}}{\mathscr{N}_o} |h^{\text{rd}}|^2 \delta^2, \tag{2.38}$$

where $\mathscr{P}_\varepsilon = 1 - \sum_{m=1}^{M} \Theta_m / M$.

It is observed, when wrongly decoded bits are null out at relay, diversity gain will be reduced as the second term in (2.38) will be null out. Therefore, relay node should only still forward the selected symbols to destination after CRC reported error when $\gamma^{(\mathrm{r})} \geqslant \gamma^{\mathrm{baseline}}$. This is equivalent to

$$(1 - \mathscr{P}_\varepsilon) \frac{P^{\mathrm{r}}}{\mathscr{N}_o} |h^{\mathrm{rd}}|^2 \delta^2 \geqslant \frac{P^{\mathrm{s}}}{\mathscr{N}_o} |h^{\mathrm{sd}}|^2 \delta^2. \tag{2.39}$$

From the condition in (2.39), we have the following condition for frame error probability as

$$\mathscr{P}_\varepsilon \leqslant 1 - \frac{P^{\mathrm{s}} |h^{\mathrm{sd}}|^2}{P^{\mathrm{r}} |h^{\mathrm{rd}}|^2}. \tag{2.40}$$

As error probability is always non-negative, therefore, the maximum decoding error probability at relay for forwarding to offer the same performance as source retransmission is given as

$$\mathscr{P}_\varepsilon^{\max} = 1 - \frac{P^{\mathrm{s}} |h^{\mathrm{sd}}|^2}{P^{\mathrm{r}} |h^{\mathrm{rd}}|^2}. \tag{2.41}$$

As indicated in (2.40), $\mathscr{P}_\varepsilon$ needs to fulfil the forward condition. To filter out the trust-able symbol at relay, a selection strategy is needed. In the following section, the proposed LS based symbol-level filtering strategy will be discussed.

It is noticed here, the stopping forward criterion in (2.41) needs the channel knowledge of RD link, which is possible available at relay through signalling.

2.3.1 Proposed Symbol Filtering Strategy

In this section, our proposed symbol filtering strategy will be discussed, which will be employed at relay to conduct the selection mask ■. After broadcasting in phase I, relay performs demodulation and decoding to the receive signals. Then the decoded symbols are fed into encoder and modulator to produce re-constructed mth symbol as $\hat{x}_m^s$. The LS of the mth received symbol at relay and the re-constructed symbol can be expressed as

$$\Delta_m = \left| h^{\mathrm{sr}} x_m^s + v_m^{\mathrm{sr}} - h^{\mathrm{sr}} \hat{x}_m^s \right|^2. \tag{2.42}$$

To determine whether mth symbol is correctly decoded or not, the Δ_m is compared with the norm of mth receive symbol as

$$\xi_m = \Delta_m - |h^{\mathrm{sr}} x_m^s + v_m^{\mathrm{sr}}|^2. \tag{2.43}$$

If $\hat{x}_m^s$ is correctly decoded (i.e. $\hat{x}_m^s = x_m^s$), the LS value (i.e. Δ_m) should be smaller than the mth receive symbol (i.e., $\xi_m < 0$). Otherwise, it will be larger than it, which indicates $\hat{x}_m^s$ is wrongly decoded. The utility function defined in (2.35) can be calculated as

$$\Theta_m = \begin{cases} 1, & \xi_m < 0 \\ 0, & \xi_m \geqslant 0. \end{cases} \tag{2.44}$$

Θ_m is calculated for all M symbols and then a selection mask ■ is produced per frame to select the trust-able symbols to be forwarded to destination. As indicated in Section 2.3 the symbol error rate per frame should be less than maximum symbol error rate per frame to maintain the diversity gain. Therefore, we have the following

$$1 - \sum_{m=1}^{M} \Theta_m / M \leqslant \mathscr{P}_\varepsilon^{\max}, \tag{2.45}$$

$$\sum_{m=1}^{M} \Theta_m \geqslant M \cdot \frac{P^{\mathrm{s}} |h^{\mathrm{sd}}|^2}{P^{\mathrm{r}} |h^{\mathrm{rd}}|^2}. \tag{2.46}$$

With the definition of Θ_m in (2.35) and the inequality in(2.46), we can immediately conclude the following result.

Theorem 1 (Relay Forwarding Criterion)**.** *To let relay to forward an erroneous frame to destination, a sufficient and necessary condition for the total selected trust-able symbols per frame to be fulfilled is*

$$\sum_{m=1}^{M} \Theta_m \geqslant M \cdot \frac{P^{\mathrm{s}} |h^{\mathrm{sd}}|^2}{P^{\mathrm{r}} |h^{\mathrm{rd}}|^2} \tag{2.47}$$

Theorem 1 defines a criterion that relay can forward the message although CRC report error.

It is noticed here, when relay forwards frame through RD link, the null-out symbols will introduce noise at destination. The selection mask, i.e., ■, can be forwarded to destination to de-noise, but this will significantly increase the signalling overhead as the frame length increasing. Without ■ at destination, the performance will be degraded. However, it is observed that the the degradation is negligible throughout the whole SNR range. In our simulation results section, the proposed approach will be demonstrated with and without selection mask to be forwarded to destination node.

2.3.2 Performance Analysis

In this section, the bit error probability (BEP) is employed to analyse performance. With the law of total probability, the BEP of the proposed scheme is

$$\Pr(\varepsilon) = \Pr(\mathscr{S}^C)\Pr(\varepsilon|\mathscr{S}^C) + (1-\Pr(\mathscr{S}^C))\Pr(\varepsilon|\mathscr{S}). \tag{2.48}$$

Here, the condition probability is defined as $\Pr(A|B) = \Pr(AB)/\Pr(B)$. The first term of (2.48) is the error probability at destination when the symbol is not selected to be forwarded. The second term is the error probability at destination when the symbol is selected.

Symbols is selected based on the LS decision in (2.44). Therefore, the probability that a symbol is not selected for retransmission $\Pr(\mathscr{S}^C)$ can be expressed as follows,

$$\Pr(\mathscr{S}^C) = \Pr(\xi_m \geqslant 0) = \Pr(|y_m^{\mathrm{sr}}| \leqslant \sqrt{\Delta_m}) \tag{2.49}$$

$$= \int_{-\sqrt{\Delta_m}}^{\sqrt{\Delta_m}} g_{y_m^{\mathrm{sr}}}(y_m^{\mathrm{sr}}) dy_m^{\mathrm{sr}}, \tag{2.50}$$

where $g_{y_m^{\mathrm{sr}}}(y_m^{\mathrm{sr}}) = \alpha \exp(\beta y_m^{\mathrm{sr}}) \exp(\chi |y_m^{\mathrm{sr}}|)$ denotes the PDF function of the low-pass equivalent received signal after channel compensation at relay (see Appendix A in[Kwo+10] for details). When mth symbol is not selected for retransmission, $\Pr(\varepsilon|\mathscr{S}^C)$ is the error probability of the SD link as

$$\Pr(\varepsilon|\mathscr{S}^C) = \mathrm{P_B}(\gamma_m^{\mathrm{sd}}). \tag{2.51}$$

When the symbol is selected, the error probability at destination after linear combining can be expressed as follows,

$$\Pr(\varepsilon|\mathscr{S}) = (1-\Pr(\varepsilon^{\mathrm{sr}}|\mathscr{S}))\Pr(\varepsilon^{\mathrm{com}}|(\varepsilon^{\mathrm{sr}})^C, \mathscr{S}) + \Pr(\varepsilon^{\mathrm{sr}}|\mathscr{S}) \cdot \Pr(\varepsilon^{\mathrm{ep}}|\varepsilon^{\mathrm{sr}}, \mathscr{S}). \tag{2.52}$$

Consequently, the BEP after combining at destination is derived by substituting (2.50), (2.51) and (2.52) into (2.48).

2.3.3 Simulation Results

Computer based Monte Carlo simulations are used to demonstrate pros/cons of the proposed SDF approach with LS based symbols level filtering. All the communication channels are generated independently according to Rayleigh distribution with unity variance. BPSK modulation scheme is used in our simulations. All transmitters use the equal transmission power. The main metric of interest is the bit error rate (BER). This is because, the proposed symbol-level filtering cannot improve the frame error rate, but the BER. The SNR is defined by average total transmit bit power (i.e. consumed at both source and relay) to noise ratio.

The first baseline is the CRC-based SDF, which will stop forward as long as CRC reporting error in frame level. The second baseline approach employed here for performance comparison is the SNR threshold based SDF investigated in [MYT08]. The pre-agreed SNR threshold is set as 2 dB. As uncoordinated wireless networks considered here, i.e., no signalling is considered, hence HARQ approach cannot be employed to improve the performance.

The simulation results were produced by employing carefully designed experiments with each have $15,000$ Monte Carlo trials. The channel gain (denoted by G) for each links was considered in two different cases as, in Case 1, $G^{\mathrm{sd}} : G^{\mathrm{sr}} : G\mathrm{rd} = 1:1:100$, and in Case 2, $G^{\mathrm{sd}} : G^{\mathrm{sr}} : G^{\cdot}G^{\mathrm{rd}} = 1:4:4$. Case 1 and 2 are corresponding

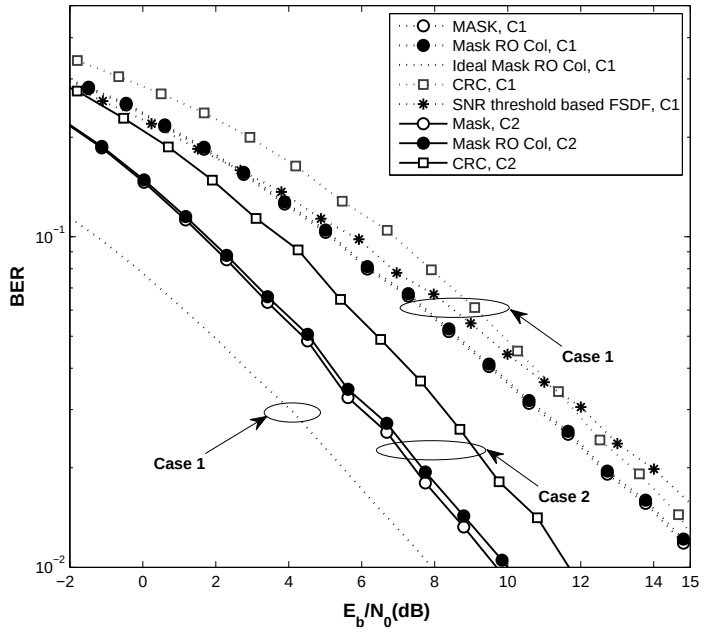

Figure 2.8: BER versus the total transmit power per bit versus noise variance for proposed approach and baselines. Uncoded frame length setup is 2048**. Channel gain setup is as shown in Section V.**

to the scenarios: the relay is close to the destination, and in the middle between the source and the destination, respectively. The employed coding scheme in our simulation is half Turbo Code and the uncoded frame length is 2048.

As it is shown in Fig. 2.8, BER performance is plotted versus the total transmit power per bit versus noise variance (e.g., $E_b/\mathcal{N}_o$) for our proposed approach and baselines. The total transmit power per bit versus noise variance is defined as the total transmit power cost per bit at both source and relay versus the noise variance. The dot lines demonstrate the performance in Case 1. The lines with solid circle marks are the proposed approach, which symbol selection mask is not forwarded to destination to significantly reduced the signalling overhead. Therefore, the noise variance is coloured when linear combining is performed as destination. The lines with square marks are the baseline of CRC based SDF, and the line with star mark is the baseline of SNR threshold based SDF. The line without mark demonstrates the ideal case which all correct symbols have been selected at relay node and forwarded to destination.

It is observed that the proposed approach outperforms both baselines along the total transmit power per bit versus noise variance. Up to 2 dB gain can be observed when comparing the proposed approach with CRC based SDF. It is also observed, that in Case 1, CRC based SDF approaches proposed approach as long as $E_b/\mathcal{N}_o$ increased. This is because more frames will pass the CRC checking at relay node when $E_b/\mathcal{N}_o$ increased. Hence, more frames will be forwarded to destination for diversity combining. It is also noticed, the SNR threshold based SDF does not approach proposed approach as long as $E_b/\mathcal{N}_o$ increased. This is due to the threshold is fixed as a pre-setup value. It is also interesting to see what the performance can achieve, when the symbol selection mask is forwarded to destination to denoise and white the noise variance. So we also plot it as the dot curve with empty circle mark. It is observed, that the performance is almost identical with when the mask is not forwarded. It is also worth to notice, the ideal symbol selection at relay (i.e., denotes by the dot curve) offer much better performance to all the rest. This is because, in Case 1, SD link is weak, hence, many errors will happen at relay. Although LS selection is proposed to be employed at relay, the performance is limited by noise.

We also plotted the performance of the proposed approach and base-line over Case 2 in Fig. 2.8. It is observed, the performances of all approaches are significantly improved compare to over Case 1. This is because that relay node is placed in the middle between source and destination. Hence, SD link is relative strong compare with Case

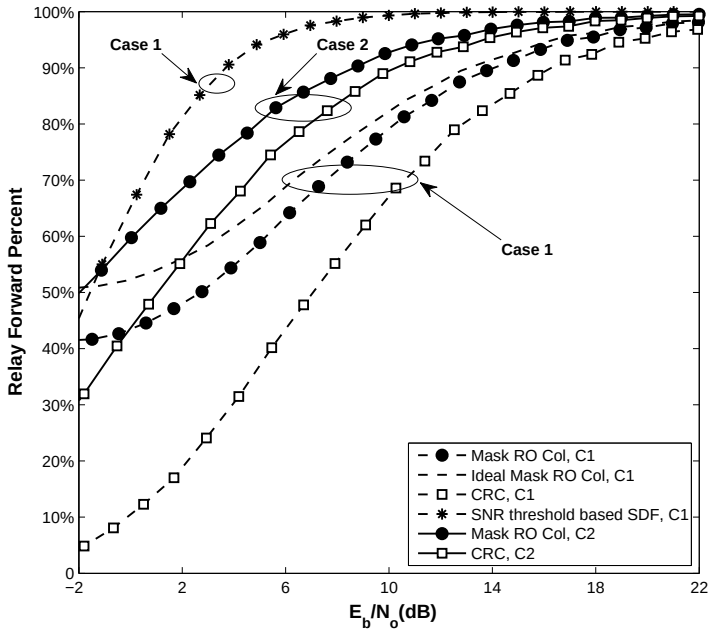

Figure 2.9: Relay forward percent versus the total transmit power per bit versus noise variance.

1. The proposed approach outperforms the CRC based SDF around 3 dB in Case 2. This is because, LS selection performance is improved as SD link channel gain is increased.

To further explain the gain of the proposed approach, we plot the relay node forward percent versus the total transmit power per bit versus noise variance in Fig. 2.9. Dashed curves demonstrate the performance in Case 1, and the solid curves demonstrate the performance in Case 2. It is observed, relay forwards least symbols with CRC based SDF, which explains why it offers worse performance. Proposed approach let relay forward more symbols compare with CRC-based SDF, hence the performance is improved. However, the curve is still away to the ideal symbol selection, therefore, there is a performance gap between the curves of these two in Fig.2.8. It is also interesting to see SNR threshold based SDF enables relay forward the most symbols to destination especially when the value of the total transmit power per bit versus noise variance is low. This is due to the threshold is pre-setup, and more errors have been forward to destination and cause the performance loss.

2.4 Conclusion

The impact of the LOS component on outage probability for the LF relaying has been investigated. The S-D link has been assumed to suffer from block Rayleigh fading whereas the S-R and R-D links undergo block Rician or Nakagami-*m* fading. The exact outage probability bound has been derived. The impact difference of Rician and Nakagami-*m* fading on outage performance has been evaluated, based on KLD analysis between the Rician and Nakagami-*m* distributions.

The majority of factor *m* values estimated in typical urban areas vary from 0.5 to 3.5 [RRC07]. The relatively large KLD between Rician and Nakagami-*m* distributions can be observed in this range. Therefore, the outage difference between the LF relaying with Rician and Nakagami-*m* model is correspondingly large. This observation indicates the flaw that Nakagami-*m* fading model cannot be represented by Rician fading model for designing and/or evaluating the theoretical limit approaching techniques with the LF relaying.

Moreover, an improved SDF with least-square based symbol level filtering has been investigated over TS1. Trusted symbols will be filtered out after CRC reporting frame error. If the Relay Forwarding Criterion is fulfilled, relay will forward a frame with selected symbols and reserve places for the unselected symbols at the destination. The

selection mask at relay can be forwarded to destination to reduce the extra noise introduced by the reserved places. However, it is also demonstrated in our simulation results that the performance degradation at destination due to these can be negligible. Simulation demonstrated the proposed relaying protocol offers up to 3 dB performance improvement than the selected baselines in terms of BER.

3. Performance Analysis of TS2

3.1 Hamming Distortion Bounds of Binary Information Sensing

We analyze the theoretical limits in AWGN channels using the Slepian-Wolf theorem for the binary information sensing network, which can be considered as a real application case of TS2. However, the limits are obtained with a strong assumption that the observations are recovered losslessly in usual Shannon sense, which is not always true. Instead, we analyze a problem that how small a Hamming distortion level the fusion center can achieve from the rate-distortion perspective by taking into account distortions of reconstructed observations. To this end, we formulate a minimization problem to obtain the lower bounds on Hamming distortion using the JSC setup with orthogonal multiple access channel (MAC) components.

In order to solve the minimization problem, we first model the source coding of the binary information sensing network by the binary CEO problem. We then reduce the binary CEO problem to a binary multiterminal source coding problem, which plays the core role in solving the main problem. An outer bound for the rate-distortion region of the binary multiterminal source coding problem is then derived by providing the converse coding proof. We establish the connection with respect to the Hamming distortion level between the binary CEO problem and the binary multiterminal source coding problem. Finally, the minimization problem is formulated in the framework of convex optimization. It should be emphasized here that our purpose is not intended to derive a tight rate-distortion bound for the binary CEO problem. Instead, we focus on the derivation of a lower bound on the Hamming distortion that can be used as a reference of the BER performance curves of the encoding/decoding algorithms.

3.2 Problem Statement

The system model of estimating a single source through two sensors/terminals is depicted in Fig. 3.1. A common i.i.d. source X produces a sequence $\mathbf{x} = [x(t)]_{t=1}^{n}$ by taking values from a binary set $\mathscr{X} = \{0,1\}$ with equal probability. Source X is observed by two nodes and forwarded to a single destination. Due to the inaccuracy of the estimation and/or limited received signal power at nodes, such as in WSN and WMN, the sequences received by the nodes may contain errors[1], and the nodes still forward the erroneous sequences to the destination, which is referred as LF [Zho+14; Lu+14]. The error probabilities $\Pr(x_1(t) \neq x(t))$ and $\Pr(x_2(t) \neq x(t))$ are denoted as p_1 and p_2, respectively, i.e., $\Pr(b_i(t) = 1) = p_i$ for the binary noise sequence $\mathbf{b}_i = [b_i(t)]_{t=1}^{n}$, $i = 1,2$. At the nodes, the noisy versions $\mathbf{x}_1 = [x_1(t)]_{t=1}^{n}$ and $\mathbf{x}_2 = [x_2(t)]_{t=1}^{n}$ of $\mathbf{x}^n$ are independently encoded by two joint source channel (JSC) encoders to generate symbol sequences $\mathbf{s}_1 = [s_1(t)]_{t=1}^{k_1}$ and $\mathbf{s}_2 = [s_2(t)]_{t=1}^{k_2}$ with coding rates $r_i = n/k_i$, $i = 1,2$. The symbol sequences $\mathbf{s}_1$ and $\mathbf{s}_2$ are then transmitted to the destination over two orthogonal AWGN channels, as

$$\mathbf{y}_i = h_i \cdot \mathbf{s}_i + \mathbf{z}_i, \quad i = 1,2, \tag{3.1}$$

where h_i and $\mathbf{z}_i = [z(t)]_{t=1}^{k_i}$ represent the channel gain and the AWGN sequence at the destination, respectively. The orthogonality can be achieved by any scheduled multiple access scheme, like time division multiple access (TDMA), i.e., $\mathbf{s}_1$ and $\mathbf{s}_2$ can be transmitted at different time intervals. The destination performs JSC decoding to form estimates $\hat{\mathbf{x}}_i$ of the sequences $\mathbf{x}_i$, $i = 1,2$. We define the expected Hamming distortion measures $E[\frac{1}{n}\sum_{t=1}^{n} d(x_i(t),\hat{x}_i(t))] \leq D_i + \varepsilon$ to evaluate the error probability $\Pr(x_i(t) \neq \hat{x}_i(t))$ with

$$d(x_i(t),\hat{x}_i(t)) = \begin{cases} 1, & \text{if} \quad x_i(t) \neq \hat{x}_i(t), \\ 0, & \text{if} \quad x_i(t) = \hat{x}_i(t), \end{cases} \tag{3.2}$$

and ε representing an arbitrarily small positive number.

Finally, the destination reconstructs the source information $\mathbf{x}^n$ of which the estimate is denoted as $\hat{\mathbf{x}}^n$ based on a decision rule from $\hat{\mathbf{x}}_1^n$ and $\hat{\mathbf{x}}_2^n$. Therefore, the distortion measure $E[\frac{1}{n}\sum_{t=1}^{n} d(x(t),\hat{x}(t))] \leq D + \varepsilon$ can be formulated as a function of D_i, $i = 1,2$, as $D = F_d(D_1,D_2)$, where function $F_d(\cdot)$ is detailed in Section 3.4. It should be emphasized here that function $D = F_d(D_1,D_2)$ limits the decoding scheme to which first reconstructs $\mathbf{x}_1^n$ and $\mathbf{x}_2^n$ and then makes the decision on $\mathbf{x}^n$ from those reconstructions (it is referred to as sequential decoding), as shown

[1] In WMN applications, the nodes correspond to the transceivers in the multiple routes. In a WMN, a source communicates with a destination through multiple intermediate nodes if they are not within the communication coverage. If errors are allowed in the messages forwarded by the intermediate nodes, the WMN can be also modeled as the model shown in Fig. 3.1 [XinISITA].

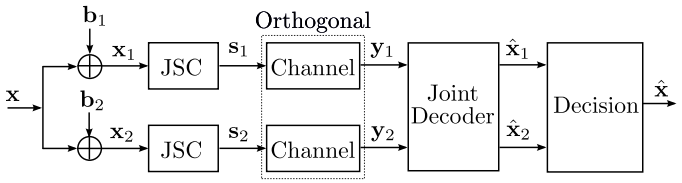

Figure 3.1: The abstract system model of estimating a single source through two independent nodes with joint source-channel coding.

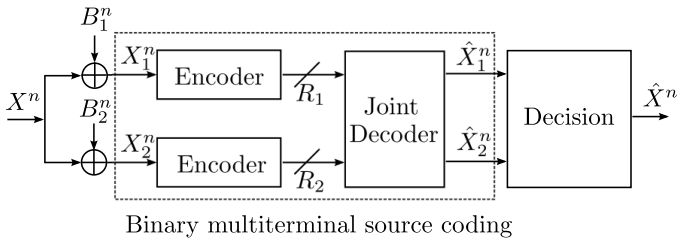

Figure 3.2: The abstract model of the binary CEO problem with two independent nodes.

in Fig. 3.1. The optimality of such a decoding scheme is an open problem, but it is definitely of interest for practical systems. Furthermore, $F_d(D_1, D_2)$ largely depends on the decision rule, i.e., there exists different function $F_d(D_1, D_2)$ for different decision rules[2].

According to the source-channel separation theorem for lossy source coding [Xiao2007], distortion D_1 and D_2 can be achieved if the following inequalities hold:

$$\begin{cases} R_1(D_1) \cdot r_1 & \leq C(\gamma_1), \\ R_2(D_2) \cdot r_2 & \leq C(\gamma_2), \end{cases} \tag{3.3}$$

where $R_i(D_i)$ is the rate-distortion function for the source coding and $C(\gamma)$ is the Shannon capacity using Gaussian codebook[3] with the argument γ denoting the SNR of the channel. As stated above, r_1 and r_2 represent end-to-end coding rates of two links. Our goal is to derive the theoretical lower bound on the Hamming distortion for the system shown in Fig. 3.1. It is equivalent to minimizing the expected Hamming distortion D through a function $F_d(D_1, D_2)$ under constraints shown in (3.3), as

$$\min_{D_1, D_2} \quad D = F_d(D_1, D_2) \tag{3.4}$$

$$\text{s.t.} \tag{3.5}$$

$$R_1(D_1) \cdot r_1 \leq C(\gamma_1),$$
$$R_2(D_2) \cdot r_2 \leq C(\gamma_2),$$

The minimization being performed in (3.4) is for a specific system which maps the average distortions D_1 and D_2 to D, since function $F_d(D_1, D_2)$ is defined for designated decision rules. To achieve this goal by solving (3.4), we turn to derive the rate-distortion function $R_i(D_i)$ for the problem shown in Fig. 3.1 and to establish the function $D = F_d(D_1, D_2)$ for the decision rule used at the destination.

[2]It has been assumed in this setup that 1) each encoder uses joint typicality encoding and binning based on random coding arguments, and the decoder performs joint typicality decoding with a sufficiently large n to achieve the average distortion D_i as in the Berger-Tung source coding problem [GK11]; 2) the errors occurring in each sequence $\mathbf{x}_i^n$ are i.i.d. In the practical system, we use random interleavers to asymptotically make this assumption practical. As shown in Section 3.5, the simulation results are consistent with the lower bound calculation based on soft combining decision.

[3]For one-dimensional signal, $C(\gamma) = \frac{1}{2}\log_2(1+2\gamma)$, and for two-dimensional signal, $C(\gamma) = \log_2(1+\gamma)$ [CT06].

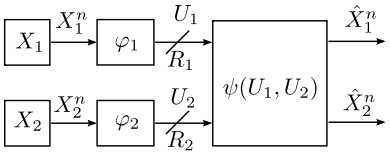

Figure 3.3: The binary multiterminal source coding problem for two correlated binary sources.

3.3 Rate-Distortion Region Analysis

3.3.1 Outer Bound on the Rate-Distortion Region

3.3.1.1 Source Coding

In network information theory, the source coding of the communication system shown in Fig. 3.1 is modeled by the binary CEO problem. The abstract model of the binary CEO problem is illustrated in Fig. 3.2. In order to derive the rate-distortion function $R_i(D_i)$, we first reduce the binary CEO problem to a binary multiterminal source coding problem. An outer bound for the rate-distortion region which is determined by the rate-distortion function $R_i(D_i)$ is then derived for the binary multiterminal source coding problem through the converse proof, as in the Gaussian case [Ooh97].

The binary multiterminal source coding problem which we consider is depicted in Fig. 3.3. Since random sources X_1^n and X_2^n originate from the common source X^n, the random variable pair (X_1, X_2) follows a joint PMF $p_{X_1X_2}(x_1, x_2) = \Pr\{X_1 = x_1, X_2 = x_2\}$ given by

$$p_{X_1X_2}(x_1, x_2) = \begin{cases} \frac{1}{2}\rho, & \text{if } x_1 \neq x_2, \\ \frac{1}{2}(1-\rho), & \text{otherwise}, \end{cases} \tag{3.6}$$

where $\rho = \Pr(x_1 \neq x_2)$ is the correlation parameter between the sources X_1 and X_2, i.e., X_2 can be seen as the output of a BSC with the crossover probability ρ where X_1 is the input. Two encoders independently encode X_1^n and X_2^n at rates R_1 and R_2 as

$$\varphi_1 : \mathscr{X}^n \to \mathscr{M}_1 = \{1, 2, \cdots, 2^{nR_1}\},$$
$$\varphi_2 : \mathscr{X}^n \to \mathscr{M}_2 = \{1, 2, \cdots, 2^{nR_2}\}.$$

The encoder output sequences $U_1 = \varphi_1(X_1^n)$ and $U_2 = \varphi_2(X_2^n)$ are transmitted to a common receiver. It jointly decodes the received samples to construct the estimates $(\hat{X}_1^n, \hat{X}_2^n)$ of the source pair (X_1^n, X_2^n) denoted as $(\hat{X}_1^n, \hat{X}_2^n) = \psi(\varphi_1(X_1^n), \varphi_2(X_2^n))$.

For given distortion values $D_1 \in [0, \frac{1}{2}]$ and $D_2 \in [0, \frac{1}{2}]$, the rate-distortion region $\mathscr{R}(D_1, D_2)$ is defined as

$$\mathscr{R}(D_1, D_2) = \Big\{(R_1, R_2) : (R_1, R_2) \text{ is admissible such that } E\frac{1}{n}\sum_{t=1}^{n} d(x_i(t), \hat{x}_i(t)) \leq D_i + \varepsilon, i = 1, 2\Big\}.$$

It should be emphasized here that the admissible rate-distortion region may *not* be applied to the binary CEO problem directly, since the strategy at the CEO is specified to two-step decoding. The admissible rate-distortion region defined above limits the problem which has the specific setup.

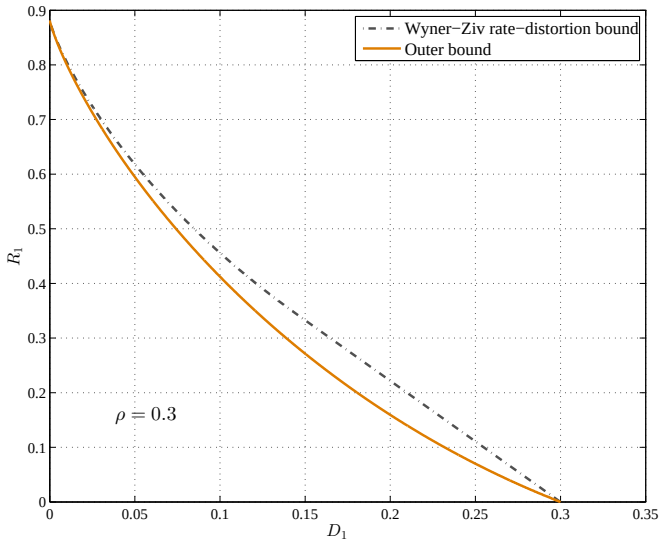

Figure 3.4: The comparison of Wyner-Ziv rate-distortion bound and derived outer bound. The correlation ρ between two sources is set at 0.3.

3.3.1.2 Main Results

In summary, the outer bound on the rate-distortion function $R_i(D_i)$ is given by

$$\begin{cases} R_1(D_1) \geq H_2[\rho * H_2^{-1}(1-R_2(D_2))] - H_2(D_1), \\ R_2(D_2) \geq H_2[\rho * H_2^{-1}(1-R_1(D_1))] - H_2(D_2), \\ \sum_{i=1}^{2} R_i(D_i) \geq 1 + H_2(\rho) - \sum_{i=1}^{2} H_2(D_i). \end{cases} \tag{3.7}$$

3.3.2 Inner Bound

As it is known that the exact rate-distortion bound for lossy multiterminal source coding problem lies between the Berger-Tung inner and outer bounds [GK11]. We also derived the rate-distortion region $\mathscr{R}^{\mathrm{i}}(D_1,D_2)$ based on the Berger-Tung inner bound [ICT15] as

$$\mathscr{R}^{\mathrm{i}}(D_1,D_2) = \mathscr{R}_1^{\mathrm{i}}(D_1) \bigcap \mathscr{R}_2^{\mathrm{i}}(D_2) \bigcap \mathscr{R}_{12}^{\mathrm{i}}(D_1,D_2) \tag{3.8}$$

with

$$\begin{cases} \mathscr{R}_1^{\mathrm{i}}(D_1) = \{(R_1,R_2) | R_1 \geq H_2(\rho * D_1 * D_2) - H_2(D_1)\}, \\ \mathscr{R}_2^{\mathrm{i}}(D_2) = \{(R_1,R_2) | R_2 \geq H_2(\rho * D_1 * D_2) - H_2(D_2)\}, \\ \mathscr{R}_{12}^{\mathrm{i}}(D_1,D_2) = \{(R_1,R_2) | \\ \quad R_1 + R_2 \geq 1 + H_2(\rho * D_1 * D_2) - \sum_{i=1}^{2} H_2(D_i)\}, \end{cases}$$

for every $0 \leq D_1, D_2 \leq \frac{1}{2}$. The detailed proof is given in Appendix D.

3.3.3 Remarks

We now show that the derived outer and inner bounds on the rate-distortion region are connected to the classical results.

Remark. *If either $R_1 = 0$ or $R_2 = 0$, i.e., one of two encoders is breakdown in the network, $\mathscr{R}^o(D_1,D_2)$ is then consistent with the classical rate-distortion function $1 - H_2(D_i)$ for the binary source.*

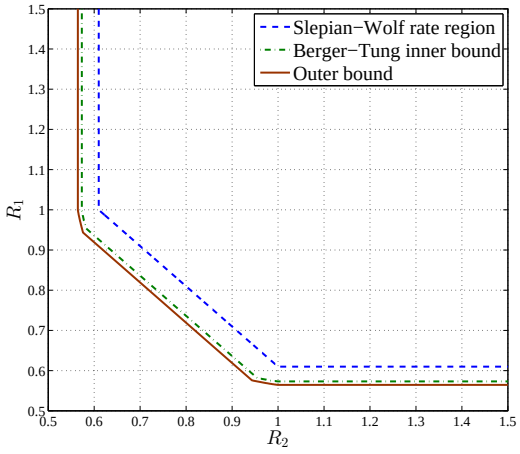

(a) $\rho = 0.15$**,** $D_1 = D_2 = 0.005$**.**

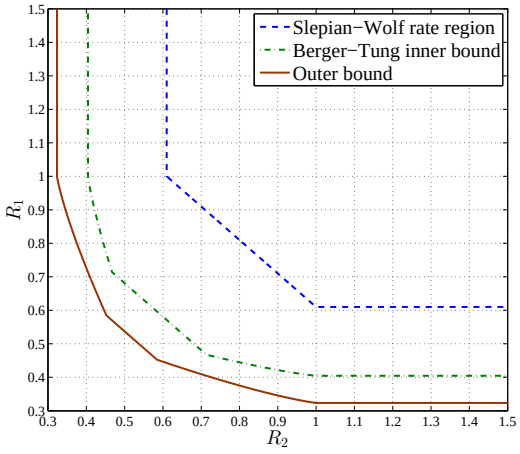

(b) $\rho = 0.15$**,** $D_1 = D_2 = 0.05$**.**

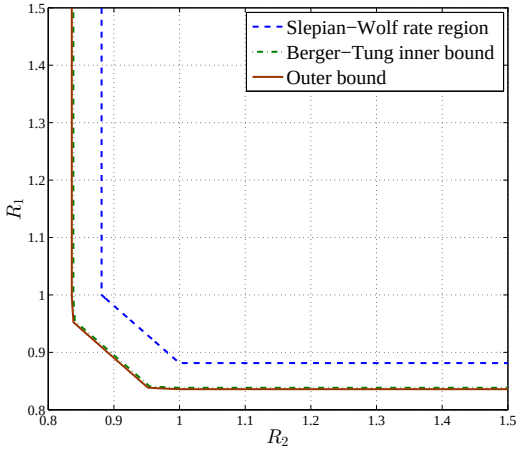

(c) $\rho = 0.3$**,** $D_1 = D_2 = 0.005$**.**

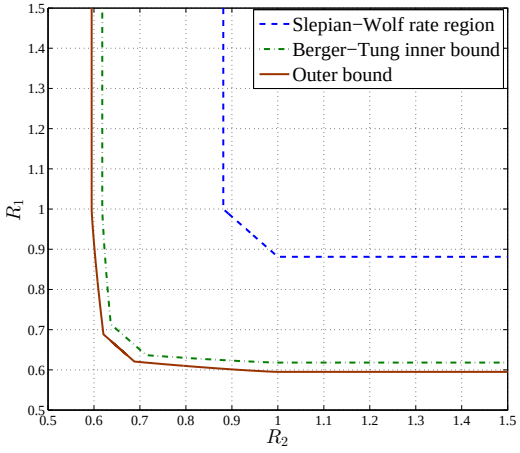

(d) $\rho = 0.3$**,** $D_1 = D_2 = 0.05$**.**

Figure 3.5: The comparison of $\mathscr{R}^{\mathbf{o}}(D_1, D_2)$, Berger-Tung inner bound and Slepian-Wolf admissible rate region.

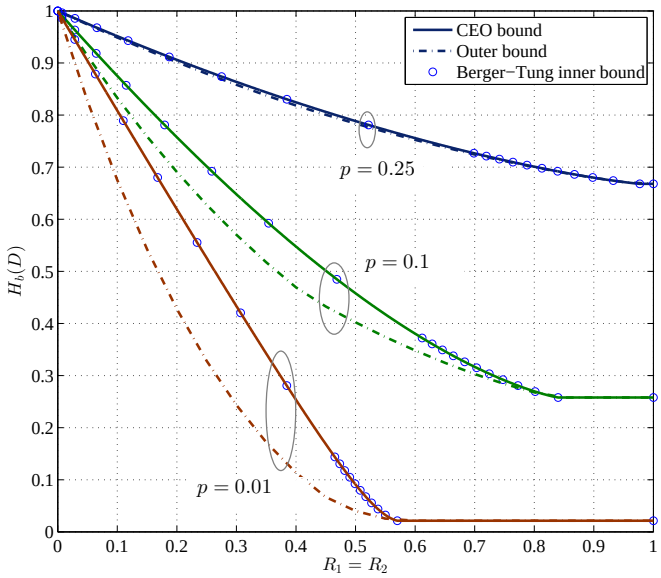

Figure 3.6: The comparison of two-step outer bound and Berger-Tung inner bound with optimal decision, and the direct outer bound of the binary CEO problem. We assume that $p = p_1 = p_2$ and $R_1 = R_2$.

Remark. *If the distortions D_1 and D_2 are required to be arbitrarily small, then $\mathscr{R}^o(D_1, D_2)$ reduces to the Slepian-Wolf rate region [SW73] for correlated binary sources if we set $D_1 \to 0$ and $D_2 \to 0$. The Slepian-Wolf rate region and $\mathscr{R}^o(D_1, D_2)$ are shown in Fig. 3.5. Obviously, it is found that by allowing nonzero distortion, the sources can be further compressed compared to the Slepian-Wolf lossless case.*

Remark. *If we are interested in reconstructing only one of the two sources, say X_1, and there is no rate limit on describing X_2^n, i.e., $R_2 \geq \frac{1}{n}H(X_2^n)$, then it is equivalent to the Wyner-Ziv compression problem [GK11]. Fig. 3.4 plots the rate-distortion bound $R_1^{WZ}(D_1)$ of the Wyner-Ziv source coding [WZ76] and our derived outer bound. In this case, $\mathscr{R}_1^o(D_1)$ is not tight, since it can be found from Fig. 3.4 that the rate-distortion region of the Wyner-Ziv problem lies inside of $\mathscr{R}_1^o(D_1)$.*

Remark. *In Fig. 3.5, the Berger-Tung inner bound for binary case $\mathscr{R}^i(D_1, D_2)$ is also presented as a reference to verify how close the bounds $\mathscr{R}^o(D_1, D_2)$ and $\mathscr{R}^i(D_1, D_2)$ are. It can be seen from the figure that they are very close to each other for small values of D_1 and D_2, i.e., the outer bound can be considered as a useful reference in the evaluation of the BER performance, even though there exists a small gap. The gap between the Berger-Tung inner bound and the derived outer bound is sensitive to both ρ and D_i. If ρ goes large and/or D_i small, the gap becomes relatively small. However, to resolve this gap, further insightful discussions are still needed as in Gaussian multiterminal source coding [Ooh97].*

Remark. *In Fig. 3.6, we compare three rate-distortion bounds for the binary CEO problem. As a reference, we directly derived the outer bound on the rate-distortion region for the two-node binary CEO problem, which is summarized in Appendix B. This outer bound is referred as direct outer bound. Our derived outer bound with optimal decision, which is stated in the next section, is not tight for the binary CEO problem. However, if the observation accuracy is low, let say, $p_1 = p_2 = 0.25$, the gap between the derived two-step outer bound and the direct outer bound is negligible. Furthermore, for large rate R_i, two bounds exactly match with each other. Hence, the derived outer bound is tight for relatively large p and/or R_i based on the results shown in Fig. 3.6, which is consistent with the above Remark. Also, it is interesting to find that the Berger-Tung inner bound with optimal decision coincides with the direct outer bound for any p_i. As a result, it is concluded that the binary CEO problem with two nodes is solved.*

3.4 Problem Formulation: Hamming Distortion Lower Bounds

3.4.1 Distortion Function

As stated in Section 3.2, distortion D is a function of distortions D_i, $i = 1,2$. Function $F_d(D_1,D_2)$ is obtained by evaluating the relationship between the binary CEO and the binary multiterminal source coding problems in terms of distortions, where the model of the relationship is shown in Fig. 3.7. The estimate $\hat{X}$ is obtained based on the decision rule from the outputs of two parallel BSCs with crossover probabilities $p_1 * D_1$, $p_2 * D_2$ and input X. The distortion D largely depends on the decision rule used by the destination. Here we only consider two decision rules. One is the soft combining decision and the other is the optimal decision.

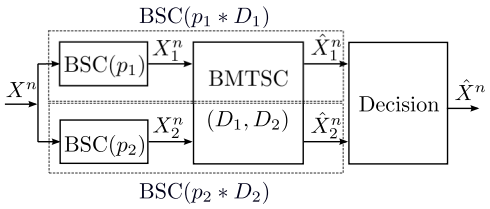

Figure 3.7: The relationship between the binary CEO and multiterminal source coding problems. BMTSC: binary multiterminal source coding.

3.4.1.1 Soft combining decision

Distortion D is obtained by evaluating the probability of an error event. Let $\theta_1 = p_1 * D_1$ and $\theta_2 = p_2 * D_2$. Without loss of generality, we assume that $\theta_1 \leq \theta_2$. Hence, the error event is composed of two independent events: node 1 makes a wrong decision and node 2 makes correct decision or both node 1 and node 2 make erroneous decisions. Therefore, the distortion D in this case is approximated by $D \cong \theta_1(1-\theta_2) + \theta_1\theta_2 = \theta_1$. It can be found that the corner point θ_1 or θ_2 in the rate-distortion region is achieved. Hence, the soft combining decision rule can be seen as being equivalent to that derived from the time sharing method.

3.4.1.2 Optimal decision

According to the rate-distortion theory for a binary source [CT06], the theoretical lower bound of the BEP floor is given in the following proposition.

Proposition 1 (Lower bound on BEP floor)**.** *Assume that a random variable $X \sim Bern(0.5)$, and X_i is the output variable of a BSC with crossover probability p_i, where $0 \leq p_i \leq \frac{1}{2}$. The minimum error probability of estimating X from X_i is given by*

$$p_{lb} = H_2^{-1}[1 + \sum_{i=1}^{L} H_2(p_i) - H(X_{\mathscr{L}})]. \tag{3.9}$$

Proof. According to the rate-distortion function for binary source [CT06], we have (3.10)

$$\begin{aligned}
1 - H_2(\tilde{d}) &\leq I(X;\hat{X}) && (3.10)\\
&\leq I(X;X_{\mathscr{L}}) && (3.11)\\
&= H(X) - H(X|X_{\mathscr{L}}) && (3.12)\\
&= 1 - H(X,X_{\mathscr{L}}) + H(X_{\mathscr{L}}) && (3.13)\\
&= 1 - \{H(X) + H(X_1|X) + \cdots + H(X_L|X)\} + H(X_{\mathscr{L}}) && (3.14)\\
&= 1 - \{1 + H_2(p_1) + \cdots + H_2(p_L)\} + H(X_{\mathscr{L}}), && (3.15)
\end{aligned}$$

where $\tilde{d}$ is a dummy variable, and the steps are justified as:
(3.11) there exists information loss in the process of obtaining $\hat{X}$ from $X_{\mathscr{L}}$,
(3.14) assume $X_i \to X \to (X_1,\cdots,X_{i-1},X_{i+1},\cdots,X_L)$ forms Markov chains, i.e., given X, X_i are independent to each other [GP79].

Thus, it is obvious from (3.15) that $\tilde{d} \geq H_2^{-1}[1+H_2(p_1)+\cdots+H_2(p_L)-H(X_{\mathscr{L}})]$. Therefore, the lower bound on the BEP floor p_{lb} in (3.9) is obtained by setting to the minimal value of $\tilde{d}$. □

Since the block length is assumed to be infinite and the code is random, an optimal lower bound on the distortion D is determined by applying **Proposition 1**, as

$$D = H_2^{-1}[H_2(\theta_1)+H_2(\theta_2)-H_2(\theta_1 * \theta_2)]. \tag{3.16}$$

It should be emphasized here that the optimal decision acts as a universal lower bound on the Hamming distortion for specific schemes which assume sequential decoding. However, in the design of practical encoding/decoding algorithms, we do not consider this decision rule.

In summary, the distortion level D of the two decision rules described above is given as

$$D = F_d(D_1,D_2) = \begin{cases} \min\{\theta_1,\theta_2\}, & \text{soft combining,} \\ H_2^{-1}[H_2(\theta_1)+H_2(\theta_2)-H_2(\theta_1*\theta_2)], & \text{optimal.} \end{cases} \tag{3.17}$$

3.4.2 Convex Optimization: Minimizing Distortion

By substituting the rate-distortion function (3.7) and (3.17) into the minimization problem (3.4), we have

$$\begin{aligned} \min_{D_1,D_2} \quad & D \\ \text{s.t.} \quad & \\ & H_2[\rho * H_2^{-1}(1-\tfrac{C(\gamma_2)}{r_2})]-H_2(D_1) \leq \frac{C(\gamma_1)}{r_1}, \\ & H_2[\rho * H_2^{-1}(1-\tfrac{C(\gamma_1)}{r_1})]-H_2(D_2) \leq \frac{C(\gamma_2)}{r_2}, \\ & 1+H_2(\rho)-H_2(D_1)-H_2(D_2) \leq \frac{C(\gamma_1)}{r_1}+\frac{C(\gamma_2)}{r_2}, \\ & D_i \leq \frac{1}{2}, \quad i=1,2, \\ & D_i \geq 0, \quad i=1,2. \end{aligned} \tag{3.18}$$

The reason of using the derived outer bound, not the Berger-Tung inner bound is that, the outer bound can be easily formulated as a convex optimization. The Berger-Tung inner bound includes term $D_1 * D_2$ in the binary entropy function which cannot be easily handled in the minimization. It is found that distortion $D = F_d(D_1,D_2)$ is monotonically increasing function on the intervals $D_i \in [0,\frac{1}{2}]$, $i=1,2$ for both the soft combining decision and optimal decision rules, and the proof is detailed in Appendix C. Furthermore, since the sequential decoding (first reconstructs $\mathbf{x}_1$ and $\mathbf{x}_2$, then makes decision on $\mathbf{x}$) is applied, we first minimize the ℓ_2-norm of a vector $[D_1,D_2]$

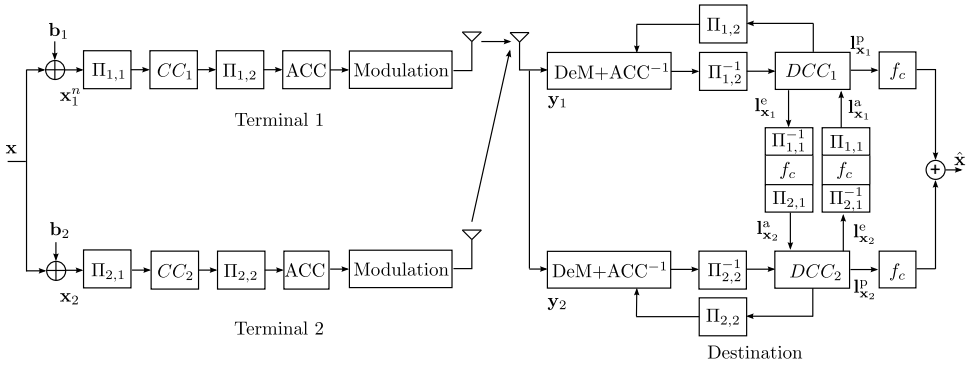

Figure 3.8: Block diagram of the encoding/decoding algorithm.

instead of directly minimizing D, as

$$\begin{aligned}
\min_{D_1,D_2} \quad & \|[D_1,D_2]\|_2 \qquad (3.19)\\
\text{s.t.} \quad & \\
-H_2(D_1)-H_2(D_2) &\le \frac{C(\gamma_1)}{r_1}+\frac{C(\gamma_2)}{r_2}-1-H_2(\rho),\\
-H_2(D_1) &\le \frac{C(\gamma_1)}{r_1}-H_2[\rho * H_2^{-1}(1-\frac{C(\gamma_2)}{r_2})],\\
-H_2(D_2) &\le \frac{C(\gamma_2)}{r_2}-H_2[\rho * H_2^{-1}(1-\frac{C(\gamma_1)}{r_1})],\\
D_i &\le \frac{1}{2}, \quad i=1,2,\\
-D_i &\le -0, \quad i=1,2,
\end{aligned}$$

to obtain the minimal values of D_1 and D_2, and then map them to D by using function $F_d(D_1,D_2)$.

It is easily found that the problem (3.19) is convex since the objective function is convex and function $-H_2(\cdot)$ is also convex. Therefore, it can be efficiently solved using convex optimization tools. Assume that the minimum values of D_1 and D_2 obtained through the convex optimization are denoted as $D_1^\star$ and $D_2^\star$, respectively. Substituting $D_1^\star$ and $D_2^\star$ into (3.17), the minimum distortion value $D^\star$ is then obtained through

$$D^\star = \begin{cases} \min\{\theta_1^\star,\theta_2^\star\}, & \text{soft combining},\\ H_2^{-1}[H_2(\theta_1^\star)+H_2(\theta_2^\star)-H_2(\theta_1^\star * \theta_2^\star)], & \text{optimal}, \end{cases} \qquad (3.20)$$

where $\theta_1^\star$ and $\theta_2^\star$ are $p_1 * D_1^\star$ and $p_2 * D_2^\star$, respectively. It should be emphasized here that the distortion D_1 or D_2 should be set to 0 in the optimization problem (3.18) if $\frac{C(\gamma_1)}{r_1}$ or $\frac{C(\gamma_2)}{r_2}$ is larger than or equal to 1, which is the binary entropy of the source X_1 and X_2. The reason is that a source can be reconstructed under an arbitrary small error probability if the source coding rate is larger than its entropy even in the case the helper does not exist [CT06].

3.5 Verification of Hamming Distortion Lower Bounds

3.5.1 Simulation Settings

We briefly explain the practical encoding/decoding algorithm [Zhou2012; Xin13CL] which is illustrated in Fig. 3.8. This algorithm is used to verify the theoretical Hamming distortion lower bounds. As illustrated in Fig. 3.8, each node encodes its erroneous sequence by using a serially concatenated memory-1 convolutional code and ACC. The encoder output sequences are then modulated and transmitted to the destination over statistically independent AWGN and block Rayleigh fading channels, where the channel gain h_i is static within each block but varies independently block-by-block. At the destination, iterative decoding process is carried out between the decoders of the convolutional code and the ACC, as well as between the two decoders of the convolutional codes through the LLR updating function f_c to modify the extrinsic LLR, according to the error probabilities p_1 and p_2.

Table 3.1: The settings of simulation parameters.

Parameter	Value
Block length n	10000 bits for AWGN and 2048 bits for fading
Block	1000 for AWGN and 10000 for fading
Interleavers	random
Encoder CC_i	Rate $1/2$, $G = (3,2)_8$, memory-1 nonrecursive systematic convolutional code
Doping ratio P_d	1
Modulation	BPSK and QPSK with natural mapping
Decoding Algorithm	log-maximum *a posteriori*
The number of iterations:	30

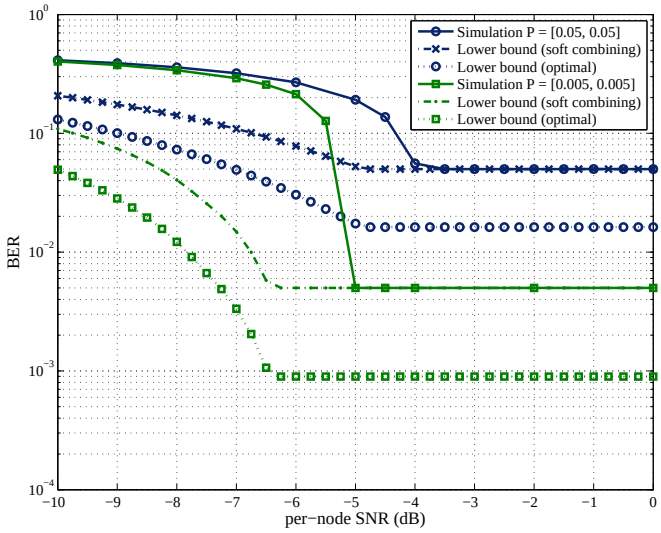

Figure 3.9: Symmetric P and SNR. BPSK is used for both nodes.

The lower bounds[4] on the Hamming distortion for different SNR values γ_1, γ_2 are obtained through solving the convex optimization problem which we presented in Section 3.4. The results are shown in Figs. 3.9–3.12 for AWGN channels and Fig. 3.13 for block Rayleigh fading channels. The common parameters used in conducting the simulations are shown in 3.1.

3.5.2 Numerical Results

Figure 3.9 shows the error probability lower bounds and the BER versus SNR when p_1, p_2 and SNRs of the two nodes are set identically; this is referred as the symmetric case. It can be found that, the BER curves obtained by simulations and the theoretical lower bounds on the Hamming distortion exhibit a similar tendency. The gap between the simulated BER and theoretical lower bound on Hamming distortion is caused by: (i) the derived outer bound is not tight, and thus smaller Hamming distortion is obtained for fixed rates; (ii) the Hamming distortion lower bound is obtained by assuming the optimal source coding rate is adopted based on separability, however, fixed coding rate is used in simulations.

Furthermore, it is clearly found that the error floor of the BER obtained by the simulation and the lower bound on the Hamming distortion based on soft combining match exactly. The reason is that if the SNRs of two nodes are large enough, the distortion levels D_1 and D_2 are almost 0, which results in the error floor being determined completely by the error probabilities p_1 and p_2. A gap clearly appears between the Hamming distortion lower bounds using the soft combining and optimal decision rules. The reason is twofold: 1) the optimality of the

[4]The terminology "lower bound" used here is due to the Hamming distortion is calculated based on the derived outer bound, even though the approximation of the objective functions is used.

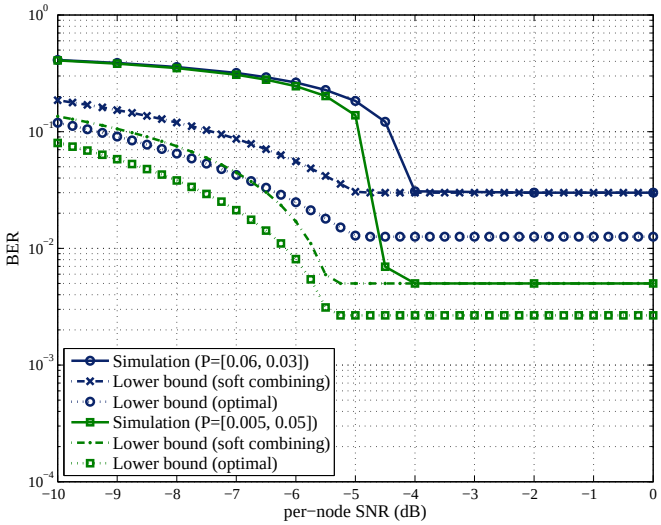

Figure 3.10: Asymmetric P and symmetric SNR. BPSK is used for both nodes.

soft combining cannot be guaranteed; 2) optimal decision is derived based on the assumption of the binary rate-distortion function without any loss during processing the information. To find a better decision rule than soft combining rule is left as a future study. However, it is clear that the Hamming distortion lower bound deriving from the optimal decision cannot be exceeded.

The impact of the variation of the error probabilities p_1, p_2 and the coding rates r_i are evaluated in AWGN channels. Fig. 3.10 shows the results for asymmetric p_1 and p_2 but symmetric SNRs. When the coding rates[5] r_1 and r_2 are set as $\frac{1}{4}$ and $\frac{1}{2}$, respectively, the BER performance shown in Fig. 3.11 is obtained. We further consider using different modulation schemes for the nodes to achieve different rates of the channel code in Fig. 3.12, where quadrature Phase Shift Keying (QPSK) is used for node 1 and BPSK for node 2. Even in these asymmetric cases, the theoretical lower bounds on the Hamming distortion can still provide us with a useful reference when we evaluate the BER performance of practical systems. Furthermore, the theoretical lower bounds on the Hamming distortion obtained based on our derived outer bound exhibit similar behaviors to those of the BER curves found by simulations.

In both the symmetric and asymmetric cases, the threshold SNR value at which turbo cliff in the BER obtained by the simulation is around 1.5 dB larger than that observed in the theoretical lower bounds in static AWGN channels. In addition, since the lower bounds on the Hamming distortion plateaus at a certain level even if the power is increased at high SNR regime, increasing the number of nodes is a proper way to improve performance in the practical deployment.

In Fig. 3.13, the channels between two nodes and the destination experience independent block Rayleigh fading. Therefore, the instantaneous SNRs of two nodes are different while the average SNRs of the two channels are the same. The lower bounds on the Hamming distortion shown in Fig. 3.13 are calculated as

$$D^{\star}_{\text{fading}} = \int_0^{+\infty} \int_0^{+\infty} D^{\star}(\gamma_1, \gamma_2) \cdot \Pr(\gamma_1) \cdot \Pr(\gamma_2) d\gamma_1 d\gamma_2, \tag{3.21}$$

where $D^{\star}(\gamma_1, \gamma_2)$ is the result of (3.20), obtained for static AWGN channels. $\Pr(\gamma_i)$ is the probability density function of the SNR γ_i, which follows the Rayleigh distribution. We use Monte Carlo method to obtain the lower bounds on the average Hamming distortion $D^{\star}_{\text{fading}}$ instead of theoretically calculating (3.21). In the Rayleigh fading case, the shape of the BER curves and the lower bounds on the Hamming distortion are almost the same. Two points need to be emphasized here. The analytical solution of (3.21) is difficult to find, because $D^{\star}(\gamma_1, \gamma_2)$ is obtained by solving the formulated convex optimization using *cvx* tool. The other point is that, the outage probability approaches 1 using the definition that the outage event happens when the package cannot *losslessly*

[5] We simply transmit the output of ACC without doping to achieve rate $\frac{1}{4}$. No optimized design of the channel code is considered.

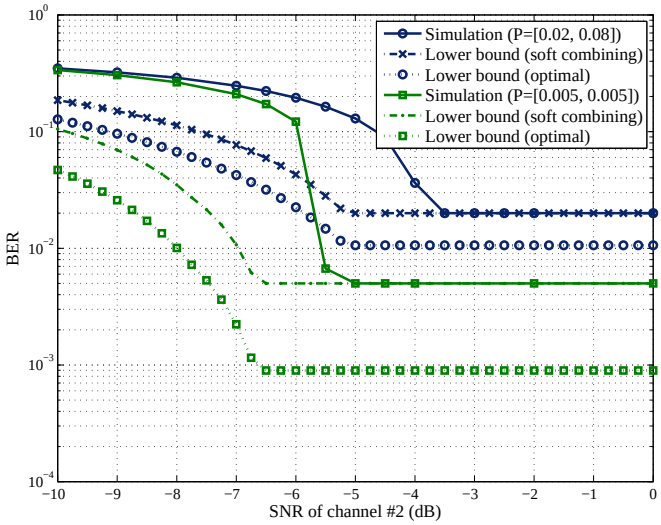

Figure 3.11: Asymmetric r_1 and r_2. The coding rates r_1 and r_2 are set at $\frac{1}{4}$ and $\frac{1}{2}$, respectively. The transmit power of two nodes is the same. BPSK is used for both nodes.

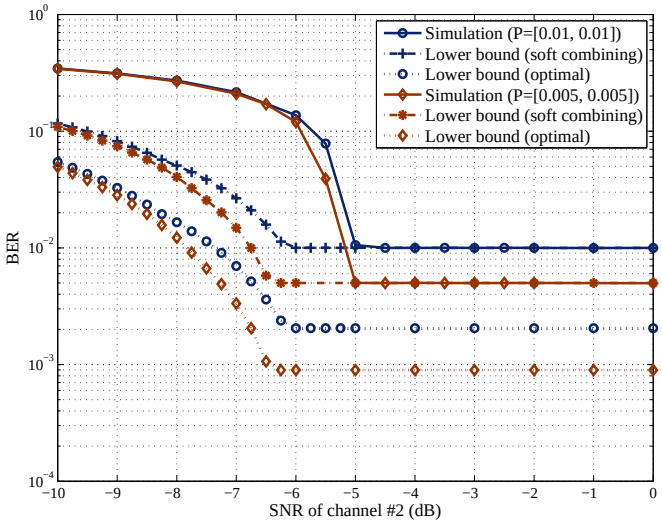

Figure 3.12: Asymmetric r_1 and r_2. The coding rates r_1 and r_2 are set at 1 and $\frac{1}{2}$, respectively. The transmit power of two nodes is the same. QPSK is used for node 1 and BPSK for node 2.

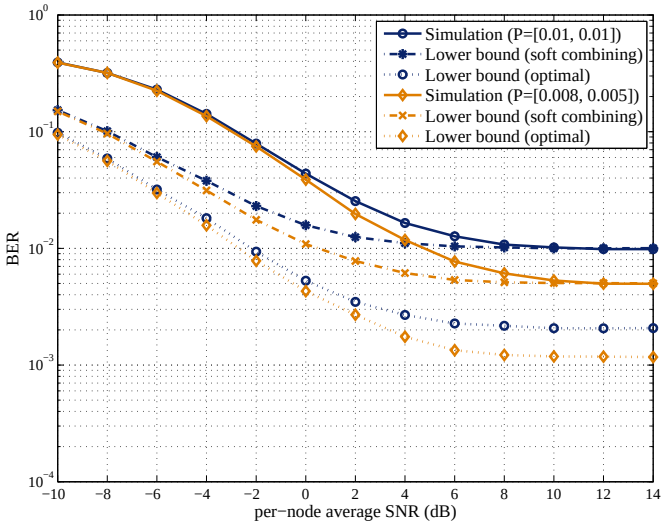

Figure 3.13: BER performances over Rayleigh fading channels. Both nodes use BPSK modulation.

recovered. Hence, the definition of outage should be changed in this case. We follow the method of using Slepian-Wolf theorem and separability to calculate the outage probability p_{out} for the situation that bit error floor is reached [ICT15, Section 4.2], where the definition of outage event is

$$\begin{cases} \text{Outage}, & D > \min\{p_1, p_2\} \\ \text{Success}, & \text{otherwise} \end{cases} \tag{3.22}$$

The detail of deriving p_{out} for two-node case is shown in Appendix E. We compare the theoretical outage probability p_{out} and the FER[6], where the results is shown in Fig. 3.14. The FER performance obtained by practical encoding/decoding algorithm are around $1 \sim 2$ dB in average SNR to the theoretical outage p_{out}.

3.6 Extension to Multiple Terminals

The outer bound on the rate-distortion region for $L = 2$ terminals is proved and discussed in detail. However, it is worth to show the possibility of extending the proposed solutions to the general binary CEO problem with an arbitrary number of terminals. In this section, the same approach where the rate-distortion region of the binary CEO problem is solved through establishing the relationship with the binary multiterminal source coding is applied to the general binary CEO problem.

3.6.1 Problem Statement

The binary multiterminal source coding which we consider is depicted in Fig. 3.15. Let the information sequence of source $X_i^n = \{x_i(t)\}_{t=1}^n$, $i = 1, 2, \cdots, L$, be binary i.i.d. It should emphasized here that X_i^n is generated from X^n through a BSC with crossover probability p_i in order to make connection with the binary CEO problem. Each encoder independently encodes the data sequences X_i^n with the coding rate R_i as

$$\varphi_i : \mathscr{X}^n \to \mathscr{M}_i = \{1, 2, \cdots, 2^{n \cdot R_i}\}, \tag{3.23}$$

where φ_i is the i-th encoder function. The encoder outputs $\varphi_i(X_i^n)$ are transmitted to a common receiver over noiseless channels. The common receiver jointly produces estimates $\hat{X}_i^n$ of the sources based on the received sequences from the agents as $\hat{X}_i^n = \psi[\varphi_1(X_1^n), \cdots, \varphi_L(X_L^n)]$, where ψ is the decoder function.

Let $d_i(x_i(t), \hat{x}_i(t))$ be the average Hamming distortion measure. For given positive numbers $D_i \in [0, 1/2]$, we define

[6]The frame is error if and only if $D > \min\{p_1, p_2\}$.

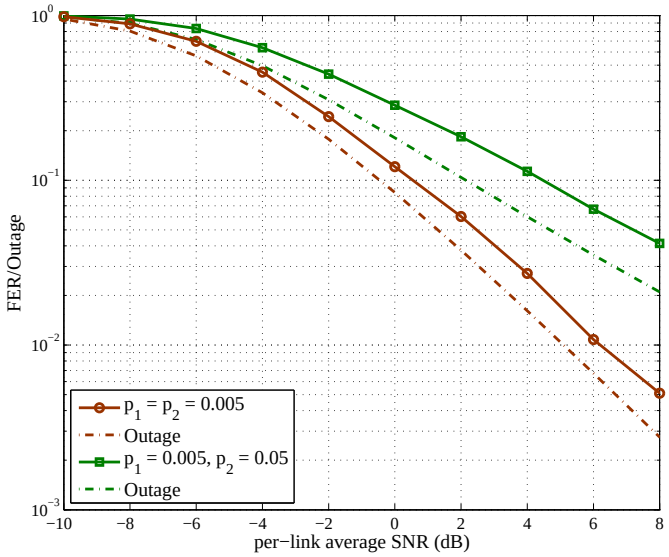

Figure 3.14: Comparison between FER and theoretical p_{out}.

the rate-distortion region $\mathscr{R}(D_{\mathscr{L}})$ as

$$\mathscr{R}(D_{\mathscr{L}}) = \{(R_{\mathscr{L}}) : (R_{\mathscr{L}}) \text{ is admissible such that } E\frac{1}{n}\sum_{t=1}^{n} d_i(x_i(t),\hat{X}_i(t)) \leq D_i + \varepsilon\},$$

where $\mathscr{L} = \{1,\cdots,L\}$, $R_{\mathscr{L}} = \{R_i | i \in \mathscr{L}\}$ and $D_{\mathscr{L}} = \{D_i | i \in \mathscr{L}\}$. We provide an outer bound $\mathscr{R}^{\text{o}}(D_{\mathscr{L}})$ for the rate-distortion region $\mathscr{R}(D_{\mathscr{L}})$ with the converse proof in the next section.

3.6.2 Rate-Distortion Region Analysis

Definition 1. $\mathscr{R}^{\text{o}}(D_{\mathscr{L}}) = \bigcap_{\mathscr{S}}\{\mathscr{R}^{\text{o}}_{\mathscr{S}}(D_{\mathscr{S}})\}$, $\forall \mathscr{S} \subseteq \mathscr{L}$ and $\mathscr{S} \neq \emptyset$, with

$$\mathscr{R}^{\text{o}}_{\mathscr{S}}(D_{\mathscr{S}}) = \Bigg\{(R_{\mathscr{S}}) : \forall R_j, j \in \mathscr{S}^c = \mathscr{L} \setminus \mathscr{S}, \sum_{i\in\mathscr{S}} R_i \geq h(\{p_{\mathscr{S}}, \alpha_{\mathscr{S}^c}\}) - h(\{\alpha_{\mathscr{S}^c}\}) - \sum_{i\in\mathscr{S}} H_2(D_i)\Bigg\}, \tag{3.24}$$

where

$$p_{\mathscr{S}} = \{p_i | i \in \mathscr{S}\}, \tag{3.25}$$
$$\alpha_{\mathscr{S}^c} = \{\alpha_j | j \in \mathscr{S}^c\}, \tag{3.26}$$
$$\alpha_j = p_j * H_2^{-1}(1 - [R_j]^-), \tag{3.27}$$

set $\mathscr{S}^c$ is the complementary set of $\mathscr{S}$ and $[a]^- = \min\{1, a\}$.

Theorem 2. $\mathscr{R}(D_{\mathscr{L}}) \subseteq \mathscr{R}^{o}(D_{\mathscr{L}})$.

3.6.2.1 Proof

Converse proof of 2. In order to easily present the proof of the outer bound, we take $L = 3$ as a basic example. Let $U_i = \varphi(X_i^n)$.

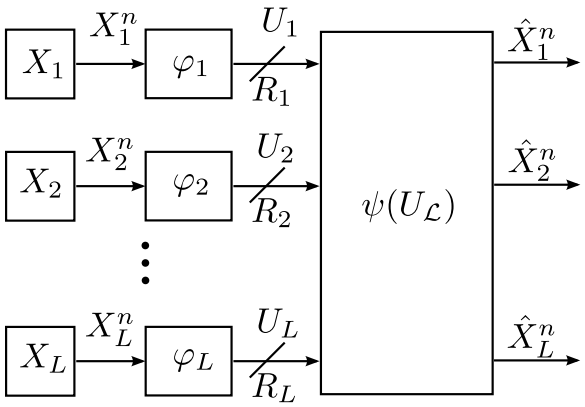

Figure 3.15: The binary multiterminal source coding problem for L correlated binary sources.

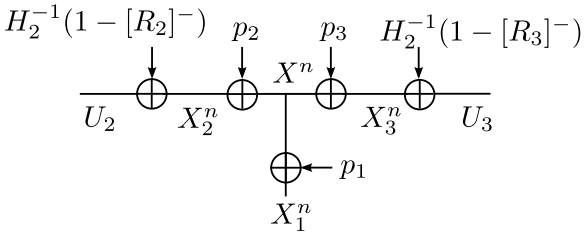

Figure 3.16: The test BSC model for proving the outer bound.

Case 1. $\mathscr{S} = \{1\}$ and $\mathscr{S}^c = \{2,3\}$. In this case, sources X_2^n and X_3^n operate as helpers for recovering X_1^n. The case belongs to the category of many-help-one problems in the network information theory. A specific two-help-one problem where the primary source, which the decoder wants to reproduce is the XOR version of two helpers was studied by Körner and Marton [KM79]. Furthermore, the many-help-one problem for correlated Gaussian sources was studied by Oohama [Ooh05] and Pandya *et al.* [Pan+04], respectively. Assume that D_1 is achieved by a rate triple (R_1, R_2, R_3), then the following equations hold:

$$\begin{aligned} n(R_1+\varepsilon) &\geq H(U_1) \\ &\geq H(U_1|U_2,U_3) && (3.28)\\ &= I(X_1^n;U_1|U_2,U_3) && (3.29)\\ &= I(X_1^n;U_1,U_2,U_3) - I(X_1^n;U_2,U_3) && (3.30)\\ &\geq I(X_1^n;\hat{X}_1^n) - I(X_1^n;U_2,U_3) && (3.31) \end{aligned}$$

where the steps are justified since
(3.28) conditioning reduces the entropy,
(3.29) U_1 is a function of X_1^n,
(3.30) the chain rule of mutual information,
(3.31) data processing inequality,

$$n(R_2+\varepsilon) \geq H(U_2) = I(X_2^n;U_2), \tag{3.32}$$

$$n(R_3+\varepsilon) \geq H(U_3) = I(X_3^n;U_3). \tag{3.33}$$

Now, we need to find the lower bound on the term $I(X_1^n;\hat{X}_1^n)$ and the upper bound on $I(X_1^n;U_2,U_3)$. As same as in $L=2$ case, the lower bound on $I(X_1^n;\hat{X}_1^n)$ is obtained by applying Fano's inequality

$$I(X_1^n;\hat{X}_1^n) \geq n - nH_2(D_1). \tag{3.34}$$

The upper bound on $I(X_1^n;U_2,U_3)$ is derived based on the test BSC model shown in Fig. 3.16 and inequalities (3.32), (3.33), as[7]

$$\begin{aligned} I(X_1^n;U_2,U_3) &= nH(X_1)+H(U_2,U_3)-H(X_1^n,U_2,U_3) \\ &\leq n+nh(\{\alpha_2,\alpha_3\})-nh(\{p_1,\alpha_2,\alpha_3\}), \end{aligned} \tag{3.35}$$

where (3.35) is obtained based on the fact that X_1^n, U_2 and U_3 are the outputs from a BSC or a cascade BSC channels when X^n is the input. By substituting (3.34) and (3.35) into (3.31) and letting ε go to 0, we conclude that

$$R_1 \geq h(\{p_1,\alpha_2,\alpha_3\})-h(\{\alpha_2,\alpha_3\})-H_2(D_1). \tag{3.36}$$

For the cases $\mathscr{S}=\{2\}$ and $\mathscr{S}=\{3\}$, the bounds can be obtained in the same way.

Case 2. $\mathscr{S}=\{1,2\}$ and $\mathscr{S}^c=\{3\}$. The source X_3^n acts as the helper to recover X_1^n and X_2^n. Gastpar derived the inner and outer bounds for the rate-distortion region of independently compressing two or more correlated sources with side information available at the decoder [Gas04]. In this case, except that (3.33) holds, the following inequalities also hold.

$$\begin{aligned} n(R_1 &+ R_2+\varepsilon) \geq H(U_1)+H(U_2) \\ &\geq H(U_1,U_2|U_3) \\ &= I(X_1^n,X_2^n;U_1,U_2|U_3) \\ &= I(X_1^n,X_2^n;U_1,U_2,U_3)-I(X_1^n,X_2^n;U_3) \\ &= I(X_1^n;U_1,U_2,U_3)+I(X_2^n;U_1,U_2,U_3|X_1^n)-I(X_1^n,X_2^n;U_3) \\ &\geq I(X_1^n;\hat{X}_1^n)+I(X_2^n;U_1,U_2,U_3,X_1^n) \\ &- I(X_1^n;X_2^n)-I(X_1^n;U_3)-I(X_2^n;U_3|X_1^n) \qquad (3.37) \\ &\geq I(X_1^n;\hat{X}_1^n)+I(X_2^n;\hat{X}_2^n) \\ &- I(X_1^n;X_2^n)-I(X_1^n;U_3)-I(X_2^n;U_3,X_1^n)+I(X_1^n;X_2^n) \\ &\geq H(X_1^n,X_2^n,U_3)-H(U_3)-n[H_2(D_1)+H_2(D_2)] \qquad (3.38) \\ &\geq n[h(\{p_1,p_2,\alpha_3\})-h(\{\alpha_3\})-H_2(D_1)-H_2(D_2)] \qquad (3.39) \end{aligned}$$

where (3.37) holds because the chain rule of mutual information and data processing inequality, (3.38) follows from several steps of elementary calculation, and (3.39) is obtained based on the same test BSC model which is shown in Fig. 3.16.

By letting ε go to 0, it is concluded that $R_1+R_2 \geq h(\{p_1,p_2,\alpha_3\})-h(\{\alpha_3\})-H_2(D_1)-H_2(D_2)$. The other two similar cases with $\mathscr{S}=\{1,3\}$ and $\mathscr{S}=\{2,3\}$ can be followed the same derivation which is shown above.

Case 3. $\mathscr{S}=\{1,2,3\}$ and $\mathscr{S}^c=\emptyset$. Assume that a rate triple (R_1,R_2,R_3) achieves the required distortions D_1, D_2 and D_3, we have the following inequalities.

$$\begin{aligned} n(R_1+R_2 &+ R_3+\varepsilon) \geq H(U_1)+H(U_2)+H(U_3) \\ &\geq H(U_1,U_2,U_3) \\ &= I(X_1^n,X_2^n,X_3^n;U_1,U_2,U_3) \\ &= I(X_1^n;U_1,U_2,U_3)+I(X_2^n,X_3^n;U_1,U_2,U_3|X_1^n) \\ &\geq I(X_1^n;\hat{X}_1^n)+I(X_2^n,X_3^n;U_1,U_2,U_3,X_1^n)-I(X_2^n,X_3^n;X_1^n) \\ &\geq I(X_1^n;\hat{X}_1^n)+I(X_2^n;U_1,U_2,U_3,X_1^n)+I(X_3^n;U_1,U_2,U_3,X_1^n|X_2^n)-I(X_2^n,X_3^n;X_1^n) \\ &\geq I(X_1^n;\hat{X}_1^n)+I(X_2^n;\hat{X}_2^n)+I(X_3^n;\hat{X}_3^n)-I(X_3^n;X_2^n)-I(X_2^n,X_3^n;X_1^n) \\ &= nh(\{p_1,p_2,p_3\})-n\sum_{i=1}^{3}H_2(D_i). \end{aligned} \tag{3.40}$$

[7] Inspired by the MGL, we establish the test BSC model to bound the mutual information. However, this bound may exist a gap to the global optimal bound. The validation of the global optimality is left as a future study. Indeed, the bound derived from the current setup can still serve as a useful reference in the power allocation and scheduling of WSNs. Some further discussions on this issue are provided in subsection 3.6.4.

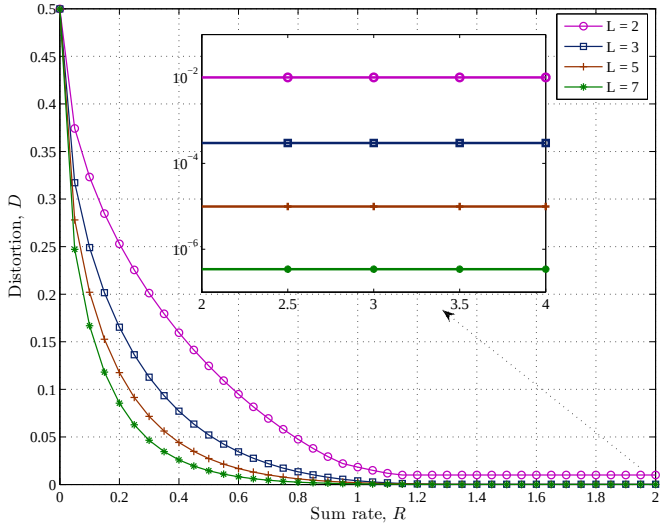

Figure 3.17: Sum rate versus distortion. The rate is equally allocated to each link. The observation error probabilities are set to 0.01**.**

The derivation of above inequalities can be straightforwardly extended to the general case having an arbitrary number of sources. In summary, we conclude that

$$\sum_{i\in\mathscr{S}} R_i \geq h(\{p_{\mathscr{S}}, \alpha_{\mathscr{S}^c}\}) - h(\{\alpha_{\mathscr{S}^c}\}) - \sum_{i\in\mathscr{S}} H_2(D_i). \tag{3.41}$$

Hence, we can conclude that $\mathscr{R}(D_{\mathscr{L}}) \subseteq \mathscr{R}^{\mathrm{o}}(D_{\mathscr{L}})$. □

Remark. *The outer bound $\mathscr{R}^{o}(D_{\mathscr{L}})$ for the rate-distortion region is a convex hull of a set of rate tuples.*

Remark. *If all the distortion levels $D_{\mathscr{L}}$ approach to* 0*, the outer bound $\mathscr{R}^{o}(D_{\mathscr{L}})$ coincides with the Slepian-Wolf theorem with multiple correlated sources [Cov75; GK11].*

Remark. *Consider the case two agents observe the same source X, i.e., $L = 2$. In this case, since $h(\cdot)$ has a very simple form, we can obtain the following rate-distortion inequalities by substituting p_i and D_i into the outer bound expression*

$$\begin{cases} R_1(D_1) \geq H_2(p_1 * \alpha_2) - H_2(D_1), \\ R_2(D_2) \geq H_2(p_2 * \alpha_1) - H_2(D_2), \\ \sum_{i=1}^{2} R_i(D_i) \geq 1 + H_2(p_1 * p_2) - \sum_{i=1}^{2} H_2(D_i), \end{cases} \tag{3.42}$$

which is consistent with the results shown in $L = 2$ case.

3.6.3 Sum Rate versus Distortion

The distortion level D is examined with respect to the sum rate R, giving fixed values of L and the observation error probabilities p_i. The results of D versus R are shown in Fig. 3.17 with different L. The distortion D is the result of

$$D = \mathrm{PB}(p_{\mathscr{L}} * D^{\star}_{\mathscr{L}}), \tag{3.43}$$

where $p_{\mathscr{L}} * D^{\star}_{\mathscr{L}} = \{p_1 * D^{\star}_1, \cdots, p_L * D^{\star}_L\}$ and $D^{\star}_{\mathscr{L}} = \{D^{\star}_i | i \in \mathscr{L}\}$ is given by

$$\begin{aligned} D^{\star}_i \quad &= \arg\min \quad \|[D_1, \cdots, D_L]\|_2 \\ &\text{s.t.} \quad \begin{cases} \sum_{i\in\mathscr{S}} H_2(D_i) \geq h(\{p_{\mathscr{S}}, \alpha_{\mathscr{S}^c}\}) - h(\{\alpha_{\mathscr{S}^c}\}) - \sum_{i\in\mathscr{S}} \frac{R}{L}, \\ 0 \leq D_i \leq 0.5, \qquad i \in \mathscr{L} \end{cases} \end{aligned} \tag{3.44}$$

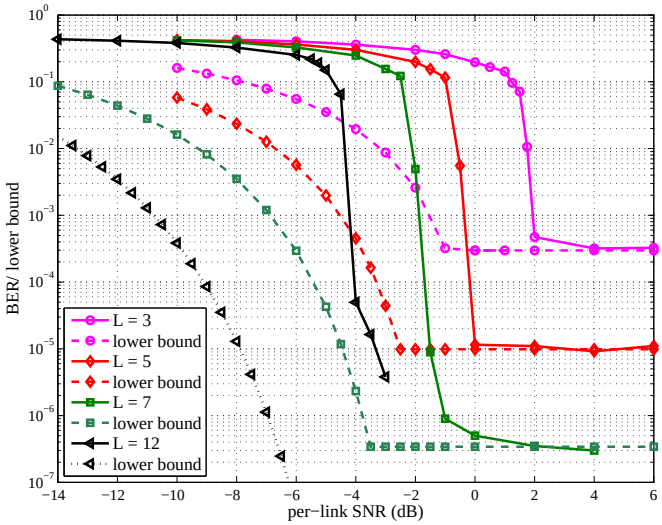

Figure 3.18: Simulation results verify the lower bounds on Hamming distortion using 16QAM and identical p_i.

and $\mathrm{PB}(\cdot)$ calculated the error probability based on the Poisson binomial process.

It should be emphasized here that the sum rate R is equally allocated to each link without considering any optimal rate allocation scheme. It can be seen from the figure that, D becomes small, if the number of links L increased and/or the sum rate R is large. However, D converges to a certain level (not equal to 0) even we increase R which is very clear in the enlarged view. The certain level is given by $\mathrm{PB}(p_{\mathscr{L}})$ by assuming the distortions D_i asymptotically approach 0. Furthermore, this level also decreased when the number of agents increases.

3.6.4 Brief Discussions of using test BSC

In the proof of the outer bound, there is an important step of bounding the mutual information term $I(X_1^n;U_2,\cdots,U_L)$ using the test BSCs. In other words, the cardinality bound on $\mathscr{U}_i$ is assumed to be 2. In [Jan09], Soumya gave a proof of reducing the cardinality bound of auxiliary RV U_i in multiterminal source coding problem. It is found that the cardinality bound can be reduced as $|\mathscr{U}_i| \leq |\mathscr{X}_i|$. Applying the result in our specified binary Hamming case, it is reasonable to set the cardinality bound $|\mathscr{U}_i|$ to 2.

Besides this, the further discussion is needed for whether it is optimal to use BSC to lower bound the conditional entropy terms, such as $H(X_1^n|U_2,U_3)$. Inspired by the proof of MGL, we use the BSC as the test channel in the derivation. However, the extension of MGL to this general setup still needs some efforts. Hence, the outer bound on the rate-distortion region is only an approximation.

3.6.5 Numerical Results

A series of simulations are performed to verify the Hamming distortion lower bound that obtained by solving the following convex optimization problem

$$\begin{aligned} \min \quad & \|[D_1,\cdots,D_L]\|_2 \\ \text{s.t.} \quad & \begin{cases} -\sum\limits_{i\in\mathscr{S}} H_2(D_i) \leq \sum\limits_{i\in\mathscr{S}} \frac{C(\gamma_i)}{r_i} - h(\{p_{\mathscr{S}},\alpha_{\mathscr{S}^c}\}) + h(\{\alpha_{\mathscr{S}^c}\}), \\ 0 \leq D_i \leq 0.5, \qquad i\in\mathscr{L} \end{cases} \end{aligned} \tag{3.45}$$

and mapping the minimal values to D using Poisson binomial process.

Figure 3.18 shows the simulation results and their corresponding Hamming distortion lower bounds for identical p_i. As we can see from the figure that, the Hamming distortion lower bounds and the simulation results have

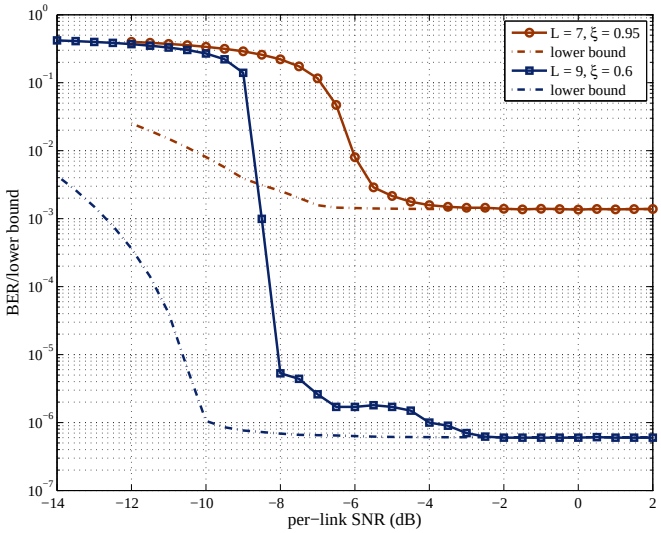

Figure 3.19: Simulation results verify the lower bounds on Hamming distortion using BPSK and logarithmic distributed p_i.

very similar tendency. However, if L goes large, the difference between the simulation results and the theoretical bounds also becomes significant. The reason is that the theoretical bounds are obtained by assuming the capacity-achieving code is used at each sensor node. To further analyze the impact of p_i variation, Fig. 3.19 shows the BER performance using the obtained p_i from logarithmic distribution. Their Hamming distortion lower bounds also presents as references. Note that in these cases, the Hamming distortion bound on D is obtained using soft combining (Appendix F) after the minimal distortions D_i of each link are available. From the simulations results, it concludes that the impact of p_i variation to the bound analysis is not significant.

Furthermore, the superiority of performing global iteration in decoding process is proved through the theoretical analysis. It is found that from Fig. 3.20, the performance gain in AWGN channels is around 5 dB for $L = 4$ and 8.5 dB for $L = 12$, respectively. Simulation results using the proposed encoding/decoding algorithm also confirm the gain. The Hamming distortion lower bound for the case global iteration is not performed is given by

$$D^{\text{noGI}} = \text{PB}(\{p_1 * H_2^{-1}(1-[C(\gamma_1)]^-), \cdots, p_L * H_2^{-1}(1-[C(\gamma_L)]^-)\}). \tag{3.46}$$

In other words, D^{noGI} is the result of solving the following convex optimization problem.

$$D^{\text{noGI}} = \text{PB}(p_{\mathscr{L}} * D_{\mathscr{L}}^{noGI\star}), \tag{3.47}$$

where $p_{\mathscr{L}} * D_{\mathscr{L}}^{noGI\star} = \{p_1 * D_1^{noGI\star}, \cdots, p_L * D_L^{noGI\star}\}$ and $D_{\mathscr{L}}^{noGI\star} = \{D_i^{noGI\star} | i \in \mathscr{L}\}$ is given by

$$\begin{aligned} \min \quad & \|[D_1, \cdots, D_L]\|_2 \\ \text{s.t.} \quad & \begin{cases} -\sum\limits_{i\in\mathscr{S}} H_2(D_i) \le \sum\limits_{i\in\mathscr{S}} \frac{C(\gamma_i)}{r_i} - |\mathscr{S}|, \\ 0 \le D_i \le 0.5, \qquad i \in \mathscr{L} \end{cases} \end{aligned} \tag{3.48}$$

Comparing the constraints of (3.45) and (3.48), it is obviously found that $|\mathscr{S}| \ge h(\{p_{\mathscr{S}}, \alpha_{\mathscr{S}^c}\}) - h(\{\alpha_{\mathscr{S}^c}\})$ with equality holding if and only if $p_i = 0.5$. Hence, the Hamming distortion lower bound D^{noGI} is greater than D.

3.7 Conclusion

We examined theoretically the lower bound on the Hamming distortion for the binary information sensing network modelled by the binary CEO problem, where several independent terminals forward the erroneous versions of a common binary source to the destination over static AWGN and block Rayleigh fading channels.

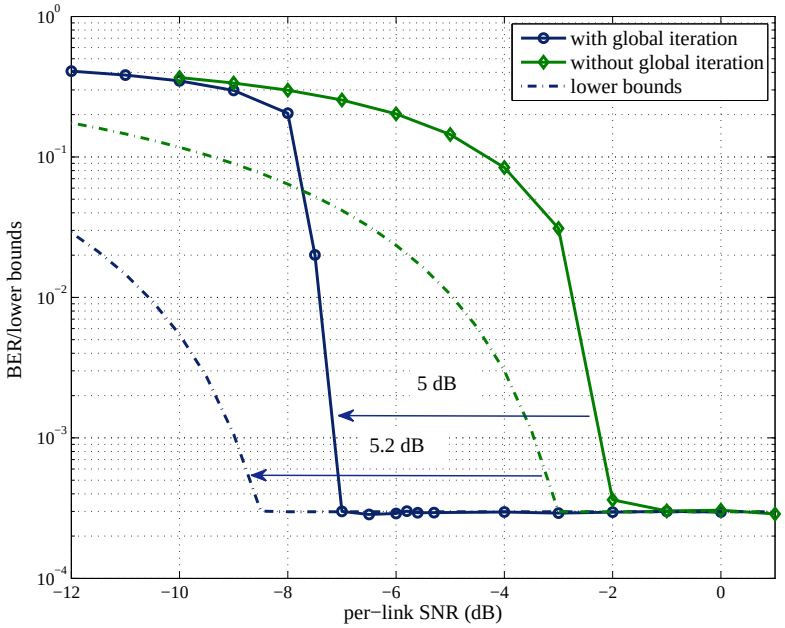

(a) $L = 4$, $p_i = 0.01$.

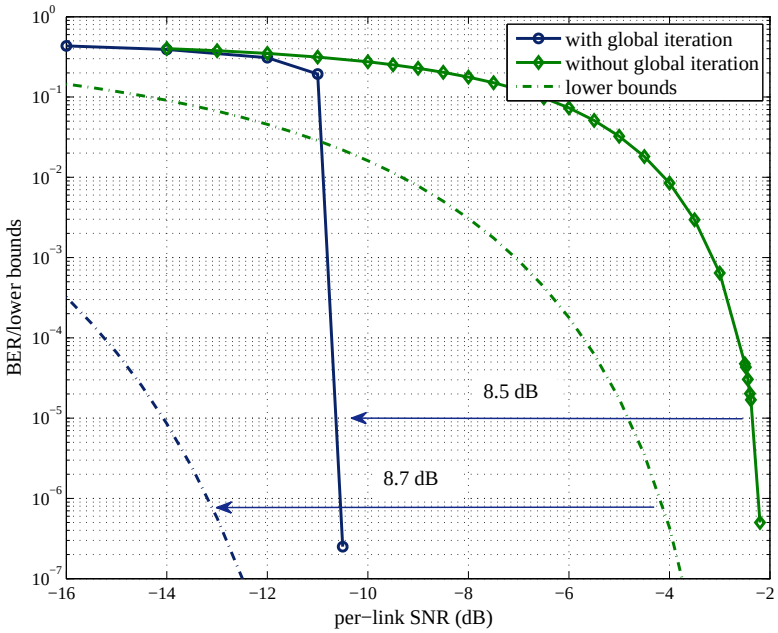

(b) $L = 12$, $p_i = 0.01$.

Figure 3.20: Comparison on theoretical Hamming distortion lower bounds by assuming whether correlation is utilized through *global iteration*.

We first considered a simple case that the number of terminals is 2. The binary CEO problem was first formulated as the binary multiterminal source coding problem, which is the core part of the binary CEO problem. The outer bound on the rate-distortion region for the binary multiterminal source coding problem was then derived based on the converse proof of the bound. The relationship between the binary CEO problem and the binary multiterminal source coding problem in terms of the distortion function has been established. According to the lossy source-channel separation theorem, the lower bound on the Hamming distortion was formulated by minimizing the distortion function subject to the inequalities between the derived outer bound and the channel capacities. The problem of obtaining the lower bound on the Hamming distortion was solved in the framework of convex optimization, and the results of Hamming distortion lower bounds only apply to schemes which use sequential decoding. Through a series of simulations, it has been shown that the BER curves obtained with a practical encoding/decoding algorithm is consistent with the result of the theoretical lower bounds on the Hamming distortion.

We further extended discussions to the binary CEO problem having arbitrary number of terminals. An approximated outer bound was derived through the converse coding proof. The outer bound on the rate-distortion region was used to obtain the theoretical lower bound on the Hamming distortion for the general binary information sensing network as the case of two terminals. Finally, we simply discussed the superiority of our proposed decoding algorithm from the rate-distortion perspective.

4. Performance Analysis of TS3

4.1 System Model

4.1.1 DF-IE System

We consider a half-duplex relay system, where one source (S) and multiple relays (F_i) cooperate to transmit to one destination (D) as shown in Fig. 4.1. To ensure orthogonal transmission,TDMA is assumed. An i.i.d binary information sequence[1] B_0 is originated by S with uniform probabilities $\Pr[B_0 = 0] = \Pr[B_0 = 1] = 0.5$. The source information sequence is encoded, modulated and broadcasted to F_i and D. Each F_i decodes the received source information sequence. The decoded information sequences B_i can differ from the source information sequence depending on the channel states between S and F_i, associated with the intra-link error probability $p_i = \Pr[B_i \neq B_0]$, [Zho+14]. The information sequences at the relays are interleaved, re-encoded and forwarded to D. All received information sequences B_0 and B_i are jointly decoded at D to retrieve B_0. The joint decoder can exploit the correlation of the information sequences and achieves tremendous performance gain in terms of the estimated source information sequence $\hat{B}_0$, [AM12b]. In literature, the decode-and-forward relaying allowing intra-link errors (DF-IE) system is also referred to as source coding with side information, [XLC04].

4.1.2 Channel Model

All channels are affected by flat Rayleigh fading (RF) and additive white Gaussian noise with mean power N_0. The PDF of the instantaneous received SNR Γ_i is exponentially distributed, thus given by

$$f_{\Gamma_i}(\gamma_i) = \frac{1}{\bar{\Gamma}_i} \exp(-\frac{\gamma_i}{\bar{\Gamma}_i}), \tag{4.1}$$

where $\bar{\Gamma}_i$ is the average SNR between S and D or F_i

$$\bar{\Gamma}_i = \frac{P_0}{N_0} \cdot d_i^{-\eta}, i \in \{0,1,2,...N\}, \tag{4.2}$$

and average SNR $\bar{\Gamma}_{2\cdot i}$ between F_i and D

$$\bar{\Gamma}_{2\cdot i} = \frac{P_i}{N_0} \cdot d_{2\cdot i}^{-\eta}, i \in \{1,2,...N\}, \tag{4.3}$$

with transmit power P_0 and P_i at S and F_i, respectively, distance d_i between S and F_i, D or F_i and D, and path loss exponent η.

4.2 Preliminaries

In this section, we define the relation between intra-link error probability and instantaneous received SNR.

4.2.1 Intra-Link Error Probability

With the RF assumption, the intra-link error probability p_i is constant over one frame, but varies transmission-by-transmission. As shown in [Zho+14] the intra-link error probability can be related to the instantaneous received SNR by

$$p_i(\gamma_i) = \begin{cases} H^{-1}\left(1 - \Phi(\Gamma_i)\right), & \text{for } \Phi^{-1}(0) \leq \Gamma_i \leq \Phi^{-1}(1) \\ 0, & \text{for } \Gamma_i \geq \Phi^{-1}(1) \end{cases} \tag{4.4}$$

based on Shannon's lossy source-channel separation theorem [CT06]. With $\Phi(\Gamma_i) = \frac{1}{R_c}\log_2(1+\Gamma_i)$, and $\Phi^{-1}(\cdot)$ is the inverse function of $\Phi(\cdot)$. The inverse function values of interest are $\Phi^{-1}(0) = 0$ and $\Phi^{-1}(1) = 2^{R_c} - 1$. The spectrum efficiency $R_c = R_{\text{cod}} \cdot R_{\text{M}}$ includes channel coding rate and modulation multiplicity. To simplify calculations, R_c is assumed to be the same for all channels. $H^{-1}(\cdot)$ is the inverse function of the binary entropy function $H(x) = -x\log_2(x) - (1-x)\log_2(1-x)$.

[1] In order to alleviate the notation, we shall drop the time index when denoting information and error sequences.

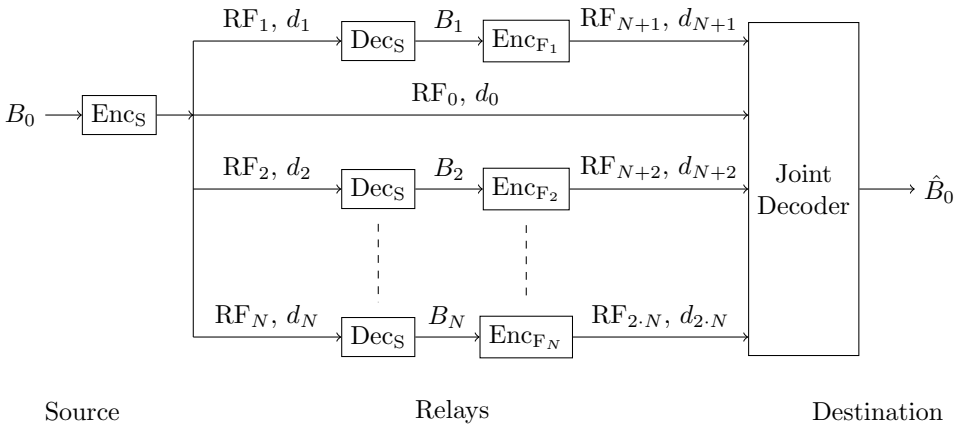

Figure 4.1: System model.

4.2.2 Slepian-Wolf Theorem

Slepian-Wolf's correlated source coding theorem states that correlation among information sequences can be exploit at the destination with distributed source coding. Iff all transmission rates R_i, measured in bits per channel use, satisfy the inequality constraints [SW73]

$$\sum_{i\in\mathscr{S}} R_i \geq H\left(\{B_i|i\in\mathscr{S}\}|\{B_j|j\in\mathscr{S}^c\}\right), \tag{4.5}$$

then all relay information sequences $B_0, B_1, \ldots, B_N$ can be recovered error-free. With set $\mathscr{S}\hat{=}\{X \mid X\subseteq\mathscr{N}_0\}$ with $\mathscr{N}_0=\{0,1,\ldots,N\}$ and $\mathscr{S}^c$ denoting the complement of $\mathscr{S}$. In literature, all sets of $N+1$-tuples $\{(R_0,R_1,...,R_N)\}$ that satisfy all constraints in (4.5) are also known as Slepian-Wolf's admissible rate region $\mathscr{R}_{\text{SW}}$.

4.3 Outage Probability

In this section, we define the DF-IE admissible rate region and establish the outage probability with N Relays. Furthermore, we carry out the mathematical calculation deploying one and two relays.

4.3.1 DF-IE Admissible Rate Region

The Slepian-Wolf theorem is well known for lossless transmission of correlated sources. Unlike the theorem for source coding with side information, the Slepian-Wolf theorem provides the admissible rate region required to recover all correlated sources. As shown in [Zho+14] the DF-IE admissible rate region with one relay can be approximated by a modified Slepian-Wolf admissible rate region. In this study, the DF-IE admissible rate region is extended to a DF-IE system with N relays. Iff all transmission rates R_i satisfy the inequality constraints

$$\sum_{i\in\mathscr{S}_0} R_i \geq H\left(\{B_i|i\in\mathscr{S}_0\}|\{B_j|j\in\mathscr{S}_0^c\}\right) \tag{4.6}$$

or

$$R_0 \geq H(B_0)=1, \tag{4.7}$$

than the source information sequence B_0 can be recovered error-free. With set $\mathscr{S}_0\hat{=}\{0\cup X \mid X\subseteq\mathscr{N}\}$ with $\mathscr{N}=\{1,\ldots,N\}$ and complement set $\mathscr{S}_0^c$ of $\mathscr{S}_0$. All sets of $N+1$-tuples $\{(R_0,R_1,...,R_N)\}$ that satisfy all constraints in (4.6) or (4.7) are the DF-IE's admissible rate region denoted with $\mathscr{R}_{\text{DF-IE}}$.

4.3.2 Outage Probability Based on $\mathscr{R}_{\text{DF-IE}}$ with N Relays

If the set of $N+1$-tuples $\{R_0,R_1,...,R_N\}$ fall outside the DF-IE admissible rate region $\mathscr{R}_{\text{DF-IE}}$ a system outage occurs. All RF channels are assumed to be i.i.d., i.e. $f_{\Gamma_1,\Gamma_2,...,\Gamma_N}(\gamma_1,\gamma_2,...,\gamma_N)=\prod_{i=1}^{N} f_{\Gamma_i}(\gamma_i)$ and with the defined

limits in (4.6) and (4.7) the outage probability can be established with

$$P_{\text{out},N} = \Pr\left[\{R_i \mid i \in \mathscr{S}_0\} \notin \mathscr{R}_{\text{DF-IE}}, \{0 \le p_j \le 0.5 \mid j \in \mathscr{S}_{\bar{0}}\}\right], \tag{4.8}$$

with set $\mathscr{S}_{\bar{0}} \hat{=} \{X \mid X \subseteq \mathscr{N}\}$. The intra-link error probability exhibits two functional domanions (4.4), consequently a case distinction is required. Hence, the outage probability is calculated by

$$= \sum_{\{p_j\} \in \mathscr{P}^{|\mathscr{S}_{\bar{0}}|}} \Pr\left[\{R_i \mid i \in \mathscr{S}_0\} \notin \mathscr{R}_{\text{DF-IE}}, \{p_j\}\right], \tag{4.9}$$

including all case distictions

$$\mathscr{P}^{|\mathscr{S}_{\bar{0}}|} = \left\{ \bigtimes_{i \in \mathscr{S}_{\bar{0}}} \mathscr{P}_i \;\middle|\; \mathscr{P}_i \in \{\{0\}, (0, 0.5]\} \right\}. \tag{4.10}$$

4.4 Outage Probability Upper Bound

In the section we derive the outage probability upper bound in four steps: (i) we reduce the set of rate constrains with the assumption of high-SNR, i.e. asymptotic analysis of outage probability, (ii) we relax the rate constraint with an upper bound for the conditional entropy, (iii) we transform these relaxed rate constraints into SNR constraints, and (iv) we calculate the outage probability upper bound for DF-IE system deploying up to four relays[2].

4.4.1 Reduction of rate constraints

We begin by decomposing the outage probability into two probability terms, for convenience, as shall become apparent soon. The first term, $P_{\text{out,a},N}$, is the probability for the violation of the loosens constrain[3] in (4.6), depending on case distinction $\mathscr{P}^{|\mathscr{S}_{\bar{0}}|}$ in (4.10) by

$$P_{\text{out,a},N} = \sum_{\{p_j\} \in \mathscr{P}^{|\mathscr{S}_{\bar{0}}|}} \Pr\left[\{R_i \mid i \in \mathscr{S}_0^{\text{sub}}\} \notin \mathscr{R}_{\text{DF-IE}}^{\text{sub}}, \{p_j\}\right], \tag{4.11}$$

where $\mathscr{S}_0^{\text{sub}}$ represent the subset of rates included in the loosens constraint and $\mathscr{R}_{\text{DF-IE}}^{\text{sub}}$ defines the subset of DF-IE admissible rate region respectively. All other rates do not have constraints. Because a subset of the rate constraints in (4.6) have being ignored in (4.11), the latter does not include all possible outage events, so that

$$P_{\text{out},N} = P_{\text{out,a},N} + \varepsilon \tag{4.12}$$

where the term ε accounts for those additional outage events. Interestingly, it turns out that, as the SNR increases, ε goes faster to zero than $P_{\text{out,a},N}$, playing no role at high-SNR. Indeed, as shown in [WG03] under a different context, the asymptotic outage behavior of a transmission link depends exclusively on the SNR distribution in the vicinity of the origin. In our case, we have an $N+1$-variate rate (or SNR, equivalently) distribution, so that it suffices to cover the probability masses in the vicinity of the $N+1$ coordinate axes. Notice that this is fulfilled in (4.11). Therefore, $P_{\text{out,a},N}$ is the asymptotic outage probability.

4.4.2 Relaxed rate constraint

The loosens constraints in (4.6) entail conditional entropies. Consequently, the conditional entropies are included in the integral bound of the asymptotic outage probability in (4.11). The conditional entropies is a non-linear

[2]Note, that the upper bound outage probability is presented in [Wol+15] deploying up to two relays, but only for a concrete realisation of the code rate and modulation scheme, $R_c = 1$.

[3]The loosens constrain defines the largest rate region among all constraints in (4.6).

function of the received SNR and contains binary convolution, entropy function and inverse entropy function.

$$H\left(\{B_i|i\in\mathscr{S}_0\}|\{B_j|j\in\mathscr{S}_0^c\}\right)=\sum_{j_1\in\mathscr{S}_0^c}H(p_{j_1})-\sum_{\{j_1,j_2\}\in\mathscr{S}_0^c}H(p_{j_1}*p_{j_2})+\sum_{\{j_1,j_2,j_3\}\in\mathscr{S}_0^c}H(p_{j_1}*p_{j_2}*p_{j_3})-\ldots\pm\sum_{\{j_1,\ldots,j_{|\mathscr{S}_0^c|}\}\in\mathscr{S}_0^c}H(p_{j_1}*\ldots*p_{j_{j_{|\mathscr{S}_0^c|}}}) \tag{4.13}$$

Unfortunately, (4.11) cannot be solved analytically. However, a upper bound for the conditional entropies exist by

$$\sum_{j_1\in\mathscr{S}_0^c}H(p_{j_1})-\sum_{\{j_1,j_2\}\in\mathscr{S}_0^c}H(p_{j_1}*p_{j_2})+\sum_{\{j_1,j_2,j_3\}\in\mathscr{S}_0^c}H(p_{j_1}*p_{j_2}*p_{j_3})+\ldots$$
$$\pm\sum_{\{j_1,j_{|\mathscr{S}_0^c|}\}\in\mathscr{S}_0^c}H(p_{j_1}*\ldots*p_{j_{j_{|\mathscr{S}_0^c|}}})\leq\min\left[H(p_{j_1}),\ldots,H(p_{j_{|\mathscr{S}_0^c|}})\right]. \tag{4.14}$$

Substituting the conditional entropy upper bound in (4.11), the outage probability upper bound $P_{\text{out,UB},N}$ can be calculated. The tightness of the bound is discussed in (4.6).

4.4.3 Transformation of rate constrains into SNR constraints

The maximum achievable value of rate R_i is related to the received SNR Γ_i by means of [Zho+14]

$$R_i=\Phi(\Gamma_i). \tag{4.15}$$

Rearranging (4.15), we obtain

$$\Gamma_i=2^{R_{ci}\cdot R_i}-1, \tag{4.16}$$

which can be readily used to rewrite (4.11) in terms of corresponding SNR constraints.

4.4.4 Calculation of outage probability upper bound

To achieve the analytical solution of the outage probability upper bound, MacLaurin series for the exponential functions $\exp(-x)\approx 1-x$ are used.

4.4.4.1 DF-IE System with One Relay

The looses constraints for DF-IE system with one relay are

$$R_0+R_1\geq 1,\ \text{for } p_1=0 \tag{4.17}$$
$$R_0\geq H(p_1),\ \text{for } 0<p_1\leq 0.5. \tag{4.18}$$

The calculation of the outage probabilities are presented in I.1. Finally, the outage probability upper bound is

$$\begin{aligned}P_{\text{out,UB},1}&=\sum_{i=1}^{2}J_{1,i}\\&=\frac{C_{1,1}}{\bar{\Gamma}_0\bar{\Gamma}_1}+\frac{C_{1,1}}{\bar{\Gamma}_0\bar{\Gamma}_2}\end{aligned} \tag{4.19}$$

with constant

$$\begin{aligned}C_{1,1}&=2^{R_c}\left[R_c\ln(2)-1\right]+1\\&=+1-2^{R_c}\sum_{n=0}^{1}(-1)^n\frac{1}{n!}R_c^n\ln^n(2).\end{aligned} \tag{4.20}$$

Case	Intra-link error probability $0 < p_i \leq 0.5$
1	$\{\varnothing\}$
2-4	$\{(1),(2),(3)\}$
5-7	$\{(1,2),(1,3),(2,3)\}$
8	$\{(1,2,3)\}$

Table 4.1: Case distinction for DF-IE system with three relay. The elements in the set define the index for the intra-link error probabilities in the range of $0 < p_i \leq 0.5$. All other intra-link error probabilities are $p_j = 0$.

Case	1	2	5	8
$R_0 \geq$	0	0	0	$\min[H(p_1),H(p_2),H(p_3)]$
$R_0+R_1 \geq$	0	0	$\min[H(p_2),H(p_3)]$	$\cdot$
$R_0+R_1+R_2 \geq$	0	$H(p_3)$	$\cdot$	$\cdot$
$R_0+R_1+R_2+R_3 \geq$	1	$\cdot$	$\cdot$	$\cdot$

Table 4.2: Looses constraints for DF-IE system with three relay.

4.4.4.2 DF-IE System with Two Relays

The looses constraints for DF-IE system with one relay are

$$R_0+R_1+R_2 \geq 1, \text{ for } p_1 = 0, p_2 = 0, \tag{4.21}$$

$$R_0+R_1 \geq H(p_1), \text{ for } p_1 = 0, 0 < p_2 \leq 0.5, \tag{4.22}$$

$$R_0 \geq H(p_1)+H(p_2)-H(p_1 * p_2), \text{ for } 0 < p_1 \leq 0.5, 0 < p_2 \leq 0.5. \tag{4.23}$$

The calculation of the outage probabilities are presented in I.2. The outage probability upper bound is

$$\begin{aligned} P_{\text{out,UB},2} &= \sum_{i=1}^{4} J_{2,i} \\ &= \frac{C_{2,1}}{\bar{\Gamma}_0\bar{\Gamma}_3\bar{\Gamma}_4} + \frac{C_{2,1}}{\bar{\Gamma}_0\bar{\Gamma}_2\bar{\Gamma}_3} + \frac{C_{2,1}}{\bar{\Gamma}_0\bar{\Gamma}_1\bar{\Gamma}_4} + \frac{C_{2,2}}{\bar{\Gamma}_0\bar{\Gamma}_1\bar{\Gamma}_2} \end{aligned} \tag{4.24}$$

with constants

$$\begin{aligned} C_{2,1} &= 2^{R_c}\left[1/2R_c^2\ln^2(2) - R_c\ln(2) + 1\right] - 1 \\ &= -1 + 2^{R_c}\sum_{n=0}^{2}(-1)^n\frac{1}{n!}R_c^n\ln^n(2) \end{aligned} \tag{4.25}$$

$$C_{2,2} = 2^{R_c}\left[2^{R_c} - 2R_c\ln(2)\right] - 1. \tag{4.26}$$

4.4.4.3 DF-IE System with Three Relays

The looses constraints for DF-IE system with three relay are presented in Tab. 4.2 with case distinction presented in Tab. 4.1.

The calculation of the outage probabilities are presented in I.3. The outage probability upper bound is

$$\begin{aligned} P_{\text{out,UB},3} &= \sum_{i=1}^{8} J_{3,i} \\ &= \frac{C_{3,1}}{\bar{\Gamma}_0\bar{\Gamma}_4\bar{\Gamma}_5\bar{\Gamma}_6} + \frac{C_{3,1}}{\bar{\Gamma}_0\bar{\Gamma}_3\bar{\Gamma}_4\bar{\Gamma}_5} + \frac{C_{3,1}}{\bar{\Gamma}_0\bar{\Gamma}_2\bar{\Gamma}_4\bar{\Gamma}_6} + \frac{C_{3,1}}{\bar{\Gamma}_0\bar{\Gamma}_1\bar{\Gamma}_5\bar{\Gamma}_6} \\ &\quad + \frac{C_{3,2}}{\bar{\Gamma}_0\bar{\Gamma}_2\bar{\Gamma}_3\bar{\Gamma}_6} + \frac{C_{3,2}}{\bar{\Gamma}_0\bar{\Gamma}_1\bar{\Gamma}_3\bar{\Gamma}_5} + \frac{C_{3,2}}{\bar{\Gamma}_0\bar{\Gamma}_1\bar{\Gamma}_2\bar{\Gamma}_6} + \frac{C_{3,3}}{\bar{\Gamma}_0\bar{\Gamma}_1\bar{\Gamma}_2\bar{\Gamma}_3} \end{aligned} \tag{4.27}$$

Case	Intra-link error probability $0 < p_i \leq 0.5$
1	$\{\varnothing\}$
2-5	$\{(1),(2),(3),(4)\}$
6-11	$\{(1,2),(1,3),(1,4),(2,3),(2,4),(3,4)\}$
12-15	$\{(1,2,3),(1,2,4),(1,3,4),(2,3,4)\}$
16	$\{(1,2,3,4)\}$

Table 4.3: Case distinction for DF-IE system with four relay. The elements in the set define the index for the intra-link error probabilities in the range of $0 < p_i \leq 0.5$. All other intra-link error probabilities are $p_j = 0$.

Case	1	2	6	12	16
$R_0 \geq$	0	0	0	0	$\min[H(p_1),H(p_2),H(p_3),H(p_4)]$
$R_0+R_1 \geq$	0	0	0	$\min[H(p_2),H(p_3),H(p_4)]$	·
$R_0+R_1+R_2 \geq$	0	0	$\min[H(p_3),H(p_4)]$		·
$R_0+R_1+R_2+R_3 \geq$	0	$H(p_4)$	·		·
$R_0+R_1+R_2+R_3+R_4 \geq$	1	·	·		·

Table 4.4: Looses constraints for DF-IE system with four relay.

with constants

$$\begin{aligned} C_{3,1} &= 2^{R_c}\left[1/6 R_c^3 \ln^3(2) - 1/2 R_c^2 \ln^2(2) + R_c \ln(2) - 1\right] + 1 \\ &= +1 - 2^{R_c} \sum_{n=0}^{3} (-1)^n \frac{1}{n!} R_c^n \ln^n(2) \end{aligned} \tag{4.28}$$

$$C_{3,2} = 2^{R_c}\left[2^{R_c} - R_c^2 \ln^2(2) - 2\right] + 1 \tag{4.29}$$

$$C_{3,3} = 2\left(2^{R_c} - 1\right)\left[2^{2R_c} - 2 \cdot 2^{R_c} R_c \ln(2) - 1\right]. \tag{4.30}$$

4.4.4.4 DF-IE System with Four Relays

The looses constraints for DF-IE system with four relay are presented in Tab. 4.4 with case distinction presented in Tab. 4.3.

The calculation of the outage probabilities are presented in I.4. The outage probability upper bound is

$$\begin{aligned} P_{\text{out,UB,4}} =& \sum_{i=1}^{16} J_{4,i} \\ =& \frac{C_{4,1}}{\bar{\Gamma}_0\bar{\Gamma}_5\bar{\Gamma}_6\bar{\Gamma}_7\bar{\Gamma}_8} \\ &+ \frac{C_{4,1}}{\bar{\Gamma}_0\bar{\Gamma}_4\bar{\Gamma}_5\bar{\Gamma}_6\bar{\Gamma}_7} + \frac{C_{4,1}}{\bar{\Gamma}_0\bar{\Gamma}_3\bar{\Gamma}_5\bar{\Gamma}_6\bar{\Gamma}_8} + \frac{C_{4,1}}{\bar{\Gamma}_0\bar{\Gamma}_2\bar{\Gamma}_5\bar{\Gamma}_7\bar{\Gamma}_8} + \frac{C_{4,1}}{\bar{\Gamma}_0\bar{\Gamma}_1\bar{\Gamma}_6\bar{\Gamma}_7\bar{\Gamma}_8} \\ &+ \frac{C_{4,2}}{\bar{\Gamma}_0\bar{\Gamma}_3\bar{\Gamma}_4\bar{\Gamma}_5\bar{\Gamma}_6} + \frac{C_{4,2}}{\bar{\Gamma}_0\bar{\Gamma}_2\bar{\Gamma}_4\bar{\Gamma}_5\bar{\Gamma}_7} + \frac{C_{4,2}}{\bar{\Gamma}_0\bar{\Gamma}_2\bar{\Gamma}_3\bar{\Gamma}_5\bar{\Gamma}_8} + \frac{C_{4,2}}{\bar{\Gamma}_0\bar{\Gamma}_1\bar{\Gamma}_4\bar{\Gamma}_6\bar{\Gamma}_7} \\ &+ \frac{C_{4,2}}{\bar{\Gamma}_0\bar{\Gamma}_1\bar{\Gamma}_3\bar{\Gamma}_6\bar{\Gamma}_8} + \frac{C_{4,2}}{\bar{\Gamma}_0\bar{\Gamma}_1\bar{\Gamma}_2\bar{\Gamma}_7\bar{\Gamma}_8} \\ &+ \frac{C_{4,3}}{\bar{\Gamma}_0\bar{\Gamma}_2\bar{\Gamma}_3\bar{\Gamma}_4\bar{\Gamma}_5} + \frac{C_{4,3}}{\bar{\Gamma}_0\bar{\Gamma}_1\bar{\Gamma}_3\bar{\Gamma}_4\bar{\Gamma}_6} + \frac{C_{4,3}}{\bar{\Gamma}_0\bar{\Gamma}_1\bar{\Gamma}_2\bar{\Gamma}_4\bar{\Gamma}_7} + \frac{C_{4,3}}{\bar{\Gamma}_0\bar{\Gamma}_1\bar{\Gamma}_2\bar{\Gamma}_3\bar{\Gamma}_8} \\ &+ \frac{C_{4,4}}{\bar{\Gamma}_0\bar{\Gamma}_1\bar{\Gamma}_2\bar{\Gamma}_3\bar{\Gamma}_4} \end{aligned} \tag{4.31}$$

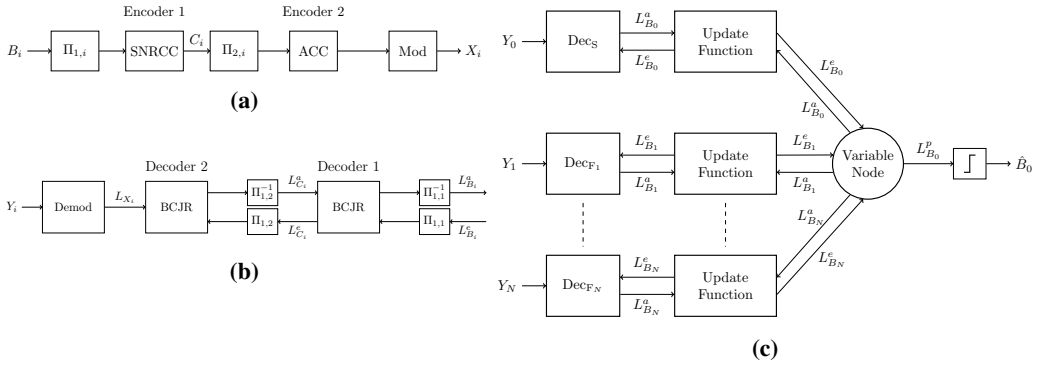

Figure 4.2: (a) Encoder, (b) decoder, and (c) joint decoder.

with constants

$$C_{4,1} = 2^{R_c}\left[1/24 R_c^4 \ln^4(2) - 1/6 R_c^3 \ln^3(2) + 1/2 R_c^2 \ln^2(2) - R_c \ln(2) + 1\right] - 1$$
$$= -1 + 2^{R_c} \sum_{n=0}^{4} (-1)^n \frac{1}{n!} R_c^n \ln^n(2), \tag{4.32}$$
$$C_{4,2} = 2^{R_c}\left[2^{R_c} - 1/3 R_c^3 \ln^3(2) - 2R_c \ln(2)\right] - 1, \tag{4.33}$$
$$C_{4,3} = 2\left(2^{R_c} - 1\right)\left[2^{2R_c} - 2 \cdot 2^{R_c} - 2^{R_c} R_c^2 \ln^2(2) + 1\right], \tag{4.34}$$
$$C_{4,4} = 6(2^{R_c} - 1)^2\left[2^{2R_c} - 2 \cdot 2^{R_c} R_c \ln(2) - 1\right]. \tag{4.35}$$

4.4.4.5 DF-IE system with N Relays

The outage probability upper bound for the DF-IE with an arbitrary N of relays can be calculated as presented. However, to derive a general expression is NP-hard do to case distinction and left for further studies.

4.4.4.6 DF-IE system with Zero Relays

We define a baseline, where no relay is included in the transmission.

$$H(B_0) \leq R_0 = \frac{1}{R_c} \log_2(1 + \Gamma_0) \tag{4.36}$$
$$P_{0,\text{out}} = \Pr[0 \leq R_0 < 1]$$
$$= \Pr\left[0 \leq \gamma_0 < 2^{R_c} - 1\right]$$
$$= \int_{\gamma_0} \frac{1}{\bar{\Gamma}_0} \exp\left(-\frac{\gamma_0}{\bar{\Gamma}_0}\right) d\gamma_0$$
$$\approx \frac{2^{R_c} - 1}{\bar{\Gamma}_0} \tag{4.37}$$

4.5 Distributed Source Coding Scheme

In this section, we briefly review the distributed source coding scheme proposed in [AM12b] and apply it to the DF-IE system in Fig. 4.1. With the distributed source coding scheme we verify the outage probability upper bound as a lower bound for the Frame-Error-Rate, i.e. $P_{\text{out,a}}(\Gamma) \leq \text{FER}(\Gamma)$, [NFR07].
Each information sequence $B_0, B_1, ..., B_N$ is interleaved denoted by Π and encoded by a twofold serially concatenated code in Enc_S and Enc_{F_i}, illustrated in Fig. 4.2a. First, a systematic non-recursive convolution code (SNRCC) and second, a doped ACC, i.e., memory-1 systematic recursive convolutional code (SRCC) are deployed. The ACC

is used to prevent an error floor at the relay decoder [PS06]. At $\mathrm{Dec_S}$ and $\mathrm{Dec_{F_i}}$, soft demapping is applied by calculating the LLR L_{X_i} with the received sequence Y_i and known channel state information. Each source and relay decoder in Fig. 4.2b has two matching Bahl-Cocke-Jelinek-Raviv (BCJR) algorithms [Bah+74]. However, to avoid heavy decoding complexity, information sequence B_0 is *decoded without iteration* at F_i. Hard decision is then performed to obtain information sequence B_i. At D, the joint decoder, illustrated in Fig. 4.2c, is structured in two main parts: first the local iteration (LI), where the information sequences are decoded with $\mathrm{Dec_S}$ and $\mathrm{Dec_{F_i}}$, and second the global iteration (GI), where the information exchange among all relay information sequences is performed. In GI the LLR update function [AM12b], based on the knowledge of p_i, updates the LLRs $L^e_{B_k}$ accordingly[4]. If the LLRs $L^e_{B_k}$ are not improving anymore, the final estimation of B_0 is determined by hard decision of the sum of all $L^e_{B_k}$. For a detailed explanation of the joint decoder, the authors refer to [AM12b].

4.6 Numerical Results

In this section, we carry out three investigations: (i) comparison of Monte Carlo simulated outage probability, outage probability upper bound and FER of distributed source coding scheme, (ii) impact of proposed power allocation scheme, and (iii) opportunistic relay selection is illustrated by means of a heat map. The common parameters used in the simulations are

- Frame length: 500 bits,
- Number of frames: 1.000.000,
- Interleavers: random,
- Generator polynomial of SNRCC: $G = ([3,1])_8$,
- Generator polynomial of SRCC: $G = ([3,1]2)_8$,
- Modulation: binary phase-shift keying (BPSK) and quadrature phase-shift keying (QPSK),
- Doping ratio of ACC: 1 for BPSK and QPSK,
- Path loss exponent: $\eta = 3.52$, [YA11],
- Number of iterations: 30 times.

In Fig. 4.4a and Fig. 4.4c we illustrate the Monte-Carlo simulated outage probability (OP-MC) and outage probability upper bound (OP-UB) for BPSK ($R_c = 0.5$) and QPSK ($R_c = 1.0$), respectively. The distence between S and D is normalized to $x_0 = 1.0$ and all relays are placed at $x_i = 0.5$ and $y_i = 0.0$, the topology is presented in Fig. 4.3. We can conclude, that the OP-UB is rather tight for the system model with few relays, i.e. the gap for DF-IE with one relay is almost zero and with two relays 0.27 dB. However, the gab increases with more relays, i.e. for DF-IE with three relays 1.23 dB and with four relays 2.5 dB. As expected, including more relays, the diversity gain increases. Additionally, with a higher order modulation scheme the outage probability increases, however the throughput increases.
In Fig. 4.4b and Fig. 4.4d we illustrate the OP-UB and FER of the joint decoder for BPSK and QPSK, respectively. The OP-UB is a good predictor of the FER. However, the FER cannot reach the OP-UP. The FER benefits from the diversity gain and with a higher order modulation scheme, the FER increase.

4.7 Conclusion

In this chapter, we analysed the outage probability of TS3. An exact analytical description of the outage probability can not be found. Therefore we introduced relaxation and reduction to the rate constraints given by the Slepian-Wolf theorem. As a result we can describe the outage probability upper bound for TS3 in general and present

[4]The intra-link error probability is assumed to be known at D.

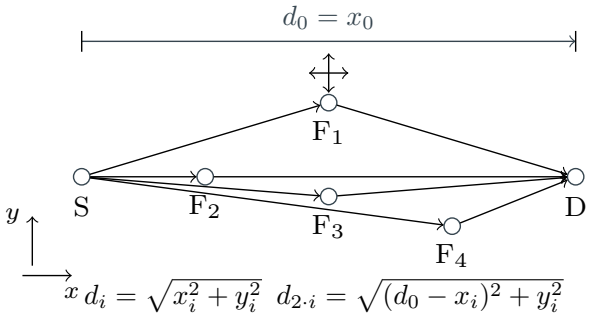

Figure 4.3: Simulation setting with up to four relay.

the analytical result for asymptotic high SNR range with up to four relays. Practical results using Monte-Carlo simulation and ACC aided turbo codes confirm the analytical result.

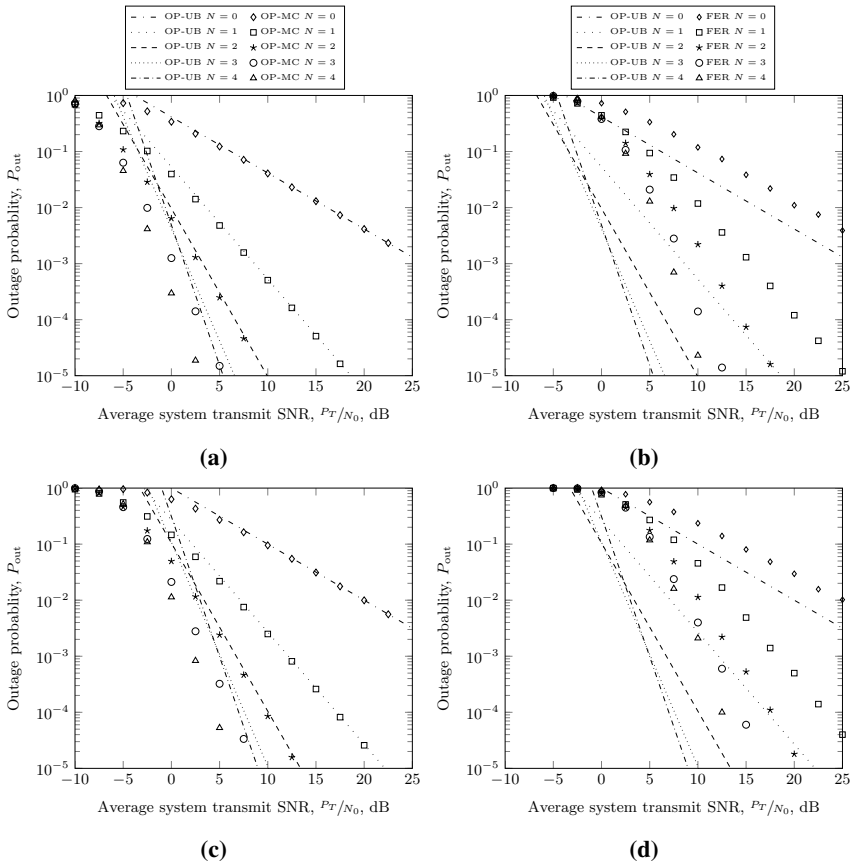

Figure 4.4: (a) Simulated outage probability (Monte-Carlo) and outage probability upper bound, (b) frame-error-rate and outage probability upper bound with BPSK, (c) simulated outage probability (Monte-Carlo) and outage probability upper bound, and (d) frame-error-rate and outage probability upper bound with QPSK.

5. Performance Analysis of TS4

5.1 System Model

The block diagram of the non-orthogonal MARC is shown in Fig 5.1. It consists of two sources, one relay, and one destination. Each node is assumed to be equipped with a single antenna and operated in a half-duplex mode. We also assume that there is no cooperation between the sources. The transmission round is divided into two time slots as compared to three time slots consumption in the conventional orthogonal MARC. During the first time slot, the uniform information sequences generated from sources A and B are encoded, modulated, and simultaneously transmitted to the relay and the destination. Let the modulated symbol sequences of sources A and B be denoted by $\mathbf{x}_{\mathrm{A}}$ and $\mathbf{x}_{\mathrm{B}}$, respectively. For convenience, we assume that each symbol has unit power. The received signal at the relay and destination during the first time-slot transmission can be expressed as

$$\mathbf{y}_{\mathrm{R},1} = \sqrt{P_{\mathrm{A}}} h_{\mathrm{AR}} \mathbf{x}_{\mathrm{A}} + \sqrt{P_{\mathrm{B}}} h_{\mathrm{BR}} \mathbf{x}_{\mathrm{B}} + \mathbf{n}_{\mathrm{R},1}, \tag{5.1}$$

$$\mathbf{y}_{\mathrm{D},1} = \sqrt{P_{\mathrm{A}}} h_{\mathrm{AD}} \mathbf{x}_{\mathrm{A}} + \sqrt{P_{\mathrm{B}}} h_{\mathrm{BD}} \mathbf{x}_{\mathrm{B}} + \mathbf{n}_{\mathrm{D},1}, \tag{5.2}$$

where all the wireless links, i.e., h_{AR}, h_{BR}, h_{AD}, and h_{BD}, suffer from independent and identically distributed (i.i.d.) Rayleigh block fading distributed as $CN(0,1)$, P_i is the transmit power at source i, for $i \in \{\mathrm{A},\mathrm{B}\}$, and each entry of additive white Gaussian noise (AWGN) vector $\mathbf{n}_{j,1}$ also follows $CN(0,1)$, for $j \in \{\mathrm{R},\mathrm{D}\}$. The average individual received SNRs can be written by

$$\gamma_{ij} = P_i |h_{ij}|^2, \text{ for } i \in \{\mathrm{A},\mathrm{B}\} \text{ and } j \in \{\mathrm{R},\mathrm{D}\}, \tag{5.3}$$

where $|h_{ij}|^2$ follows exponential distribution with unit mean and unit variance. The pdf of γ_{ij} can be expressed as

$$p(\gamma_{ij}) = \frac{1}{P_i} \exp(-\frac{\gamma_{ij}}{P_i}), \text{ for } i \in \{\mathrm{A},\mathrm{B}\} \text{ and } j \in \{\mathrm{R},\mathrm{D}\}. \tag{5.4}$$

Because the relay is not interested in the original information of the sources, the relay directly estimates the bit-wise XOR of the data sequences transmitted by sources A and B. Regardless of the correctness of the estimation, the relay re-encodes and modulates the estimated XOR version to $\mathbf{x}_{\mathrm{R}}$ and forwards it to the destination during the second time slot. The received signal at the destination during the second time-slot transmission is given by

$$\mathbf{y}_{\mathrm{D},2} = \sqrt{P_{\mathrm{R}}} h_{\mathrm{RD}} \mathbf{x}_{\mathrm{R}} + \mathbf{n}_{\mathrm{D},2}, \tag{5.5}$$

where P_{R} denotes the transmit power at the relay, h_{RD} is the i.i.d. Rayleigh block fading distributed as $CN(0,1)$, and each entry of $\mathbf{n}_{\mathrm{D},2}$ also follows $CN(0,1)$.

5.2 Source-to-Relay Transmission

We assume that source A (U_{A}) and source B (U_{B}) are correlated, which can be modeled by bit-flipping model,

$$U_{\mathrm{A}} = U_{\mathrm{B}} \oplus U, \tag{5.6}$$

where $\Pr(U=1) = p_u$. In this sense, the bit-wise XOR version of U_A and U_B, i.e., $U_{\mathrm{A}\oplus\mathrm{B}} = U_{\mathrm{A}} \oplus U_{\mathrm{B}}$, has the following probability mass function (PMF) $\Pr(U_{\mathrm{A}\oplus\mathrm{B}} = 1) = p_u$ and $\Pr(U_{\mathrm{A}\oplus\mathrm{B}} = 0) = 1 - p_u$.

For the transmission from the sources to the relay, we introduce the concept of PNC at the relay. The estimated bit-wise XOR is treated as a helper for the MAC transmission from the sources to the destination. For the purpose of tractability, the XMAC, shown in (5.1), is approximated by a virtual P2P channel with transmission of non-uniform/uniform binary i.i.d sources (i.e., $0 \le p_u \le 0.5$). The virtual channel is in the form of

$$h = \begin{cases} h_{\mathrm{AR}}, & \text{if } |h_{\mathrm{AR}}| < |h_{\mathrm{BR}}|, \\ h_{\mathrm{BR}}, & \text{if } |h_{\mathrm{AR}}| \ge |h_{\mathrm{BR}}|. \end{cases} \tag{5.7}$$

Assuming that $P_{\mathrm{A}} = P_{\mathrm{B}} = P$, the received signal for this virtual channel can be written by

$$\mathbf{y}_{\mathrm{V}} = \sqrt{P} h \mathbf{x} + \mathbf{n}, \tag{5.8}$$

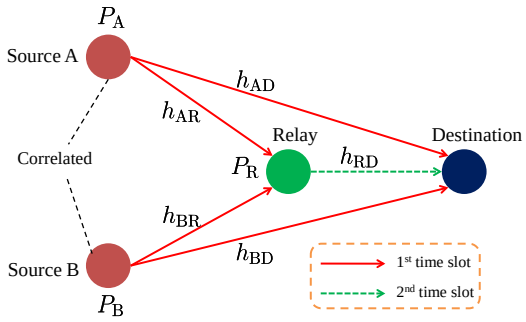

Figure 5.1: The block diagram of the non-orthogonal MARC.

where $\mathbf{x}$ is the modulated symbol sequence of the XOR version of $\mathbf{x}_A$ and $\mathbf{x}_B$, and each entry of additive noise vector $\mathbf{n}$ follows $CN(0,1)$. Further details of the virtual channel aregiven in Appendix J.

The pdf of the average SNR of the virtual channel has been changed into

$$p(\gamma_V) = \frac{2}{P}\exp(-\frac{2\gamma_V}{P}). \tag{5.9}$$

Referring to the lossy source channel separation theorem [Xiaobo2014; LZM15], we obtain

$$R_D(p_e)R_c \leq C(\gamma_V), \tag{5.10}$$

where $R_D(\cdot)$ represents the rate distortion function, $C(a) = \log_2(1+a)$ is the capacity function under the assumption of Gaussian signaling, and R_c is the multiplication of channel coding rate and modulation order, i.e., transmission rate, for the virtual P2P channel. Setting $\Phi(\gamma_V) = C(\gamma_V)/R_c$, the calculation of the Hamming distortion for the virtual channel, i.e., p_e, in (5.10) can be computed by

$$p_e = \begin{cases} H_b^{-1}[H_b(p_u) - \Phi(\gamma_V)], & \text{for } \Phi^{-1}(0) \leq \gamma_V \leq \Phi^{-1}[H_b(p_u)], \\ 0, & \text{for } \gamma_V \geq \Phi^{-1}[H_b(p_u)], \end{cases} \tag{5.11}$$

where $H_b(p) = -p\log_2(p) - (1-p)\log_2(1-p)$ denotes the binary entropy function, $H_b^{-1}(\cdot)$ denotes its inverse function, and $\Phi^{-1}(a) = 2^{aR_c} - 1$ is the inverse function of $\Phi(\cdot)$. The approximated closed from expression of $H_b^{-1}(\cdot)$ is given in [Zho+14]. The relationship between the decoded version of $U_{A\oplus B}$ (denoted by $\hat{U}_{A\oplus B}$) and the original one can also be modeled by bit-flipping model with correlation p_e,

$$\hat{U}_{A\oplus B} = U_{A\oplus B} \oplus E, \tag{5.12}$$

where $\Pr(E=1) = p_e$.

5.3 MAC with a Helper

The source-to-destination transmission combined with relay-to-destination transmission can be regarded as MAC with a helper, as shown in Fig. 5.2. The capacity region is unknown. Instead, we take the intersection of the Slepian-Wolf compression rate region and the MAC capacity region into consideration to obtain an achievable rate region [CT06]. This derivation is based on the sufficient conditions for lossless communication.

The Slepian-Wolf compression rate region without the helper can be represented by

$$R_{s,A} \geq H(U_A|U_B) = H_b(p_u), \tag{5.13}$$
$$R_{s,B} \geq H(U_B|U_A) = H_b(p_u), \tag{5.14}$$
$$R_{s,A} + R_{s,B} \geq H(U_A, U_B) = 1 + H_b(p_u), \tag{5.15}$$

where $R_{s,A}$ and $R_{s,B}$ are the compression rates of sources A and B, respectively. With the aid of the helper, the Slepian-Wolf compression rate region [He16] will be enlarged to

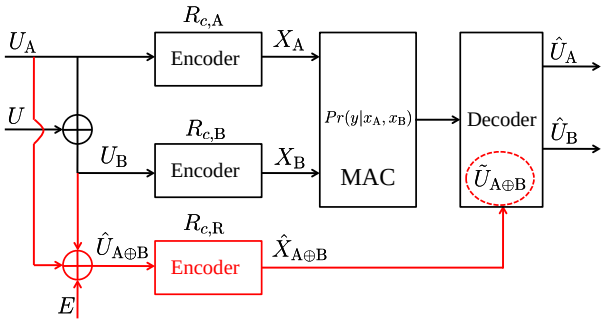

Figure 5.2: Illustration of MAC with a helper.

$$R_{s,\mathrm{A}} \geq H(U_\mathrm{A}|U_\mathrm{B},\tilde{U}_{\mathrm{A}\oplus\mathrm{B}}) = H_b(p_u)+H_b(p_e*p_d)-H_b(p_u*p_e*p_d), \tag{5.16}$$
$$R_{s,\mathrm{B}} \geq H(U_\mathrm{B}|U_\mathrm{A},\tilde{U}_{\mathrm{A}\oplus\mathrm{B}}) = H_b(p_u)+H_b(p_e*p_d)-H_b(p_u*p_e*p_d), \tag{5.17}$$
$$R_{s,\mathrm{A}}+R_{s,\mathrm{B}} \geq H(U_\mathrm{A},U_\mathrm{B}|\tilde{U}_{\mathrm{A}\oplus\mathrm{B}}) = 1+H_b(p_u)+H_b(p_e*p_d)-H_b(p_u*p_e*p_d), \tag{5.18}$$

where $\tilde{U}_{\mathrm{A}\oplus\mathrm{B}}$ is the estimated error version of $\hat{U}_{\mathrm{A}\oplus\mathrm{B}}$ with correlation p_d at the destination and $a*b=a(1-b)+(1-a)b$. The relationship between $\tilde{U}_{\mathrm{A}\oplus\mathrm{B}}$ and $\hat{U}_{\mathrm{A}\oplus\mathrm{B}}$ can be modeled by

$$\tilde{U}_{\mathrm{A}\oplus\mathrm{B}} = \hat{U}_{\mathrm{A}\oplus\mathrm{B}} \oplus D, \tag{5.19}$$

where $\Pr(D=1)=p_d$. Similar to (5.11), p_d can be calculated as

$$p_d = \begin{cases} H_b^{-1}[H_b(p_u*p_e)-\Phi(\gamma_{\mathrm{R,D}})], & \text{for } \Phi^{-1}(0) \leq \gamma_{\mathrm{R,D}} \leq \Phi^{-1}[H_b(p_u*p_e)], \\ 0, & \text{for } \gamma_{\mathrm{R,D}} \geq \Phi^{-1}(H_b(p_u*p_e)). \end{cases} \tag{5.20}$$

More details on derivation of (5.16)–(5.18) can be found in [Xiaobo2014; LZM15].

According to the lossless source channel separation theorem, the MAC capacity region is determined by

$$R_{s,\mathrm{A}}R_{c,\mathrm{A}} \leq C(\gamma_{\mathrm{A,D}}), \tag{5.21}$$
$$R_{s,\mathrm{B}}R_{c,\mathrm{B}} \leq C(\gamma_{\mathrm{B,D}}), \tag{5.22}$$
$$R_{s,\mathrm{A}}R_{c,\mathrm{A}}+R_{s,\mathrm{B}}R_{c,\mathrm{B}} \leq C(\gamma_{\mathrm{A,D}}+\gamma_{\mathrm{B,D}}), \tag{5.23}$$

where $R_{c,\mathrm{A}}$ and $R_{c,\mathrm{B}}$ are the transmission rates of sources A and B, respectively. The achievable rate region is the intersection part determined by (5.16)–(5.18) and (5.21)–(5.23).

5.3.1 An Example

Let's show a detailed example to illustrate the achievable rate region. We set $R_{c,\mathrm{A}}=R_{c,\mathrm{B}}=1/2$, $p_u=p_e=p_d=0.1$, and $\gamma_{\mathrm{A,D}}=\gamma_{\mathrm{B,D}}=0$ dB. The achievable rate region is shown in Fig. 5.3. The achievable rate region is affected by many factors such as the values of $R_{c,\mathrm{A}}$, $R_{c,\mathrm{B}}$, P, p_u, p_e, and p_d. We mainly focus on the factors p_e and p_d, which are determined by the XMAC channel and the relay-to-destination link.

5.3.2 Outage Probability

For simplicity, we assume the same transmission rate for the two sources, i.e., $R_{c,\mathrm{A}}=R_{c,\mathrm{B}}=R_c$. Consequently, we define the event of successful transmission as

$$\begin{aligned}\mathbb{S} = \{&H_b(p_u)+H_b(p_e*p_d)-H_b(p_u*p_e*p_d) \leq C(\gamma_{\mathrm{A,D}})/R_c \\ &\wedge H_b(p_u)+H_b(p_e*p_d)-H_b(p_u*p_e*p_d) \leq C(\gamma_{\mathrm{B,D}})/R_c \wedge \\ &1+H_b(p_u)+H_b(p_e*p_d)-H_b(p_u*p_e*p_d) \leq C(\gamma_{\mathrm{A,D}}+\gamma_{\mathrm{B,D}})/R_c\},\end{aligned} \tag{5.24}$$

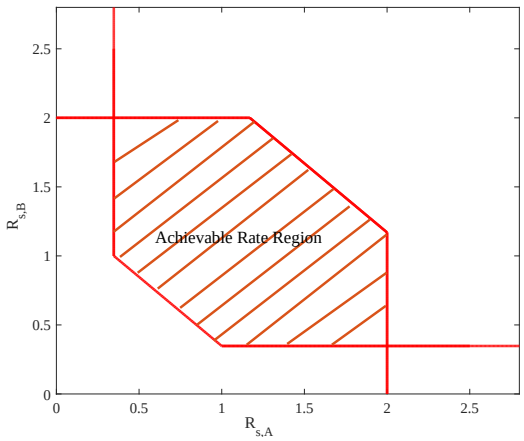

Figure 5.3: The achievable rate region for the MAC with a helper.

where $\wedge$ denotes logical "and" operation. Therefore, the outage probability can be expressed as

$$P_{\text{out}} = 1 - \Pr\{\mathbb{S}\}. \tag{5.25}$$

Because the derived achievable rate region for the MAC with a helper is smaller than its actual capacity region, the outage probability is correspondingly an upper bound.

Depending on the success or failure of source-to-relay XMAC and relay-to-destination channel, we can rewrite the $\Pr\{\mathbb{S}\}$ in (5.25) as

$$\Pr\{\mathbb{S}\} = \sum_{i=1}^{4} \Pr\{\mathbb{S}|\mathbb{C}_i\}\Pr\{\mathbb{C}_i\}, \tag{5.26}$$

where

$$\begin{aligned}
\mathbb{C}_1 &= \{p_e = 0 \wedge p_d = 0\},\\
\mathbb{C}_2 &= \{p_e = 0 \wedge p_d \neq 0\},\\
\mathbb{C}_3 &= \{p_e \neq 0 \wedge p_d = 0\},\\
\mathbb{C}_4 &= \{p_e \neq 0 \wedge p_d \neq 0\}.
\end{aligned} \tag{5.27}$$

All of the above four events will be transferred into different intervals of a two-dimensional vector consisting of γ_{V}, $\gamma_{\text{R,D}}$. In addition to the effect of direct links from sources to destination, i.e., $\gamma_{\text{A,D}}$ and $\gamma_{\text{B,D}}$, the probability of successful transmission $\Pr\{\mathbb{S}\}$ can be calculated by four-fold integrals, i.e.,

$$\Pr\{\mathbb{S}|\mathbb{C}_i\}\Pr\{\mathbb{C}_i\} = \iiiint\limits_{\mathbb{V}_i} p(\gamma_{\text{V}})p(\gamma_{\text{R,D}})p(\gamma_{\text{A,D}})p(\gamma_{\text{B,D}})d\gamma_{\text{V}}d\gamma_{\text{R,D}}d\gamma_{\text{A,D}}d\gamma_{\text{B,D}}, \tag{5.28}$$

where

$$\mathbb{V}_1 = \{\gamma_{\text{A,D}} \geq \Phi^{-1}(0) \wedge \gamma_{\text{B,D}} \geq \Phi^{-1}(0) \wedge \gamma_{\text{A,D}} + \gamma_{\text{B,D}} \geq \Phi^{-1}(1), \wedge \gamma_{\text{V}} \geq \Phi^{-1}[H_b(p_u)] \wedge \gamma_{\text{R,D}} \geq \Phi^{-1}[H_b(p_u)]\}, \tag{5.29}$$

$$\begin{aligned}
\mathbb{V}_2 = \{&\gamma_{\text{A,D}} \geq \Phi^{-1}[H_b(p_u) + H_b(p_d) - H_b(p_u * p_d)] \wedge \gamma_{\text{B,D}} \geq \Phi^{-1}[H_b(p_u) + H_b(p_d) - H_b(p_u * p_d)] \wedge\\
&\gamma_{\text{A,D}} + \gamma_{\text{B,D}} \geq \Phi^{-1}[1 + H_b(p_u) + H_b(p_d) - H_b(p_u * p_d)] \wedge \gamma_{\text{V}} \geq \Phi^{-1}[H_b(p_u)] \wedge \Phi^{-1}(0) \leq \gamma_{\text{R,D}} \leq \Phi^{-1}[H_b(p_u)]\},
\end{aligned} \tag{5.30}$$

$$\begin{aligned}
\mathbb{V}_3 = \{&\gamma_{\text{A,D}} \geq \Phi^{-1}[H_b(p_u) + H_b(p_e) - H_b(p_u * p_e)] \wedge \gamma_{\text{B,D}} \geq \Phi^{-1}[H_b(p_u) + H_b(p_e) - H_b(p_u * p_e)] \wedge\\
&\gamma_{\text{A,D}} + \gamma_{\text{B,D}} \geq \Phi^{-1}[1 + H_b(p_u) + H_b(p_e) - H_b(p_u * p_e)] \wedge \Phi^{-1}(0) \leq \gamma_{\text{V}} \leq \Phi^{-1}[H_b(p_u)] \wedge \gamma_{\text{R,D}} \geq \Phi^{-1}[H_b(p_u * p_e)]\},
\end{aligned} \tag{5.31}$$

$$\begin{aligned}
\mathbb{V}_4 = \{&\gamma_{\text{A,D}} \geq \Phi^{-1}[H_b(p_u) + H_b(p_e * p_d) - H_b(p_u * p_e * p_d)] \wedge \gamma_{\text{B,D}} \geq \Phi^{-1}[H_b(p_u) + H_b(p_e * p_d) - H_b(p_u * p_e * p_d)] \wedge\\
&\gamma_{\text{A,D}} + \gamma_{\text{B,D}} \geq \Phi^{-1}[1 + H_b(p_u) + H_b(p_e * p_d) - H_b(p_u * p_e * p_d)] \wedge \Phi^{-1}(0) \leq \gamma_{\text{V}} \leq \Phi^{-1}[H_b(p_u)]\\
&\wedge \Phi^{-1}(0) \leq \gamma_{\text{R,D}} \leq \Phi^{-1}[H_b(p_u * p_e)]\}.
\end{aligned} \tag{5.32}$$

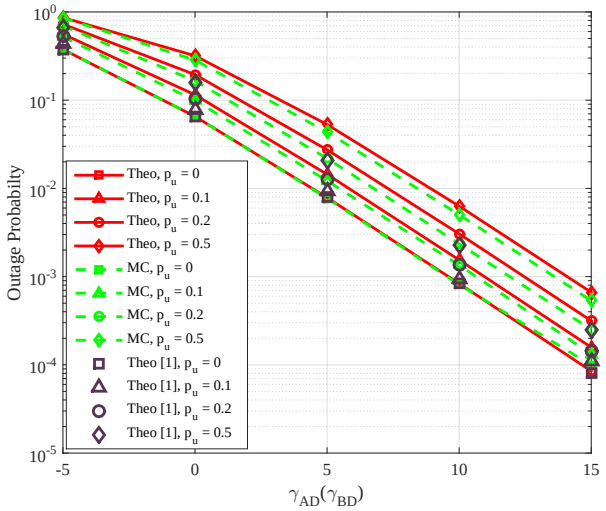

Figure 5.4: Outage probability vs SNR for Scenario One.

5.4 Simulation Results

In this section, we draw the theoretical results in terms of the outage probability over the non-orthogonal MARC and compare them to the corresponding Monte Carlo computer simulations. Practical simulations using turbo codes are left for future investigation. The case of perfect intra links from [Xiaobo2014] is considered as a benchmark scheme. All the transmission rates are set to be 0.5. The correlation of the sources ranges from 0 to 0.5, which includes transmission of independent sources as well. We assume that the transmit power has the following relationship: $P_A = P_B = P_R$. The simulation results are provided in Fig. 5.4, where "Theo" represents the theoretical results of the outage probability for the non-orthogonal MARC given by (5.25), "MC" represents the Monte Carlo simulation results of the outage probability for the non-orthogonal MARC given by (5.16)–(5.18) and (5.21)–(5.23), and "Theo [1]" represents the theoretical results of the outage probability for the orthogonal MARC from [Xiaobo2014] with error-free intra links. Compared to the case in [Xiaobo2014], the performance loss is very limited for the non-orthogonal MARC with imperfect intra links, especially when the correlation of the sources is high. Second order diversity can be achieved for all the levels of correlation. As shown in Fig. 5.4, the Monte Carlo simulations closely approximate the theoretical analysis.

5.4.1 Scenario One

In this scenario, we assume that $d_{RD} = d_{AR} = d_{BR} = d_{AD} = d_{BD}$. In other words, the average SNRs have the following relationship: $\gamma_{RD} = \gamma_{AR} = \gamma_{BR} = \gamma_{AD} = \gamma_{BD}$. The simulation results are provided in Fig. 5.4 Compared to the case in [Xiaobo2014], the performance loss is very limited for the non-orthogonal MARCs, especially when the correlation of the sources is high. Second order diversity can be achieved for all the levels of correlation. However, there exists minor mismatch between the theoretical analysis and Monte-Carlo simulations.

5.4.2 Scenario Two

In this scenario, we assume $d_{RD} = d_{AR} = d_{BR} = 0.6 \times d_{AD} = 0.6 \times d_{BD}$. In other words, the average SNRs have the following relationship: $\gamma_{RD} = \gamma_{AR} = \gamma_{BR} = \gamma_{AD} + 7.81\text{dB} = \gamma_{BD} + 7.81\text{dB}$. The simulation results are shown in Fig. 5.5. Similar to Scenario One, the same tendency and diversity order are obtained in Scenario Two. However, the performance gap between different levels of correlation is not obvious. Therefore, we don't provide the theoretical analysis of the perfect intra-link case here. It is not difficult to observe that the Monte-Carlo simulations closely follow the theoretical analysis in this scenario.

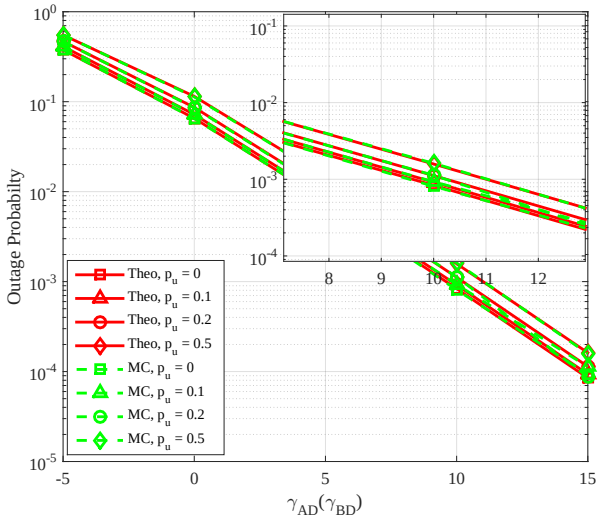

Figure 5.5: Outage probability vs SNR for Scenario Two.

5.4.3 Scenario Three

In this scenario, we assume $d_{AR} = d_{BR} = 0.4 \times d_{AD} = 0.4 \times d_{BD}$ and $d_{RD} = 0.8 \times d_{AD} = 0.8 \times d_{BD}$. In other words, the average SNRs have the following relationship: $\gamma_{AR} = \gamma_{BR} = \gamma_{AD} + 14.01\text{dB} = \gamma_{BD} + 14.01\text{dB}$ and $\gamma_{RD} = \gamma_{AD} + 3.40\text{dB} = \gamma_{BD} + 3.40\text{dB}$. The simulation results are presented in Fig. 5.6.

5.4.4 Scenario Four

In this scenario, we assume $d_{AR} = d_{BR} = 0.8 \times d_{AD} = 0.8 \times d_{BD}$ and $d_{RD} = 0.8 \times d_{AD} = 0.8 \times d_{BD}$. In other words, the average SNRs have the following relationship: $\gamma_{AR} = \gamma_{BR} = \gamma_{AD} + 3.40\text{dB} = \gamma_{BD} + 3.40\text{dB}$ and $\gamma_{RD} = \gamma_{AD} + 14.01\text{dB} = \gamma_{BD} + 14.01\text{dB}$. The simulation results are shown in Fig. 5.7.

5.5 Conclusion

We have calculated the outage probability for the transmission of correlated sources over non-orthogonal fading MARC, which is based on the sufficient conditions of lossless communication over MAC with the aid of a helper. For the purpose of tractability, first hop transmission from sources to the relay has been represented by an approximated virtual P2P channel validated through intensive numerical simulations. Subsequently, the closed form expression of the capacity for the considered XMAC has been derived using the approximated virtual channel. Finally, it has been shown that the performance results of the non-orthogonal MARC approach its orthogonal counterpart with perfect intra links.

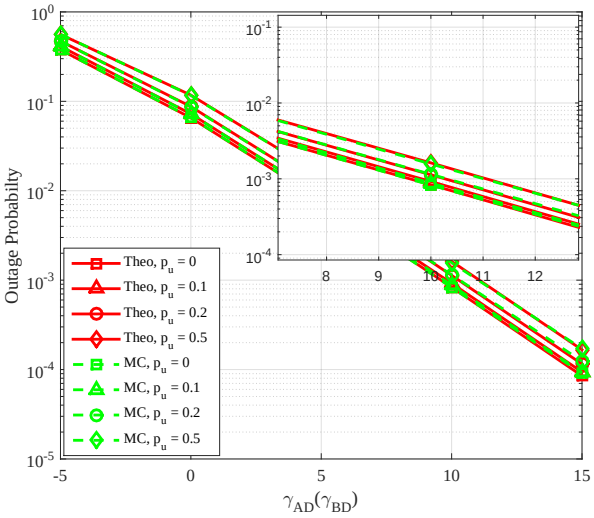

Figure 5.6: Outage probability vs SNR for Scenario Three.

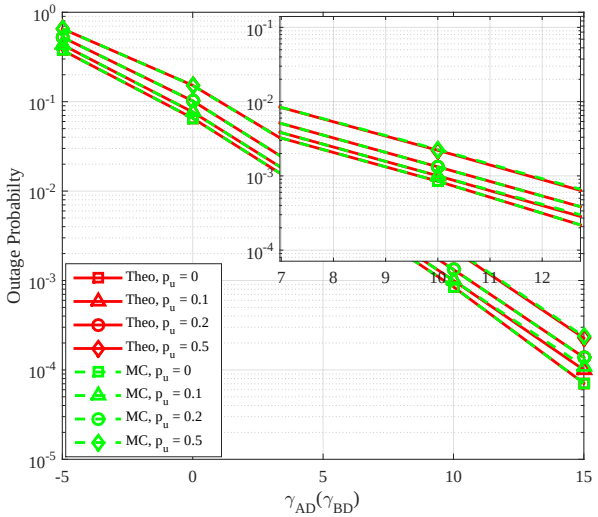

Figure 5.7: Outage probability vs SNR for Scenario Four.

6. Conclusion

In this deliverable, based on the input from [ICT15], we have presented theoretical results for reasonable extensions/generalizations of the four toy scenarios (i.e., TS1, TS2, TS3 and TS4) defined in [ICT15] along with the links-on-the-fly concept. Since the benefits of exploiting the links-on-the-fly concept over other baseline schemes were intensively studied in [ICT15], we mainly focus on this concept in this deliverable while adding the new extension scenarios and/or generalization to the performance limit analysis. Like [ICT15], the distributed lossless/lossy source coding theorems, Shannon's lossy source/channel separation theorem, source coding with a helper, Slepian-Wolf theorem and their extensions or combinations are the key tools for the performance limit analysis of the four toy scenarios. For some of the TSs, approximated closed form expression for the outage probability and validation via practical simulations are provided.

We exploit the theorem of source coding with a helper to determine the achievable rate region of TS1, which decides the outage probability of the whole system through three-fold integrals by taking into account the instantaneous SNR of the wireless links. As we all know that, second order diversity can be achieved if all the wireless links suffer from i.i.d Rayleigh block fading without LOS component. However, higher order diversity can be achieved if the LOS component is introduced. We analyze the outage probability of TS1 over Rician and Nakagami-m block fading. KLD distance between the two distributions is analyzed to provide guidelines for the diversity and coding gain analysis. A more practical SDF scheme without knowing the noise variance at the receiver side, named least square based symbol level filtering, has been proposed to improve the BER performance compared to SNR threshold based SDF scheme.

The main problem originated from TS2 is the CEO problem when all the source-to-relay links are lossy. We derive even tighter outer bound on the rate distortion region for the binary CEO problem based on the converse proof of the bound when the number of terminals is two. In practice, the KPI is the BER performance, which is a measurement of the system reliability. Therefore, we further derive the Hamming distortion for the CEO problem by saving a convex optimization problem, which could be regarded as the lower bound of the BER performance obtained via practical simulations. An extension to arbitrary number of terminal is also studied regarding the outer bound of the rate distortion region and lower bound of Hamming distortion. Practical simulation results for both AWGN and Rayleigh fading channels are provided to verify the tightness of the derived lower bound of Hamming distortion.

As an extension of TS1 or TS2, there exist multiple relays in TS3 to assist the source to forward the information sequences to the destination. The exact achievable rate region for TS3 is extremely challenging to obtain since it falls into the category of source coding with multiple helpers. Therefore, for the purpose of tractability, we relax and reduce the rate constraints based on Slepian-Wolf theorem. Approximated closed form expression for the upper bound of outage probability is obtained for the asymptotic high SNR range and up to four relays. Practical results using Monte Carlo simulations and ACC aided turbo codes illustrate that the derived upper bound of the outage probability is tight when the number of relays is small compared to the Monte Carlo simulation results.

TS4 is extended from an orthogonal multiple access relay channel (MARC) to a non-orthogonal MARC, and the outage probability of non-orthogonal MARC is derived by using the theorem of MAC with a helper. The first hop transmission from sources to the relay is represented by an approximated virtual P2P channel validated through intensive numerical simulation results. In this sense, we get the closed form expression for the capacity of the considered XMAC. It is shown that the performance results of the non-orthogonal MARC approach its orthogonal counterpart with perfect intra link while the throughput of the non-orthogonal MARC system could be significantly improved.

7. References

[AHGAD11] G. Al-Habian, A. Ghrayeb, and M. HasM. Hasna. Abu-Dayya. "Threshold-Based Relaying in Coded Cooperative Networks". In: *IEEE Trans. Veh. Technol.* 60.1 (2011), pp. 123–135.

[AM12a] K. Anwar and T. Matsumoto. "Accumulator-Assisted Distributed Turbo Codes for Relay Systems Exploiting Source-Relay Correlation". In: *IEEE Commun. Lett.* 16.7 (2012), pp. 1114–1117.

[AM12b] K. Anwar and T. Matsumoto. "Iterative Spatial Demapping for Two Correlated Sources with Power Control over Fading MAC". In: *Proc. of IEEE VTC*. 2012, pp. 1–7.

[Bah+74] L. Bahl, J. Cocke, F. Jelinek, and J. Raviv. "Optimal Decoding of Linear Codes for Minimizing Symbol Error Rate (Corresp.)" In: *IEEE Trans. on Inform. Theory* 20.2 (Mar. 1974), pp. 284–287.

[Ber n] Toby Berger. "Multiterminal source coding". In: *The Information Theory Approach to Communications, G. Longo*. Vol. 229. 0Ed. New York, Springer-Verlag, 1978, pp. 171–231.

[CAM12] Meng Cheng, K. Anwar, and T. Matsumoto. "Outage Analysis of Correlated Source Transmission in Block Rayleigh Fading Channels". In: *Proceedings of the IEEE Vehicular Technology Conference*. 2012, pp. 1–5.

[Cou12] Thomas Alexander Courtade. "Two Problems in Multiterminal Information Theory". PhD thesis. Department of Electrical Engineering, University of California, Los Angeles, 2012.

[Cov75] T.M. Cover. "A proof of the data compression theorem of Slepian and Wolf for ergodic sources (Corresp.)" In: *IEEE Transactions on Information Theory* 21.2 (1975), pp. 226–228. ISSN: 0018-9448.

[CT06] Thomas M. Cover and Joy A. Thomas. *Elements of Information theory 2nd Edition*. USA: John Wiley & Sons, Inc., 2006.

[Gas04] M. Gastpar. "The Wyner-Ziv problem with multiple sources". In: *IEEE Transactions on Information Theory* 50.11 (2004), pp. 2762–2768. ISSN: 0018-9448.

[GFZ05] J. Garcia-Frias and Ying Zhao. "Near-Shannon/Slepian-Wolf Performance for Unknown Correlated Sources Over AWGN Channels". In: *IEEE Trans. Commun.* 53.4 (2005), pp. 555–559. ISSN: 0090-6778.

[GK11] A.E. Gamal and Y.H. Kim. *Network Information Theory*. Cambridge University Press, 2011.

[Gol05] Andrea Goldsmith. *Wireless Communications*. Stanford University, USA: Cambridge University Press, 2005.

[GP79] S. Gel'fand and M. Pinsker. "Coding of Sources on the basis of observations with incomplete information (in Russian)". In: *Problemy Peredachi Informatsii (Problem of Infromation Transmission)* 25.2 (1979), pp. 219–221.

[GR07] I. S. Gradshteyn and I. M. Ryzhik. *Table of Integrals, Series, and Products*. Seventh. Burlington, MA, USA: Elsevier/Academic Press, 2007. ISBN: 0-12-373637-4.

[He16] J. He, I. Hussain, V. Tervo, M. Juntti, and T. Matsumoto. "Performance Analysis for Transmission of Correlated Sources over Non-Orthogonal MARCs". In: *Proc. of IEEE ISTC*. 2016.

[ICT15] ICT-619555 RESCUE Deliverable. *D1.2.1-Assessment on Feasibility, Achievability, and Limits*. Tech. rep. 2015.

[Jan09] Soumya Jana. "Alphabet sizes of auxiliary random variables in canonical inner bounds". In: *Proceedings of the 43rd Annual Conference on Information Sciences and Systems (CISS)*. 2009, pp. 67–71.

[KM79] J. Körner and K. Marton. "How to encode the modulo-two sum of binary sources (Corresp.)" In: *IEEE Transactions on Information Theory* 25.2 (1979), pp. 219–221. ISSN: 0018-9448.

[Kwo+10] T. Kwon, S. Lim, W. Seo, and D. Hong. "LLR-based symbol selective transmission with a near-optimal threshold to minimize BEP for demodulation-forward relay systems". In: *IEEE Trans. Wireless Commun.* 9.2 (2010), pp. 540–545.

[Li+06] Y. Li, B. Vucetic, T. F. Wong, and M. Dohler. "Distributed Turbo coding with soft information relaying in multihop relay networks". In: *IEEE J. Sel. Area Commun.* 24.11 (2006), pp. 2040–2050.

[Lu+14] Pen-Shun Lu, Xiaobo Zhou, K. Anwar, and T. Matsumoto. “Joint Adaptive Network–Channel Coding for Energy-Efficient Multiple-Access Relaying”. In: *IEEE Trans. Veh. Technol.* 63.5 (2014), pp. 2298–2305.

[LZM15] Pen-Shun Lu, Xiaobo Zhou, and T. Matsumoto. “Outage Probabilities of Orthogonal Multiple-Access Relaying Techniques With Imperfect Source-Relay Links”. In: *IEEE Trans. Wireless Commun.* 14.4 (2015), pp. 2269–2280.

[MYT08] Y. Ma, N. Yi, and R. Tafazolli. “Bit and power loading for OFDM-based three-node relaying communications”. In: *IEEE Trans. Signal Process.* 56.7 (2008), pp. 3236–3247.

[NFR07] K.D. Nguyen, A.G. Fabregas, and L.K. Rasmussen. “Analysis and Computation of the Outage Probability of Discrete-Input Block-Fading Channels”. In: *Information Theory, 2007. ISIT 2007. IEEE International Symposium on*. 2007, pp. 1196–1200.

[Nos06] T. E. T. E. Hunter. Nosratinia. “Diversity through coded cooperation”. In: *IEEE Trans. Wireless Commun.* 5.2 (2006), pp. 283–289.

[Ooh05] Y. Oohama. “Rate-distortion theory for Gaussian multiterminal source coding systems with several side informations at the decoder”. In: *IEEE Transactions on Information Theory* 51.7 (2005), pp. 2577–2593. ISSN: 0018-9448.

[Ooh97] Y. Oohama. “Gaussian Multiterminal Source Coding”. In: *IEEE Transactions on Information Theory* 43.6 (1997), pp. 1912–1923.

[Pan+04] A. Pandya, A. Kansal, G. Pottie, and M. Srivastava. “Lossy source coding of multiple Gaussian sources: m-helper problem”. In: *Proceedings of the IEEE Information Theory Workshop (ITW)*. 2004, pp. 34–38.

[PAR08] R. C. Palat, A. Annamalai, and H. Reed. “Log-Likelihood-Ratio based Selective Decode and Forward Cooperative Communication”. In: *IEEE VTC Spring 2008*. 2008, pp. 615–618.

[PS06] Stephan Pfletschinger and Frieder Sanzi. “Error Floor Removal for Bit-Interleaved Coded Modulation with Iterative Detection”. In: *IEEE Trans. on Wireless Communications* 5.11 (2006), pp. 3174–3181.

[RRC07] Lorenzo Rubio, Juan Reig, and Narcís Cardona. “Evaluation of Nakagami fading behaviour based on measurements in urban scenarios”. In: 61.2 (2007), p. 135. ISSN: 1434-8411.

[SA05] M. K. Simon and M. S. Alouini. *Digital Communications over Fading Channels*. Wiley, 2005.

[SW73] D. Slepian and J.K. Wolf. “Noiseless Coding of Correlated Information Sources”. In: *IEEE Transactions on Information Theory* 19.4 (July 1973), pp. 471–480.

[Voj06] M. R. M. R. Souryal. R. Vojcic. “Performance of Amplify-and-Forward and Decode-and-Forward Relaying in Rayleigh Fading with Turbo Codes”. In: *IEEE ICASP*. Vol. 4. 2006, pp. 681–684.

[WG03] Zhengdao Wang and G. B. Giannakis. “A simple and general parameterization quantifying performance in fading channels”. In: *IEEE Trans. Commun.* 51.8 (2003), pp. 1389–1398. ISSN: 0090-6778.

[Wol+15] Albrecht Wolf, Maximilian Matthé, Andreas Festag, and Gerhard Fettweis. “Outage Based Power Allocation for a Lossy Forwarding Two-Relaying System”. In: *Proceedings of the Computer Aided Modelling and Design of Communication Links and Networks (CAMAD’15)*. London, UK, Sept. 2015.

[WZ76] A.D. Wyner and J. Ziv. “The rate-distortion function for source coding with side information at the decoder”. In: *IEEE Transactions on Information Theory* 22.1 (1976), pp. 1–10. ISSN: 0018-9448.

[Xiao2007] Jin-Jun Xiao and Zhi-Quan Luo. “Multiterminal Source-Channel Communication Over an Orthogonal Multiple-Access Channel”. In: *IEEE Transactions on Information Theory* 53.9 (2007), pp. 3255–3264. ISSN: 0018-9448.

[Xiaobo2014] Xiaobo Zhou, Pen-Shun Lu, K. Anwar, and T. Matsumoto. “Correlated Sources Transmission in Orthogonal Multiple Access Relay Channel: Theoretical Analysis and Performance Evaluation”. In: *IEEE Trans. Wireless Commun.* 13.3 (2014), pp. 1424–1435.

[Xin13CL] Xin He, Xiaobo Zhou, K. Anwar, and T. Matsumoto. “Estimation of Observation Error Probability in Wireless Sensor Networks”. In: *IEEE Communications Letters* 17.6 (2013), pp. 1073–1076.

[XinISITA] Xin He, Xiaobo Zhou, K. Anwar, and T. Matsumoto. “Wireless mesh networks allowing intra-link errors: CEO problem viewpoint”. In: *Proceedings of the International Symposium on Information Theory and Its Applications (ISITA)*. Hawaii, USA, 2012, pp. 61–65.

[XLC04] Z. Xiong, A.D. Liveris, and S. Cheng. “Distributed source coding for sensor networks”. In: *IEEE Signal Processing Magazine* 21.5 (2004), pp. 80–94.

[YA11] R. Youssef and A. G. i. Amat. “Distributed Serially Concatenated Codes for Multi-Source Cooperative Relay Networks”. In: *IEEE Transactions on Wireless Communications* 10.1 (2011), pp. 253–263. ISSN: 1536-1276.

[YMT08] N. Yi, Y. Ma, and R. Tafazolli. “Doubly differential communication assisted with cooperative relay”. In: *Proc. IEEE VTC 08 Spring*. Marina Bay, Singapore, 2008, pp. 644–647.

[Zho+14] Xiaobo Zhou, Meng Cheng, Xin He, and Tad Matsumoto. “Exact and Approximated Outage Probability Analyses for Decode-and-Forward Relaying System Allowing Intra-Link Errors”. In: *IEEE Transactions on Wireless Communications* 13.12 (Dec. 2014), pp. 7062–7071.

[Zhou2012] Xiaobo Zhou, Xin He, Khoirul Anwar, and Tad Matsumoto. “GREAT-CEO: larGe scale distRibuted dEcision mAking Technique for wireless Chief Executive Officer problems”. In: *IEICE Transactions on Communications* E95-B.12 (2012), pp. 3654–3662.

Appendix A Calculation of the Inner Bound

The Berger-Tung inner bound on the rate-distortion region for the binary case with Hamming distortion is calculated based on the test BSCs. By using the Markov property and the chain rules of entropy and mutual information, $\mathscr{R}^{\mathrm{i}}(D_1, D_2)$ shown in (3.9) is obtained in the following way

$$\begin{aligned} R_1 &\geq I(X_1;V_1|V_2) \\ &= H(V_1|V_2) - H(V_1|X_1,V_2) && \text{(A.1)} \\ &= H(V_1|V_2) - H(V_1|X_1) && \text{(A.2)} \\ &= H_2(D_1 * p_1 * p_2 * D_2) - H_2(D_1) \\ R_2 &\geq H_2(D_1 * p_1 * p_2 * D_2) - H_2(D_2) && \text{(A.3)} \end{aligned}$$

$$\begin{aligned} R_1 + R_2 &\geq I(X_1,X_2;V_1,V_2) \\ &= H(V_1,V_2) - H(V_1,V_2|X_1,X_2) \\ &= H(V_1) + H(V_1|V_2) - H(V_1|X_1,X_2) - H(V_2|X_1,X_2,V_1) && \text{(A.4)} \\ &= 1 + H_2(D_1 * p_1 * p_2 * D_2) - H(V_1|X_1) - H(V_2|X_1,X_2) && \text{(A.5)} \\ &= 1 + H_2(D_1 * p_1 * p_2 * D_2) - H(V_1|X_1) - H(V_2|X_2) && \text{(A.6)} \\ &= 1 + H_2(D_1 * p_1 * p_2 * D_2) - H_2(D_1) - H_2(D_2) \end{aligned}$$

where the steps are justified, with:
(D.1) the chain rule for mutual information,
(D.2) given X_1, V_1 and V_2 are conditionally independent,
(D.3) symmetric to the calculation of R_1,
(D.4) the chain rule for entropy,
(D.5) given X_1, X_2 and V_1 are conditionally independent, also, V_1 and V_2 are conditionally independent given X_1 and X_2,
(D.6) given X_2, X_1 and V_2 are conditionally independent.

It should be emphasized here that the timing sharing variable Q is not involved in the above calculation, while the equations are based on [Ber n]. In order to visually present the Berger-Tung inner bound, the rate-distortion region is divided into three parts, as

(a) for some $0 \leq \tilde{d} \leq D_2$

$$\begin{cases} R_1 \geq H_2(D_1 * p_1 * p_2 * \tilde{d}) - H_2(D_1), \\ R_2 \geq 1 - H_2(\tilde{d}), \end{cases} \tag{A.7}$$

(b) for some $0 \leq \tilde{d} \leq D_1$

$$\begin{cases} R_2 \geq H_2(D_2 * p_1 * p_2 * \tilde{d}) - H_2(D_2) \\ R_1 \geq 1 - H_2(\tilde{d}); \end{cases} \tag{A.8}$$

(c)

$$R_1 + R_2 \geq 1 + H_2(D_1 * p_1 * p_2 * D_2) - H_2(D_1) - H_2(D_2), \tag{A.9}$$

where $\tilde{d}$ is a dummy variable. We calculate the rates R_1, R_2 as well as $R_1 + R_2$ with given D_1 and D_2, respectively, and then plot the rate-distortion region by combining the three parts shown above, which is similar to the time sharing concept.

Appendix B Direct Outer Bound for the Two-node Binary CEO Problem

Let

$$\mathscr{R}_L(D) = \Big\{(R_1,\cdots,R_L,D): \quad \text{there exists } \varphi_1,\cdots,\varphi_L,\psi) \quad \text{such that}$$

$$\frac{1}{n}\log|\varphi_i| \le R_i \tag{B.1}$$

$$\frac{1}{n}Ed(X^n,\hat{X}^n) = \frac{1}{n}\sum_{t=1}^{n} Ed(X(t),\hat{X}(t)) \le D\Big\}. \tag{B.2}$$

be the rate-distortion region of the binary CEO problem with $d(,)$ being the Hamming distortion measure and $|\varphi_i| = 2^{nR_i}$ denoting the range of cardinality of φ_i. Our aim is to derive a good outer bound on $\mathscr{R}_L(D)$. Assume that $(R_1,R_2,D) \in \mathscr{R}_L(D)$ and define

$$\begin{cases} U_i = \varphi_i(X_i^n) \\ \tilde{X}_t = [X(1),\cdots,X(t-1),X(t+1),\cdots,X(n)] \\ \varepsilon_t = \Pr\{x_i \neq \hat{x}_i\}. \end{cases} \tag{B.3}$$

Then we can obtain the inequality as

$$\frac{1}{n}H(X^n|\hat{X}^n) \le H_2(D). \tag{B.4}$$

A proof of (B.4) is shown as follows.

$$\begin{aligned} \frac{1}{n}H(X^n|\hat{X}^n) &= \frac{1}{n}\sum_{t=1}^{n} H(X(t)|X^{t-1}\hat{X}^n) && \text{(B.5)} \\ &\le \frac{1}{n}\sum_{t=1}^{n} H(X(t)|\hat{X}(t)) && \text{(B.6)} \\ &\le \frac{1}{n}\sum_{t=1}^{n} (\varepsilon_t(\log(|\mathscr{X}|-1)) + H_2(\varepsilon_t)) && \text{(B.7)} \\ &= \frac{1}{n}\sum_{t=1}^{n} H_2(\varepsilon_t) && \text{(B.8)} \\ &\le H_2(\frac{1}{n}\sum_{t=1}^{n}\varepsilon_t) && \text{(B.9)} \\ &\le H_2(D) && \text{(B.10)} \end{aligned}$$

with the steps being justified by
(B.5) chain rule of entropy,
(B.6) conditioning reduces entropy,
(B.7) Fano's inequality,
(B.9) Jensen's inequality and H_2 is concave,
(B.10) definition.

Based on the assumption $(R_1,R_2,D) \in \mathscr{R}_L(D)$ and several steps of basic calculation, we have

$$\begin{cases} R_i & \ge \frac{1}{n}\sum_{t=1}^{n} I(U_i;X_i(t)|U_{\mathscr{L}\setminus i},\tilde{X}_t) \\ R_{\text{sum}} & \ge \frac{1}{n}\sum_{t=1}^{n} I(U_{\mathscr{L}};X_{\mathscr{L}}(t)|\tilde{X}_t) \\ H_2(D) & \ge \frac{1}{n}H(X|U_{\mathscr{L}}) \end{cases}, \tag{B.11}$$

and the outer bound on $\mathscr{R}_L(D)$ as

$$\begin{aligned}\mathscr{R}_L^{\mathrm{o}}(D) = \Big\{ (R_{\mathscr{L}}) : & R_i \geq I(U_i; X_i | U_{\mathscr{L}\setminus i}) \\ & R_{\mathrm{sum}} \geq I(U_{\mathscr{L}}; X_{\mathscr{L}}) \\ & H_2(D) \geq H(X|U_{\mathscr{L}}) \\ & \text{for some } U_i \text{ with independent Markov chains} \\ & U_i \to X_i \to X \to X_{\mathscr{L}\setminus i} \to U_{\mathscr{L}\setminus i} \\ & X \to (X_1, \cdots, X_L) \to (U_1, \cdots, U_L) \\ & |\mathscr{U}_i| \leq |\mathscr{X}_i| + 7 \Big\}. \end{aligned} \tag{B.12}$$

The proof of $\mathscr{R}_L(D) \subseteq \mathscr{R}_L^{\mathrm{o}}(D)$ is based on the lossless CEO problem originated by Gel'fand and Pinsker [GP79] and is omitted here.

The outer bound $\mathscr{R}_L^{\mathrm{o}}(D)$ needs to be computed using a good parametrization method. Similar to the quadratic Gaussian CEO problem, we introduce following terms

$$\eta_i = I(X_i; U_i | X) \text{ for all } i \in \mathscr{L} \tag{B.13}$$

to parameterize the outer bound. Then $\mathscr{R}_L^{\mathrm{o}}(D)$ is represented by

$$\begin{cases} R_i & \geq \eta_i + H(X|U_{\mathscr{L}\setminus i}) - H_2(D) \\ R_{\mathrm{sum}} & \geq 1 - H_2(D) + \sum_{i=1}^{L} \eta_i \end{cases} \tag{B.14}$$

The term η_i can be easily obtained by MGL. Then the questions remain for future study are a series of minimization problems, denoted as $\min H(X|U_{\mathscr{S}})$ with $\mathscr{S} \subseteq \mathscr{L}$. So far, in this dissertation, we use test BSC to obtain the minimal value on $H(X|U_1, U_2)$ for the two-node case. It is found that the results of using test BSC consistent with that of using a brute-force search over a fine mesh of conditional distributions $p_{U_i|X_i}(u_i|x_i)$ [Cou12].

Appendix C Monotonicity of Distortion D

Majority decision. $D = \min\{\theta_1, \theta_2\}$. Since θ_i, $i = 1,2$ is the result of the binary convolution of p_i and D_i, θ_i is obviously increasing as D_i is increasing, when p_i is fixed.

Optimal decision. $D = H_2^{-1}[H_2(\theta_1) + H_2(\theta_2) - H_2(\theta_1 * \theta_2)]$.

In this case, D is a composite function of $H_2^{-1}(\cdot)$ and $H_2(\theta_1) + H_2(\theta_2) - H_2(\theta_1 * \theta_2)$. Since the function $H_2^{-1}(\cdot)$ is monotonically increasing, we only need to prove that $g(\theta_1, \theta_2) = H_2(\theta_1) + H_2(\theta_2) - H_2(\theta_1 * \theta_2)$ is also an increasing function of θ_1 and θ_2.

Assume θ_2 is fixed. The partial derivative $\frac{\partial g(\theta_1,\theta_2)}{\partial \theta_1}$ on θ_1 is

$$\frac{\partial g(\theta_1, \theta_2)}{\partial \theta_1} = \log \frac{1-\theta_1}{\theta_1} - (1-2\theta_2) \cdot \log \frac{1-\theta_1 * \theta_2}{\theta_1 * \theta_2}. \tag{C.1}$$

In order to prove that (C.1) is nonnegative, we should prove

$$\frac{1-\theta_1}{\theta_1} \geq \left(\frac{1-\theta_1 * \theta_2}{\theta_1 * \theta_2}\right)^{(1-2\theta_2)}. \tag{C.2}$$

The above always holds according to the monotonically increasing property of function $\log(\cdot)$. As $0 \leq \theta_i \leq \frac{1}{2}$, $i = 1,2$ and $0 \leq \theta_1 * \theta_2 \leq \frac{1}{2}$ is assumed, the following inequalities are obtained after several steps of elementary calculation

$$\frac{1-\theta_1}{\theta_1} \geq \left(\frac{1-\theta_1}{\theta_1}\right)^{(1-2\theta_2)} \geq \left(\frac{1-\theta_1 * \theta_2}{\theta_1 * \theta_2}\right)^{(1-2\theta_2)}. \tag{C.3}$$

Therefore, it is found that (C.1) can not take negative values according to (C.3). Symmetrically, we can assume θ_1 is fixed, and show that the partial derivative $\frac{\partial g(\theta_1,\theta_2)}{\partial \theta_2}$ on θ_2 is also nonnegative. Hence, $g(\theta_1, \theta_2)$ is increasing in the dimension of θ_1 and θ_2, respectively. Based on the above two cases, it is concluded that the distortion D is increasing with respect to D_1 and D_2.

Appendix D Calculation of the Inner Bound

The Berger-Tung inner bound on the rate-distortion region for the binary case with Hamming distortion is calculated based on the test BSCs. By using the Markov property and the chain rules of entropy and mutual information, $\mathscr{R}^{\mathrm{i}}(D_1, D_2)$ shown in (3.9) is obtained in the following way

$$\begin{aligned} R_1 &\geq I(X_1;V_1|V_2) \\ &= H(V_1|V_2) - H(V_1|X_1,V_2) && \text{(D.1)} \\ &= H(V_1|V_2) - H(V_1|X_1) && \text{(D.2)} \\ &= H_2(D_1 * p_1 * p_2 * D_2) - H_2(D_1) \\ R_2 &\geq H_2(D_1 * p_1 * p_2 * D_2) - H_2(D_2) && \text{(D.3)} \end{aligned}$$

$$\begin{aligned} R_1 + R_2 &\geq I(X_1,X_2;V_1,V_2) \\ &= H(V_1,V_2) - H(V_1,V_2|X_1,X_2) \\ &= H(V_1) + H(V_1|V_2) - H(V_1|X_1,X_2) - H(V_2|X_1,X_2,V_1) && \text{(D.4)} \\ &= 1 + H_2(D_1 * p_1 * p_2 * D_2) - H(V_1|X_1) - H(V_2|X_1,X_2) && \text{(D.5)} \\ &= 1 + H_2(D_1 * p_1 * p_2 * D_2) - H(V_1|X_1) - H(V_2|X_2) && \text{(D.6)} \\ &= 1 + H_2(D_1 * p_1 * p_2 * D_2) - H_2(D_1) - H_2(D_2) \end{aligned}$$

where the steps are justified, with:
(D.1) the chain rule for mutual information,
(D.2) given X_1, V_1 and V_2 are conditionally independent,
(D.3) symmetric to the calculation of R_1,
(D.4) the chain rule for entropy,
(D.5) given X_1, X_2 and V_1 are conditionally independent, also, V_1 and V_2 are conditionally independent given X_1 and X_2,
(D.6) given X_2, X_1 and V_2 are conditionally independent.

It should be emphasized here that the timing sharing variable Q is not involved in the above calculation, while the equations are based on [Ber n]. In order to visually present the Berger-Tung inner bound, the rate-distortion region is divided into three parts, as

(a) for some $0 \leq \tilde{d} \leq D_2$

$$\begin{cases} R_1 \geq H_2(D_1 * p_1 * p_2 * \tilde{d}) - H_2(D_1), \\ R_2 \geq 1 - H_2(\tilde{d}), \end{cases} \qquad \text{(D.7)}$$

(b) for some $0 \leq \tilde{d} \leq D_1$

$$\begin{cases} R_2 \geq H_2(D_2 * p_1 * p_2 * \tilde{d}) - H_2(D_2) \\ R_1 \geq 1 - H_2(\tilde{d}); \end{cases} \qquad \text{(D.8)}$$

(c)

$$R_1 + R_2 \geq 1 + H_2(D_1 * p_1 * p_2 * D_2) - H_2(D_1) - H_2(D_2), \qquad \text{(D.9)}$$

where $\tilde{d}$ is a dummy variable. We calculate the rates R_1, R_2 as well as $R_1 + R_2$ with given D_1 and D_2, respectively, and then plot the rate-distortion region by combining the three parts shown above, which is similar to the time sharing concept.

Appendix E Outage Probability Derivation

Following the method of deriving the outage probability for one-way relaying network [CAM12], the outage probability p_{out} of binary information sensing over Rayleigh fading channels is obtained. Based on the Slepian-Wolf theorem, if the rate pair (R_1, R_2) falls into parts 1 and 2, as shown in Fig. E.1, both the correlated sources can be recovers in arbitrarily small error probability. Furthermore, if (R_1, R_2) is in part 3 or 4, source 2 or 1 can be losslessly recovered. Define P_i, $i = 1,2,3,4$ as the probabilities that (R_1, R_2) falls into part i, respectively, then based on the definition of the outage event, p_{out} is expresses as

$$p_{\text{out}} = \begin{cases} 1-(P_1+P_2+P_4), & p_1 < p_2 \\ 1-(P_1+P_2+P_3), & p_1 > p_2 \\ 1-(P_1+P_2+P_3+P_4), & p_1 = p_2 \end{cases}. \tag{E.1}$$

Note that outage happens if and only if the final distortion D is larger than $\min\{p_1, p_2\}$, and thus, the sensor with smaller p_i or both sensors if $p_1 = p_2$ dominate the performance. In the calculation of outage probability, P_3 and/or P_4 should be subtracted accordingly. Now, we need to compute P_1, P_2, P_3 and P_4.

Assume the instantaneous SNR γ_i, $i = 1,2$ follows Rayleigh fading, as

$$p_{\Gamma_i}(\gamma_i) = \frac{1}{\Gamma_i} \exp(-\frac{\gamma_i}{\Gamma_i}). \tag{E.2}$$

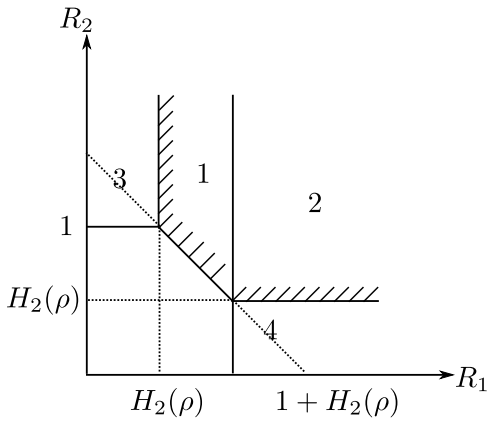

Figure E.1: Slepian-Wolf rate region for analyzing outage probability.

Based on the Slepain-Wolf theorem and separability of source and channel, we have

$$\begin{aligned}
P_1 &= \Pr\{H_2(\rho) < R_1 < 1, R_1 + R_2 > 1 + H_2(\rho)\} \\
&= \Pr\{2^{r_1 H_2(\rho)} - 1 < \gamma_1 < 2^{r_1} - 1, 2^{[r_2(1+H_2(\rho)) - \frac{r_2}{r_1}\log(1+\gamma_1)]} - 1 < \gamma_2\} \\
&= \int_{2^{r_1 H_2(\rho)}-1}^{2^{r_1}-1} \int_{2^{[r_2(1+H_2(\rho)) - \frac{r_2}{r_1}\log(1+\gamma_1)]}-1}^{+\infty} p_{\Gamma_1}(\gamma_1) p_{\Gamma_2}(\gamma_2) d\gamma_1 d\gamma_2 \\
&= \frac{1}{\Gamma_1} \int_{2^{r_1 H_2(\rho)}-1}^{2^{r_1}-1} \exp(-\frac{\gamma_1}{\Gamma_1}) \left[\exp(-\frac{\gamma_1}{\Gamma_1})\right]_{2^{[r_2(1+H_2(\rho)) - \frac{r_2}{r_1}\log(1+\gamma_1)]}-1}^{+\infty} d\gamma_1 \\
&= \frac{1}{\Gamma_1} \int_{2^{r_1 H_2(\rho)}-1}^{2^{r_1}-1} \exp(\frac{1}{\Gamma_2} - \frac{\gamma_1}{\Gamma_1} - \frac{2^{r_2(1+H_2(\rho))}}{\Gamma_2 (1+\gamma_1)^{\frac{r_2}{r_1}}}) d\gamma_1, \qquad \text{(E.3)} \\
P_2 &= \Pr\{R_1 > 1, R_2 > H_2(\rho)\} \\
&= \Pr\{2^{r_1} - 1 < \gamma_1 < \infty, 2^{r_2 H_2(\rho)} - 1 < \gamma_2 < \infty\} \\
&= \int_{2^{r_1}-1}^{+\infty} \int_{2^{r_2 H_2(\rho)}-1}^{+\infty} p_{\Gamma_1}(\gamma_1) p_{\Gamma_2}(\gamma_2) d\gamma_1 d\gamma_2 \\
&= \int_{2^{r_1}-1}^{+\infty} p_{\Gamma_1}(\gamma_1) d\gamma_1 \int_{2^{r_2 H_2(\rho)}-1}^{+\infty} p_{\Gamma_2}(\gamma_2) d\gamma_2 \\
&= \exp[-(\frac{2^{r_1}-1}{\Gamma_1} + \frac{2^{r_2 H_2(\rho)} - 1}{\Gamma_2})], \qquad \text{(E.4)} \\
P_3 &= \Pr\{0 < R_1 < H_2(\rho), R_2 > 1\} \\
&= \Pr\{0 < \gamma_1 < 2^{r_1 H_2(\rho)} - 1, 2^{r_2} - 1 < \gamma_2 < \infty\} \\
&= \int_{0}^{2^{r_1 H_2(\rho)}-1} \int_{2^{r_2}-1}^{+\infty} p_{\Gamma_1}(\gamma_1) p_{\Gamma_2}(\gamma_2) d\gamma_1 d\gamma_2 \\
&= \int_{0}^{2^{r_1 H_2(\rho)}-1} p_{\Gamma_1}(\gamma_1) d\gamma_1 \int_{2^{r_2}-1}^{+\infty} p_{\Gamma_2}(\gamma_2) d\gamma_2 \\
&= [1 - \exp(-\frac{2^{r_1 H_2(\rho)} - 1}{\Gamma_1})] \exp(-\frac{2^{r_2}-1}{\Gamma_2}). \qquad \text{(E.5)}
\end{aligned}$$

Similarly,

$$P_4 = [1 - \exp(-\frac{2^{r_2 H_2(\rho)} - 1}{\Gamma_2})] \exp(-\frac{2^{r_1}-1}{\Gamma_1}). \qquad \text{(E.6)}$$

The outage is then obtained by (E.1) depending on the values of p_1 and p_2. Note that the derivation is using the capacity function with two-dimensional signal. The outage probability can be similarly calculated for the one-dimensional signal.

Appendix F BEP Floor of Soft Combining Decision

For the case p_i are various over links, the BEP floor obtained by Poisson-binomial process is not accurate. Thus, the BEP floor needs to be analyzed by taking soft combining into account. In soft combining decision, the LLR sequence is weighted by p_i using function f_c. It is equivalent to a weighted majority voting, for which the hard decision of $\hat{x}$ follows

$$\hat{x} = \begin{cases} 1, & \mathbf{w}\mathbf{v}^{\mathrm{T}} > 0 \\ 0, & \text{otherwise} \end{cases} \tag{F.1}$$

where $\mathbf{w} = [\log \frac{1-p_1}{p_1}, \cdots, \log \frac{1-p_L}{p_L}]$ and $\mathbf{v} = \mathrm{sign}([l_1^{\mathrm{p}}, \cdots, l_L^{\mathrm{p}}])$, with $\mathrm{sign}(\cdot)$ taking the sign of its argument, i.e., 1 for positive numbers, -1 for negative numbers. Similar to the Poisson binomial process by assuming that 0 is transmitted, the BEP floor is given by

$$p_e = \Pr\{\sum_{k\in\mathscr{V}_+} w_k > \sum_{j\in\mathscr{V}_-} w_j\} + \frac{1}{2}\Pr\{\sum_{k\in\mathscr{V}_+} w_k = \sum_{j\in\mathscr{V}_-} w_j\}, \tag{F.2}$$

where $\mathscr{V}_+ = \{i|v_i = +1\}$ and $\mathscr{V}_- = \{i|v_i = -1\}$. Note that the difference between the BEP floor using Poisson binomial process and (F.2) is that, the error is determined by the number of 1's and 0's in Poisson binomial, and the weights of positive and negative signs in soft combining, respectively. To compute (F.2), it needs to carry out the search of the possible combinations of w_i over the power set of $\{1, \cdots, L\}$.

Appendix G Rate-distortion Region Visualization

Similar to the time sharing concept, the rate-distortion region is divided into three parts, as

(a) for some $0 \leq \tilde{d} \leq d_2$

$$\begin{cases} R_1 & \geq & H_b(d_1 * p_1 * p_2 * \tilde{d}) - H_b(d_1), \\ R_2 & \geq & 1 - H_b(\tilde{d}), \end{cases} \tag{G.1}$$

(b) for some $0 \leq \tilde{d} \leq d_1$

$$\begin{cases} R_2 & \geq & H_b(d_2 * p_1 * p_2 * \tilde{d}) - H_b(d_2) \\ R_1 & \geq & 1 - H_b(\tilde{d}); \end{cases} \tag{G.2}$$

(c)

$$R_{\text{sum}} \geq 1 + H_b(d_1 * p_1 * p_2 * d_2) - H_b(d_1) - H_b(d_2), \tag{G.3}$$

where $\tilde{d}$ is a dummy variable. We calculate the rates R_1, R_2 as well as R_{sum} with given d_1 and d_2, respectively, and then plot the rate-distortion region by combining the three parts shown above.

Appendix H Sum Rate of Multiple Users Case

In general, the sum rate requirement R_{sum} in the Berger-Tung inner bound is given as

$$R_{\text{sum}} \geq I(\mathbf{u}_1, \mathbf{u}_2, \cdots, \mathbf{u}_K; \mathbf{v}_1, \mathbf{v}_2, \cdots, \mathbf{v}_K), \tag{H.1}$$

however, deriving this mutual information is not easy, instead, we assume $d_1, d_2, \cdots, d_K$ are relatively small. Thus, we only need to calculate the joint entropy $H(\mathbf{U})$ to obtain the sum rate.

Given the fact that u_k, $k = 1, \cdots, K$ is the result of passing u through a BSC with crossover probability p_k, where u_k and u represent the realizations of $\mathbf{u}_k$ and $\mathbf{u}$, respectively, the joint probability $\Pr(u_1, u_2, \cdots, u_K)$ is formulated as

$$\Pr(u_1, u_2, \cdots, u_K) = \Pr(u=0) \prod_{i \in \mathbb{A}} (1-p_i) \prod_{j \in \mathbb{A}^{\text{C}}} p_j + \Pr(u=1) \prod_{i \in \mathbb{A}} p_i \prod_{j \in \mathbb{A}^{\text{C}}} (1-p_j), \tag{H.2}$$

where $\mathbb{A}$ is the set of the index k if $u_k = 0$, $k = 1, \cdots, K$ and $\mathbb{A}^{\text{C}}$ is the complementary set of the set $\mathbb{A}$. For example, setting $K = 3$ with $u_1 = 0$, $u_2 = 1$ and $u_3 = 0$, the set $\mathbb{A}$ is equal to $\{1, 3\}$ and $\mathbb{A}^{\text{C}} = \{2\}$.

Therefore, the joint entropy $H(\mathbf{U})$ which is equivalent to the information rate R_{sum} is calculated as

$$H(\mathbf{U}) = -\sum_{u_k \in \{0,1\}} \Pr(u_1, u_2, \cdots, u_K) \log_2(\Pr(u_1, u_2, \cdots, u_K)). \tag{H.3}$$

Appendix I Exact and High-SNR Expressions of Outage Probability

I.1 Exact and High-SNR Expressions for $J_{1,1}, J_{1,2}$

Substituting (4.16) into the rate inequalities in (4.6), $J_{1,1}$ and $J_{1,2}$ can be expressed in terms of SNR constraints. These expressions can be evaluated by integrating the joint pdf $f(\gamma_1,...,\gamma_N) = f(\gamma_1)\cdot...\cdot f(\gamma_N)$ over the corresponding ranges. In the last step we approximate the exponential function with the high SNR assumption.

$$\begin{aligned}
J_{1,1} =& \Pr[0 \le R_0 < 1, 0 \le R_1 < 1-R_0, p_1 = 0] \\
=& \Pr\left[0 \le \gamma_0 < 2^{R_c}-1, 0 \le \gamma_2 < 2^{R_c-\Psi(\gamma_0)}-1, 2^{R_c}-1 \le \gamma_1\right] \\
=& \exp\left(-\frac{2^{R_c}-1}{\bar{\Gamma}_1}\right) \int_{\gamma_0} \frac{1}{\bar{\Gamma}_0} \exp\left(-\frac{\gamma_0}{\bar{\Gamma}_0}\right) \left[1-\exp\left(-\frac{2^{R_c-\Psi(\gamma_0)}-1}{\bar{\Gamma}_2}\right)\right] d\gamma_0 \\
\approx& \frac{1}{\bar{\Gamma}_0\bar{\Gamma}_2} \int_{\gamma_0=0}^{2^{R_c}-1} \left[\frac{2^{R_c}}{1+\gamma_0}-1\right] d\gamma_0
\end{aligned} \tag{I.1}$$

$$\begin{aligned}
J_{1,2} =& \Pr[0 \le R_0 < H(p_1), 0 \le R_1, 0 < p_1 \le 0.5] \\
=& \Pr\left[0 \le \gamma_0 < 2^{R_c-\Psi(\gamma_1)}-1, 0 \le \gamma_2, 0 \le \gamma_1 < 2^{R_c}-1\right] \\
=& \int_{\gamma_1} \frac{1}{\bar{\Gamma}_1} \exp\left(-\frac{\gamma_1}{\bar{\Gamma}_1}\right) \left[1-\exp\left(-\frac{2^{R_c-\Psi(\gamma_1)}-1}{\bar{\Gamma}_0}\right)\right] d\gamma_1 \\
\approx& \frac{1}{\bar{\Gamma}_0\bar{\Gamma}_1} \int_{\gamma_1=0}^{2^{R_c}-1} \left[\frac{2^{R_c}}{1+\gamma_1}-1\right] d\gamma_1
\end{aligned} \tag{I.2}$$

I.2 Exact and High-SNR Expressions for $J_{2,1}, J_{2,2}, J_{2,4}$

Substituting (4.16) into the rate inequalities in (4.6), $J_{2,1}, J_{2,2}$ and $J_{2,4}$ can be expressed in terms of SNR constraints. These expressions can be evaluated by integrating the joint pdf $f(\gamma_1,...,\gamma_N) = f(\gamma_1)\cdot...\cdot f(\gamma_N)$ over the corresponding ranges. In the last step we approximate the exponential function with the high SNR assumption.

$$\begin{aligned}
J_{2,1} =& \Pr[0 \le R_0 < 1, 0 \le R_1 < 1-R_0, 0 \le R_2 < 1-R_0-R_1, p_1 = 0, p_2 = 0] \\
=& \Pr\Big[0 \le \gamma_0 < 2^{R_c}-1, 0 \le \gamma_3 < 2^{R_c-\Psi(\gamma_0)}-1, 0 \le \gamma_4 < 2^{R_c-\Psi(\gamma_0)-\Psi(\gamma_3)}-1, \\
& 2^{R_c}-1 \le \gamma_1, 2^{R_c}-1 \le \gamma_2\Big]. \\
=& \exp\left(-\frac{2^{R_c}-1}{\bar{\Gamma}_1}\right) \exp\left(-\frac{2^{R_c}-1}{\bar{\Gamma}_2}\right) \int_{\gamma_0}\int_{\gamma_3} \frac{1}{\bar{\Gamma}_0} \exp\left(-\frac{\gamma_0}{\bar{\Gamma}_0}\right) \\
& \times \frac{1}{\bar{\Gamma}_3} \exp\left(-\frac{\gamma_3}{\bar{\Gamma}_3}\right) \left[1-\exp\left(-\frac{2^{R_c-\Psi(\gamma_0)-\Psi(\gamma_3)}-1}{\bar{\Gamma}_4}\right)\right] d\gamma_0 d\gamma_3 \\
\approx& \frac{1}{\bar{\Gamma}_0}\frac{1}{\bar{\Gamma}_3}\frac{1}{\bar{\Gamma}_4} \int_{\gamma_0=0}^{2^{R_c}-1} \int_{\gamma_3=0}^{2^{R_c-\Psi(\gamma_0)}-1} \left[\frac{2^{R_c}}{(1+\gamma_0)(1+\gamma_3)}-1\right] d\gamma_0 d\gamma_3
\end{aligned} \tag{I.3}$$

$$
\begin{aligned}
J_{2,2} =& \Pr[0 \le R_0 < H(p_2), 0 \le R_1 < H(p_2) - R_0, 0 \le R_2, p_1 = 0, 0 < p_2 \le 0.5] \\
=& \Pr\Big[0 \le \gamma_0 < 2^{R_c - \Psi(\gamma_2)} - 1, 0 \le \gamma_3 < 2^{R_c - \Psi(\gamma_0) - \Psi(\gamma_2)} - 1, \\
& \quad 0 \le \gamma_4, 2^{R_c} - 1 \le \gamma_1, 0 \le \gamma_2 < 2^{R_c} - 1\Big] \\
=& \exp\left(-\frac{2^{R_c}-1}{\bar{\Gamma}_1}\right) \int_{\gamma_0} \int_{\gamma_2} \frac{1}{\bar{\Gamma}_0} \exp\left(-\frac{\gamma_0}{\bar{\Gamma}_0}\right) \\
& \times \frac{1}{\bar{\Gamma}_2} \exp\left(-\frac{\gamma_2}{\bar{\Gamma}_2}\right) \left[1 - \exp\left(-\frac{2^{R_c - \Psi(\gamma_0) - \Psi(\gamma_2)} - 1}{\bar{\Gamma}_3}\right)\right] d\gamma_0 d\gamma_2 \\
\approx& \frac{1}{\bar{\Gamma}_0} \frac{1}{\bar{\Gamma}_2} \frac{1}{\bar{\Gamma}_3} \int_{\gamma_0=0}^{2^{R_c - \Psi(\gamma_2)} - 1} \int_{\gamma_2=0}^{2^{R_c}-1} \left[\frac{2^{R_c}}{(1+\gamma_0)(1+\gamma_2)} - 1\right] d\gamma_0 d\gamma_2
\end{aligned} \tag{I.4}
$$

$$
\begin{aligned}
J_{2,4} =& \Pr[0 \le R_0 < H(p_1) + H(p_2) - H(p_1 * p_2), 0 \le R_1, 0 \le R_2, 0 \le p_1 \le 0.5, 0 < p_2 \le 0.5] \\
=& \Pr\left[0 \le \gamma_0 < 2^{2R_c - \Psi(\gamma_1) - \Psi(\gamma_2) - R_c \Upsilon(\gamma_1, \gamma_2)} - 1, 0 \le \gamma_3, 0 \le \gamma_4, 0 \le \gamma_1 < 2^{R_c} - 1, 0 \le \gamma_2 < 2^{R_c} - 1\right] \\
=& \int_{\gamma_1} \int_{\gamma_2} \frac{1}{\bar{\Gamma}_1} \exp\left(-\frac{\gamma_1}{\bar{\Gamma}_1}\right) \frac{1}{\bar{\Gamma}_2} \exp\left(-\frac{\gamma_2}{\bar{\Gamma}_2}\right) \left[1 - \exp\left(-\frac{2^{2R_c - \Psi(\gamma_1) - \Psi(\gamma_2) - R_c \Upsilon(\gamma_1, \gamma_2)} - 1}{\bar{\Gamma}_0}\right)\right] d\gamma_1 d\gamma_2 \\
\approx& \frac{1}{\bar{\Gamma}_0 \bar{\Gamma}_1 \bar{\Gamma}_2} \int_{\gamma_1=0}^{2^{R_c}-1} \int_{\gamma_2=0}^{2^{R_c}-1} \left[\frac{2^{R_c}}{1 + \max[\Psi(\gamma_1), \Psi(\gamma_2)]} - 1\right] d\gamma_1 d\gamma_2
\end{aligned} \tag{I.5}
$$

with $\Upsilon(\gamma_1, \gamma_2) = H\left(H^{-1}(1 - \frac{1}{R_c}\Psi(\gamma_1)) * H^{-1}(1 - \frac{1}{R_c}\Psi(\gamma_2))\right)$, with binary convolution $x_1 * x_2$, defined in

I.3 Exact and High-SNR Expressions for $J_{3,1}, J_{3,2}, J_{3,5}, J_{3,8}$

Substituting (4.16) into the rate inequalities in (4.6), $J_{3,1}, J_{3,2}, J_{3,5}$ and $J_{3,8}$ can be expressed in terms of SNR constraints. These expressions can be evaluated by integrating the joint pdf $f(\gamma_1, ..., \gamma_N) = f(\gamma_1) \cdot ... \cdot f(\gamma_N)$ over the corresponding ranges. In the last step we approximate the exponential function with the high SNR assumption.

$$
\begin{aligned}
J_{3,1} =& \Pr[0 \le R_0 < 1, 0 \le R_1 < 1 - R_0, 0 \le R_2 < 1 - R_0 - R_1, 0 \le R_3 < 1 - R_0 - R_1 - R_2, p_1 = 0, p_2 = 0, p_3 = 0] \\
=& \Pr[0 \le \gamma_0 < 2^{R_c} - 1, 0 \le \gamma_4 < 2^{R_c - \Phi(\gamma_0)} - 1, 0 \le \gamma_5 < 2^{R_c - \Phi(\gamma_0) - \Phi(\gamma_4)} - 1, 0 \le \gamma_6 < 2^{R_c - \Phi(\gamma_0) - \Phi(\gamma_4) - \Phi(\gamma_5)} - 1, \\
& 2^{R_c} - 1 \le \gamma_1, 2^{R_c} - 1 \le \gamma_2, 2^{R_c} - 1 \le \gamma_3]. \\
\approx& \frac{1}{\bar{\Gamma}_0 \bar{\Gamma}_4 \bar{\Gamma}_5} \int_{\gamma_0} \int_{\gamma_4} \int_{\gamma_5} \left(\frac{2^{R_c - \Phi(\gamma_0) - \Phi(\gamma_4) - \Phi(\gamma_5)} - 1}{\bar{\Gamma}_6}\right) d\gamma_0 d\gamma_4 d\gamma_5
\end{aligned} \tag{I.6}
$$

$$
\begin{aligned}
J_{3,2} =& \Pr[0 \le R_0 < H(p_3), 0 \le R_1 < H(p_3) - R_0, 0 \le R_2 < H(p_3) - R_0 - R_1, 0 \le R_3, p_1 = 0, p_2 = 0, 0 < p_3 \le 0.5] \\
=& \Pr[0 \le \gamma_0 < 2^{R_c - \Phi(\gamma_3)} - 1, 0 \le \gamma_4 < 2^{R_c - \Phi(\gamma_0) - \Phi(\gamma_3)} - 1, 0 \le \gamma_5 < 2^{R_c - \Phi(\gamma_0) - \Phi(\gamma_3) - \Phi(\gamma_4)} - 1, 0 \le \gamma_6, \\
& 2^{R_c} - 1 \le \gamma_1, 2^{R_c} - 1 \le \gamma_2, 0 \le \gamma_3 < 2^{R_c} - 1]. \\
\approx& \frac{1}{\bar{\Gamma}_0 \bar{\Gamma}_3 \bar{\Gamma}_4 \bar{\Gamma}_5} \int_{\gamma_0} \int_{\gamma_3} \int_{\gamma_4} \left[\frac{2^{R_c}}{(1+\gamma_0)(1+\gamma_3)(1+\gamma_4)} - 1\right] d\gamma_0 d\gamma_3 d\gamma_4
\end{aligned} \tag{I.7}
$$

$$
\begin{aligned}
J_{3,5} =&\Pr[0 \le R_0 < \min\left[H(p_2), H(p_3)\right], 0 \le R_1 < \min\left[H(p_2), H(p_3)\right] - R_0, 0 \le < R_2, 0 \le R_3, \\
&p_1 = 0, 0 < p_2 \le 0.5, 0 < p_3 \le 0.5] \\
=&\Pr[0 \le \gamma_0 < 2^{R_c - \max[\Phi(\gamma_2), \Phi(\gamma_3)]} - 1, 0 \le \gamma_4 < 2^{R_c - \Phi(\gamma_0) - \max[\Phi(\gamma_2), \Phi(\gamma_3)]} - 1, 0 \le \gamma_5, 0 \le \gamma_6, \\
&2^{R_c} - 1 \le \gamma_1, 0 \le \gamma_2 < 2^{R_c} - 1, 0 \le \gamma_3 < 2^{R_c} - 1]. \\
\approx&\frac{1}{\bar{\Gamma}_0 \bar{\Gamma}_2 \bar{\Gamma}_3 \bar{\Gamma}_4} \int_{\gamma_0} \int_{\gamma_2} \int_{\gamma_3} \left[\frac{2^{R_c}}{(1+\gamma_0)(1+\max(\gamma_2, \gamma_3))} - 1 \right] d\gamma_0 d\gamma_2 \gamma_3
\end{aligned}
\tag{I.8}
$$

$$
\begin{aligned}
J_{3,8} =&\Pr[0 \le R_0 < \min\left[H(p_1), H(p_2), H(p_3)\right], 0 \le R_1, 0 \le R_2, 0 \le R_3, \\
&0 < p_1 \le 0.5, 0 < p_2 \le 0.5, 0 < p_3 \le 0.5] \\
=&\Pr[0 \le \gamma_0 < 2^{R_c - \max[\Phi(\gamma_1), \Phi(\gamma_2), \Phi(\gamma_3)]} - 1, 0 \le \gamma_4, 0 \le \gamma_5, 0 \le \gamma_6, \\
&0 \le \gamma_1 < 2^{R_c} - 1, 0 \le \gamma_2 < 2^{R_c} - 1, 0 \le \gamma_3 < 2^{R_c} - 1]. \\
\approx&\frac{1}{\bar{\Gamma}_0 \bar{\Gamma}_1 \bar{\Gamma}_2 \bar{\Gamma}_3} \int_{\gamma_1} \int_{\gamma_2} \int_{\gamma_3} \left[\frac{2^{R_c}}{(1+\max(\gamma_1, \gamma_2, \gamma_3))} - 1 \right] d\gamma_1 d\gamma_2 d\gamma_3
\end{aligned}
\tag{I.9}
$$

I.4 Exact and High-SNR Expressions for $J_{4,1}, J_{4,2}, J_{4,6}, J_{4,12}, J_{4,16}$

Substituting (4.16) into the rate inequalities in (4.6), $J_{4,1}, J_{4,2}, J_{4,6}, J_{4,12}$ and $J_{4,16}$ can be expressed in terms of SNR constraints. These expressions can be evaluated by integrating the joint pdf $f(\gamma_1, ..., \gamma_N) = f(\gamma_1) \cdot ... \cdot f(\gamma_N)$ over the corresponding ranges. In the last step we approximate the exponential function with the high SNR assumption.

$$
\begin{aligned}
J_{4,1} =&\Pr[0 \le R_0 < 1, 0 \le R_1 < 1 - R_0, 0 \le R_2 < 1 - R_0 - R_1, 0 \le R_3 < 1 - R_0 - R_1 - R_2, \\
&0 \le R_4 < 1 - R_0 - R_1 - R_2 - R_3, p_1 = 0, p_2 = 0, p_3 = 0, p_4 = 0] \\
=&\Pr[0 \le \gamma_0 < 2^{R_c} - 1, 0 \le \gamma_5 < 2^{R_c - \Phi(\gamma_0)} - 1, 0 \le \gamma_6 < 2^{R_c - \Phi(\gamma_0) - \Phi(\gamma_5)} - 1, 0 \le \gamma_7 < 2^{R_c - \Phi(\gamma_0) - \Phi(\gamma_5) - \Phi(\gamma_6)} - 1, \\
&0 \le \gamma_8 < 2^{R_c - \Phi(\gamma_0) - \Phi(\gamma_5) - \Phi(\gamma_6) - \Phi(\gamma_7)} - 1, 2^{R_c} - 1 \le \gamma_1, 2^{R_c} - 1 \le \gamma_2, 2^{R_c} - 1 \le \gamma_3, 2^{R_c} - 1 \le \gamma_4]. \\
\approx&\frac{1}{\bar{\Gamma}_0 \bar{\Gamma}_5 \bar{\Gamma}_6 \bar{\Gamma}_7 \bar{\Gamma}_8} \int_{\gamma_0} \int_{\gamma_5} \int_{\gamma_6} \int_{\gamma_7} \left[\frac{2^{R_c}}{(1+\gamma_0)(1+\gamma_5)(1+\gamma_6)(1+\gamma_7)} - 1 \right] d\gamma_0 d\gamma_5 d\gamma_6 d\gamma_7
\end{aligned}
\tag{I.10}
$$

$$
\begin{aligned}
J_{4,2} =&\Pr[0 \le R_0 < H(p_4), 0 \le R_1 < H(p_4) - R_0, 0 \le R_2 < H(p_4) - R_0 - R_1, 0 \le R_3 < H(p_4) - R_0 - R_1 - R_2, \\
&0 \le R_4, p_1 = 0, p_2 = 0, p_3 = 0, 0 < p_4 \le 0.5] \\
=&\Pr[0 \le \gamma_0 < 2^{R_c - \Phi(\gamma_4)} - 1, 0 \le \gamma_5 < 2^{R_c - \Phi(\gamma_0) - \Phi(\gamma_4)} - 1, 0 \le \gamma_6 < 2^{R_c - \Phi(\gamma_0) - \Phi(\gamma_4) - \Phi(\gamma_5)} - 1, \\
&0 \le \gamma_7 < 2^{R_c - \Phi(\gamma_0) - \Phi(\gamma_4) - \Phi(\gamma_5) - \Phi(\gamma_6)} - 1, 0 \le \gamma_8, 2^{R_c} - 1 \le \gamma_1, \\
&2^{R_c} - 1 \le \gamma_2, 2^{R_c} - 1 \le \gamma_3, 0 \le \gamma_4 < 2^{R_c} - 1]. \\
\approx&\frac{1}{\bar{\Gamma}_0 \bar{\Gamma}_4 \bar{\Gamma}_5 \bar{\Gamma}_6 \bar{\Gamma}_7} \int_{\gamma_0} \int_{\gamma_4} \int_{\gamma_5} \int_{\gamma_6} \left[\frac{2^{R_c}}{(1+\gamma_0)(1+\gamma_4)(1+\gamma_5)(1+\gamma_6)} - 1 \right] d\gamma_0 d\gamma_4 d\gamma_5 d\gamma_6
\end{aligned}
\tag{I.11}
$$

$$
\begin{aligned}
J_{4,6} =& \Pr[0 \le R_0 < \min[H(p_3), H(p_4)], 0 \le R_1 < \min[H(p_3), H(p_4)] - R_0, 0 \le R_2 < \min[H(p_3), H(p_4)] - R_0 - R_1, \\
& 0 \le R_3 < \infty, 0 \le R_4, p_1 = 0, p_2 = 0, 0 < p_3 \le 0.5, 0 < p_4 \le 0.5] \\
=& \Pr[0 \le \gamma_0 < 2^{R_c - \max[\Phi(\gamma_3), \Phi(\gamma_4)]} - 1, 0 \le \gamma_5 < 2^{R_c - \Phi(\gamma_0) - \max[\Phi(\gamma_3), \Phi(\gamma_4)]} - 1, \\
& 0 \le \gamma_6 < 2^{R_c - \Phi(\gamma_0) - \max[\Phi(\gamma_3), \Phi(\gamma_4)] - \Phi(\gamma_5)} - 1, 0 \le \gamma_7, 0 \le \gamma_8, 2^{R_c} - 1 \le \gamma_1, \\
& 2^{R_c} - 1 \le \gamma_2, 0 \le \gamma_3 < 2^{R_c} - 1, 0 \le \gamma_4 < 2^{R_c} - 1]. \\
\approx & \frac{1}{\bar{\Gamma}_0 \bar{\Gamma}_3 \bar{\Gamma}_4 \bar{\Gamma}_5 \bar{\Gamma}_6} \int_{\gamma_0} \int_{\gamma_3} \int_{\gamma_4} \int_{\gamma_5} \left[\frac{2^{R_c}}{(1+\gamma_0)(1+\max[\gamma_3, \gamma_4])(1+\gamma_5)} - 1 \right] d\gamma_0 d\gamma_3 d\gamma_4 d\gamma_5
\end{aligned}
\tag{I.12}
$$

$$
\begin{aligned}
J_{4,12} =& \Pr[0 \le R_0 < \min[H(p_2), H(p_3), H(p_4)], 0 \le R_1 < \min[H(p_2), H(p_3), H(p_4)] - R_0, 0 \le R_2, \\
& 0 \le R_3 < \infty, 0 < R_4, p_1 = 0, 0 < p_2 \le 0.5, 0 < p_3 \le 0.5, 0 < p_4 \le 0.5] \\
=& \Pr[0 \le \gamma_0 < 2^{R_c - \max[\Phi(\gamma_2), \Phi(\gamma_3), \Phi(\gamma_4)]} - 1, 0 \le \gamma_5 < 2^{R_c - \Phi(\gamma_0) - \max[\Phi(\gamma_2), \Phi(\gamma_3), \Phi(\gamma_4)]} - 1, \\
& 0 \le \gamma_6, 0 \le \gamma_7, 0 \le \gamma_8, 2^{R_c} - 1 \le \gamma_1, \\
& 0 \le \gamma_2 < 2^{R_c} - 1, 0 \le \gamma_3 < 2^{R_c} - 1, 0 \le \gamma_4 < 2^{R_c} - 1]. \\
\approx & \frac{1}{\bar{\Gamma}_0 \bar{\Gamma}_2 \bar{\Gamma}_3 \bar{\Gamma}_4 \bar{\Gamma}_5} \int_{\gamma_0} \int_{\gamma_2} \int_{\gamma_3} \int_{\gamma_4} \left[\frac{2^{R_c}}{(1+\gamma_0)(1+\max[\gamma_2, \gamma_3, \gamma_4])} - 1 \right] d\gamma_0 d\gamma_2 d\gamma_3 d\gamma_4
\end{aligned}
\tag{I.13}
$$

$$
\begin{aligned}
J_{4,16} =& \Pr[0 \le R_0 < \min[H(p_1), H(p_2), H(p_3), H(p_4)], 0 \le R_1, 0 \le R_2, \\
& 0 \le R_3 < \infty, 0 \le R_4, 0 < p_2 \le 0.5, 0 < p_2 \le 0.5, 0 < p_3 \le 0.5, 0 < p_4 \le 0.5] \\
=& \Pr[0 \le \gamma_0 < 2^{R_c - \max[\Phi(\gamma_2), \Phi(\gamma_3), \Phi(\gamma_4)]} - 1, \\
& 0 \le \gamma_5, 0 \le \gamma_6, 0 \le \gamma_7, 0 \le \gamma_8, \\
& 0 \le \gamma_1 < 2^{R_c} - 1, 0 \le \gamma_2 < 2^{R_c} - 1, 0 \le \gamma_3 < 2^{R_c} - 1, 0 \le \gamma_4 < 2^{R_c} - 1]. \\
\approx & \frac{1}{\bar{\Gamma}_0 \bar{\Gamma}_1 \bar{\Gamma}_2 \bar{\Gamma}_3 \bar{\Gamma}_4} \int_{\gamma_1} \int_{\gamma_2} \int_{\gamma_3} \int_{\gamma_4} \left[\frac{2^{R_c}}{(1+\max[\gamma_1, \gamma_2, \gamma_3, \gamma_4])} - 1 \right] d\gamma_0 d\gamma_2 d\gamma_3 d\gamma_4
\end{aligned}
\tag{I.14}
$$

Appendix J Virtual Channel Representation

The received signal from the XMAC channel is shown in (5.1). Assuming that BPSK modulation is applied for the XMAC channel. Then, the LLR information of the XMAC channel can be expressed as

$$L_{\mathrm{X}} = \ln\Big(\frac{\exp(-|y_{\mathrm{R},1} - \sqrt{P}(h_{\mathrm{AR}} + h_{\mathrm{BR}})|^2) + \exp(-|y_{\mathrm{R},1} + \sqrt{P}(h_{\mathrm{AR}} + h_{\mathrm{BR}})|^2)}{\exp(-|y_{\mathrm{R},1} - \sqrt{P}(h_{\mathrm{AR}} - h_{\mathrm{BR}})|^2) + \exp(-|y_{\mathrm{R},1} + \sqrt{P}(h_{\mathrm{AR}} - h_{\mathrm{BR}})|^2)}\Big), \tag{J.1}$$

where $|\cdot|$ denotes the absolute value. Similarly, the LLR information for the virtual channel can be expressed as

$$L_{\mathrm{V}} = \ln\Big(\exp(-|y_{\mathrm{V}} - \sqrt{P}h|^2)/\exp(-|y_{\mathrm{V}} + \sqrt{P}h|^2)\Big). \tag{J.2}$$

The performance of the relay is mainly determined by the iterative decoder. From decoding perspective, the only difference between the XMAC and the virtual channel is the input from channel to the decoder. Therefore, we investigate the output LLRs of both channels. As observed from Fig. J.1, the pdfs of L_{X} and L_{V} are quite similar, especially in medium and high SNR regimes.

The constellation-constrained capacities of the XMAC and the virtual channel under the constraint of BPSK modulation are shown in Fig. J.2. The constellation-constrained capacity of the P2P fading channel (e.g., $h = h_{\mathrm{AR}}$ in (5.8)) is given as a benchmark scheme. As shown in the figure, the constellation-constrained capacities of the XMAC and the virtual channel are also very close to each other, especially in medium and high SNR regimes.

To further confirm the accuracy of the approximation of the two channels, we run practical simulations using rate-1/2 ACC aided turbo code [AM12a] for the XMAC channel and evaluate the frame error rate (FER) performance. Moreover, we calculate the theoretical outage probability based on the virtual channel. The simulation results are provided in Fig. J.3. The performance gap is within 4 dB for all the levels of correlation.

Therefore, we can conclude that the XMAC channel and the virtual channel are closely approximated. Consequently, the capacity of the virtual channel under the constraint of Gaussian signaling can be simplified by

$$C_{\mathrm{V}} = \log_2(1 + P|h|^2), \tag{J.3}$$

where $|h|^2$ also follows exponential distribution, i.e., $p(|h|^2) = 2\exp(-2|h|^2)$. It is straightforward to show that the corresponding average SNR of the virtual channel follows (5.9).

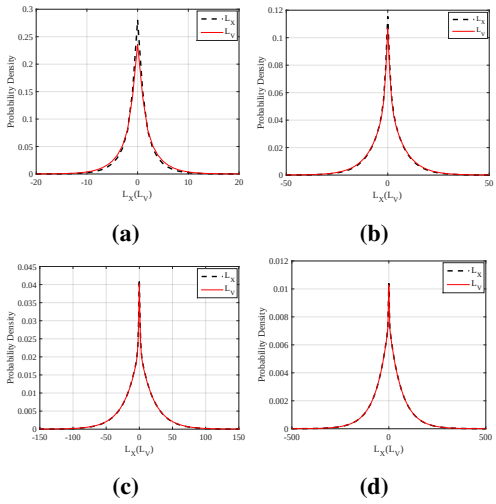

Figure J.1: (a) SNR = 0dB, (b) SNR =5dB, (c) SNR = 10dB and (d) SNR =15dB.

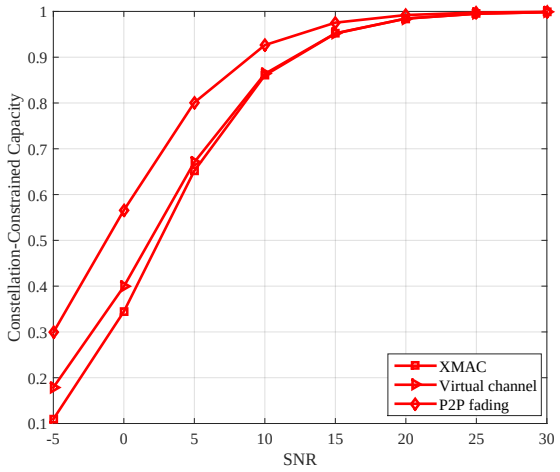

Figure J.2: Constellation-constrained capacities of the XMAC and the virtual channel under BPSK modulation.

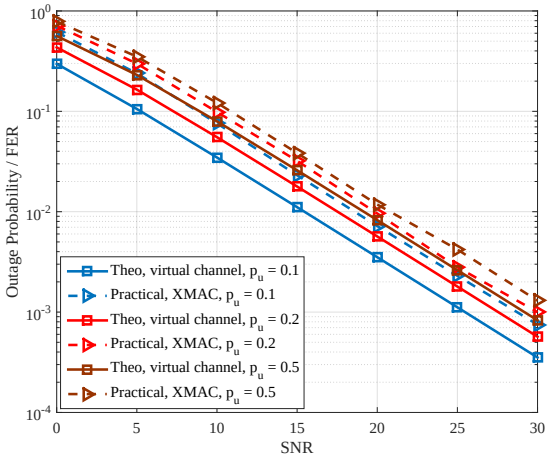

Figure J.3: Comparison between theoretical outage probability of the virtual channel and FER of the XMAC using practical ACC aided turbo code.

Appendix K Derivation of (5.16) - (5.18)

According to the chain rule for entropy, the joint entropy of U_{A}, U_{B}, $\hat{U}_{\mathrm{A}\oplus\mathrm{B}}$, and $\tilde{U}_{\mathrm{A}\oplus\mathrm{B}}$ can be written by

$$H(U_{\mathrm{A}},U_{\mathrm{B}},\hat{U}_{\mathrm{A}\oplus\mathrm{B}},\tilde{U}_{\mathrm{A}\oplus\mathrm{B}}) = H(U_{\mathrm{A}})+H(U_{\mathrm{B}}|U_{\mathrm{A}})+H(\hat{U}_{\mathrm{A}\oplus\mathrm{B}}|U_{\mathrm{A}},U_{\mathrm{B}})+H(\tilde{U}_{\mathrm{A}\oplus\mathrm{B}}|U_{\mathrm{A}},U_{\mathrm{B}},\hat{U}_{\mathrm{A}\oplus\mathrm{B}}), \tag{K.1}$$

where $H(U_{\mathrm{A}}) = 1$, $H(U_{\mathrm{B}}|U_{\mathrm{A}}) = H_b(p_u)$, $H(\hat{U}_{\mathrm{A}\oplus\mathrm{B}}|U_{\mathrm{A}},U_{\mathrm{B}}) = H_b(p_e)$, and $H(\tilde{U}_{\mathrm{A}\oplus\mathrm{B}}|U_{\mathrm{A}},U_{\mathrm{B}},\hat{U}_{\mathrm{A}\oplus\mathrm{B}}) = H_b(p_d)$.

Moreover, we can also express $H(U_{\mathrm{A}},U_{\mathrm{B}},\hat{U}_{\mathrm{A}\oplus\mathrm{B}},\tilde{U}_{\mathrm{A}\oplus\mathrm{B}})$ in the form of

$$H(U_{\mathrm{A}},U_{\mathrm{B}},\hat{U}_{\mathrm{A}\oplus\mathrm{B}},\tilde{U}_{\mathrm{A}\oplus\mathrm{B}}) = H(\tilde{U}_{\mathrm{A}\oplus\mathrm{B}})+H(U_{\mathrm{A}},U_{\mathrm{B}}|\tilde{U}_{\mathrm{A}\oplus\mathrm{B}})+H(\hat{U}_{\mathrm{A}\oplus\mathrm{B}}|U_{\mathrm{A}},U_{\mathrm{B}},\tilde{U}_{\mathrm{A}\oplus\mathrm{B}}), \tag{K.2}$$

where $H(\tilde{U}_{\mathrm{A}\oplus\mathrm{B}}) = H_b(p_u * p_e * p_d)$.

We have the following expression for the conditional mutual information,

$$\begin{aligned} &I(\hat{U}_{\mathrm{A}\oplus\mathrm{B}};\tilde{U}_{\mathrm{A}\oplus\mathrm{B}}|U_{\mathrm{A}},U_{\mathrm{B}}) = H(\hat{U}_{\mathrm{A}\oplus\mathrm{B}}|U_{\mathrm{A}},U_{\mathrm{B}})-H(\hat{U}_{\mathrm{A}\oplus\mathrm{B}}|U_{\mathrm{A}},U_{\mathrm{B}},\tilde{U}_{\mathrm{A}\oplus\mathrm{B}}) \\ &= H(\tilde{U}_{\mathrm{A}\oplus\mathrm{B}}|U_{\mathrm{A}},U_{\mathrm{B}})-H(\tilde{U}_{\mathrm{A}\oplus\mathrm{B}}|U_{\mathrm{A}},U_{\mathrm{B}},\hat{U}_{\mathrm{A}\oplus\mathrm{B}}). \end{aligned} \tag{K.3}$$

Referring to (K.3), we can get

$$H(\hat{U}_{\mathrm{A}\oplus\mathrm{B}}|U_{\mathrm{A}},U_{\mathrm{B}},\tilde{U}_{\mathrm{A}\oplus\mathrm{B}}) = H_b(p_e)+H_b(p_d)-H_b(p_e * p_d). \tag{K.4}$$

By combing (K.1), (K.2), and (K.4), we can obtain

$$H(U_{\mathrm{A}},U_{\mathrm{B}}|\tilde{U}_{\mathrm{A}\oplus\mathrm{B}}) = 1+H_b(p_u)+H_b(p_e * p_d)-H_b(p_u * p_e * p_d). \tag{K.5}$$

For the term $H(U_{\mathrm{A}}|U_{\mathrm{B}},\tilde{U}_{\mathrm{A}\oplus\mathrm{B}})$ in (5.16), we can refer to the following derivation

$$H(U_{\mathrm{A}}|U_{\mathrm{B}},\tilde{U}_{\mathrm{A}\oplus\mathrm{B}}) = H(U_{\mathrm{A}},U_{\mathrm{B}}|\tilde{U}_{\mathrm{A}\oplus\mathrm{B}})-H(U_{\mathrm{B}}|\tilde{U}_{\mathrm{A}\oplus\mathrm{B}}), \tag{K.6}$$

where $H(U_{\mathrm{B}}|\tilde{U}_{\mathrm{A}\oplus\mathrm{B}}) = 1$. Then, we get

$$H(U_{\mathrm{A}}|U_{\mathrm{B}},\tilde{U}_{\mathrm{A}\oplus\mathrm{B}}) = H_b(p_u)+H_b(p_e * p_d)-H_b(p_u * p_e * p_d). \tag{K.7}$$

Due to the symmetry property of U_{A} and U_{B}, it is easy to get

$$H(U_{\mathrm{B}}|U_{\mathrm{A}},\tilde{U}_{\mathrm{A}\oplus\mathrm{B}}) = H_b(p_u)+H_b(p_e * p_d)-H_b(p_u * p_e * p_d). \tag{K.8}$$

Appendix L Derivation of (5.28)

For the purpose of better illustration, we set $\Theta(p_u,\gamma_{\mathrm{R,D}}) = H_b(p_u)+H_b(p_d)-H_b(p_u*p_d)$, $\Gamma(p_u,\gamma_{\mathrm{V}}) = H_b(p_u)+H_b(p_e)-H_b(p_u*p_e)$, $\Lambda(p_u,\gamma_{\mathrm{V}},\gamma_{\mathrm{R,D}}) = H_b(p_u)+H_b(p_e*p_d)-H_b(p_u*p_e*p_d)$, and $\Upsilon(p_u,\gamma_{\mathrm{V}}) = H_b(p_u*p_e)$. The details of each components included in (5.28) are shown in (L.1)-(L.4).

$$\Pr\{\mathbb{S}|\mathbb{C}_1\}\Pr\{\mathbb{C}_1\} = \iiiint\limits_{\mathbb{V}_1} p(\gamma_{\mathrm{V}})p(\gamma_{\mathrm{R,D}})p(\gamma_{\mathrm{A,D}})p(\gamma_{\mathrm{B,D}})d\gamma_{\mathrm{V}}d\gamma_{\mathrm{R,D}}d\gamma_{\mathrm{A,D}}d\gamma_{\mathrm{B,D}}$$

$$= \int_{\Phi^{-1}[H_b(p_u)]}^{\infty} p(\gamma_{\mathrm{V}})d\gamma_{\mathrm{V}} \int_{\Phi^{-1}[H_b(p_u)]}^{\infty} p(\gamma_{\mathrm{R,D}})d\gamma_{\mathrm{R,D}} \int_{\Phi^{-1}(0)}^{\Phi^{-1}(1)} p(\gamma_{\mathrm{A,D}})d\gamma_{\mathrm{A,D}} \int_{\Phi^{-1}(1)-\gamma_{\mathrm{A,D}}}^{\infty} p(\gamma_{\mathrm{B,D}})d\gamma_{\mathrm{B,D}}$$
$$+ \int_{\Phi^{-1}[H_b(p_u)]}^{\infty} p(\gamma_{\mathrm{V}})d\gamma_{\mathrm{V}} \int_{\Phi^{-1}[H_b(p_u)]}^{\infty} p(\gamma_{\mathrm{R,D}})d\gamma_{\mathrm{R,D}} \int_{\Phi^{-1}(1)}^{\infty} p(\gamma_{\mathrm{A,D}})d\gamma_{\mathrm{A,D}} \int_{0}^{\infty} p(\gamma_{\mathrm{B,D}})d\gamma_{\mathrm{B,D}}, \quad \text{(L.1)}$$

$$\Pr\{\mathbb{S}|\mathbb{C}_2\}\Pr\{\mathbb{C}_2\} = \iiiint\limits_{\mathbb{V}_2} p(\gamma_{\mathrm{V}})p(\gamma_{\mathrm{R,D}})p(\gamma_{\mathrm{A,D}})p(\gamma_{\mathrm{B,D}})d\gamma_{\mathrm{V}}d\gamma_{\mathrm{R,D}}d\gamma_{\mathrm{A,D}}d\gamma_{\mathrm{B,D}}$$

$$= \int_{\Phi^{-1}[H_b(p_u)]}^{\infty} p(\gamma_{\mathrm{V}})d\gamma_{\mathrm{V}} \int_{\Phi^{-1}(0)}^{\Phi^{-1}[H_b(p_u)]} p(\gamma_{\mathrm{R,D}})d\gamma_{\mathrm{R,D}} \int_{\Phi^{-1}[\Theta(p_u,\gamma_{\mathrm{R,D}})]}^{\Phi^{-1}(1)} p(\gamma_{\mathrm{A,D}})d\gamma_{\mathrm{A,D}} \int_{\Phi^{-1}[1+\Theta(p_u,\gamma_{\mathrm{R,D}})]-\gamma_{\mathrm{A,D}}}^{\infty} p(\gamma_{\mathrm{B,D}})d\gamma_{\mathrm{B,D}}$$
$$+ \int_{\Phi^{-1}[H_b(p_u)]}^{\infty} p(\gamma_{\mathrm{V}})d\gamma_{\mathrm{V}} \int_{\Phi^{-1}(0)}^{\Phi^{-1}[H_b(p_u)]} p(\gamma_{\mathrm{R,D}})d\gamma_{\mathrm{R,D}} \int_{\Phi^{-1}(1)}^{\infty} p(\gamma_{\mathrm{A,D}})d\gamma_{\mathrm{A,D}} \int_{\Phi^{-1}[\Theta(p_u,\gamma_{\mathrm{R,D}})]}^{\infty} p(\gamma_{\mathrm{B,D}})d\gamma_{\mathrm{B,D}}, \quad \text{(L.2)}$$

$$\Pr\{\mathbb{S}|\mathbb{C}_3\}\Pr\{\mathbb{C}_3\} = \iiiint\limits_{\mathbb{V}_3} p(\gamma_{\mathrm{V}})p(\gamma_{\mathrm{R,D}})p(\gamma_{\mathrm{A,D}})p(\gamma_{\mathrm{B,D}})d\gamma_{\mathrm{V}}d\gamma_{\mathrm{R,D}}d\gamma_{\mathrm{A,D}}d\gamma_{\mathrm{B,D}}$$

$$= \int_{\Phi^{-1}(0)}^{\Phi^{-1}[H_b(p_u)]} p(\gamma_{\mathrm{V}})d\gamma_{\mathrm{V}} \int_{\Phi^{-1}[\Upsilon(p_u,\gamma_{\mathrm{V}})]}^{\infty} p(\gamma_{\mathrm{R,D}})d\gamma_{\mathrm{R,D}} \int_{\Phi^{-1}[\Gamma(p_u,\gamma_{\mathrm{V}})]}^{\Phi^{-1}(1)} p(\gamma_{\mathrm{A,D}})d\gamma_{\mathrm{A,D}} \int_{\Phi^{-1}[1+\Gamma(p_u,\gamma_{\mathrm{V}})]-\gamma_{\mathrm{A,D}}}^{\infty} p(\gamma_{\mathrm{B,D}})d\gamma_{\mathrm{B,D}}$$
$$+ \int_{\Phi^{-1}(0)}^{\Phi^{-1}[H_b(p_u)]} p(\gamma_{\mathrm{V}})d\gamma_{\mathrm{V}} \int_{\Phi^{-1}[\Upsilon(p_u,\gamma_{\mathrm{V}})]}^{\infty} p(\gamma_{\mathrm{R,D}})d\gamma_{\mathrm{R,D}} \int_{\Phi^{-1}(1)}^{\infty} p(\gamma_{\mathrm{A,D}})d\gamma_{\mathrm{A,D}} \int_{\Phi^{-1}[\Gamma(p_u,\gamma_{\mathrm{V}})]}^{\infty} p(\gamma_{\mathrm{B,D}})d\gamma_{\mathrm{B,D}}, \quad \text{(L.3)}$$

$$\Pr\{\mathbb{S}|\mathbb{C}_4\}\Pr\{\mathbb{C}_4\} = \iiiint\limits_{\mathbb{V}_4} p(\gamma_{\mathrm{V}})p(\gamma_{\mathrm{R,D}})p(\gamma_{\mathrm{A,D}})p(\gamma_{\mathrm{B,D}})d\gamma_{\mathrm{V}}d\gamma_{\mathrm{R,D}}d\gamma_{\mathrm{A,D}}d\gamma_{\mathrm{B,D}}$$

$$= \int_{\Phi^{-1}(0)}^{\Phi^{-1}[H_b(p_u)]} p(\gamma_{\mathrm{V}})d\gamma_{\mathrm{V}} \int_{\Phi^{-1}(0)}^{\Phi^{-1}[\Upsilon(p_u,\gamma_{\mathrm{V}})]} p(\gamma_{\mathrm{R,D}})d\gamma_{\mathrm{R,D}} \int_{\Phi^{-1}[\Lambda(p_u,\gamma_{\mathrm{V}},\gamma_{\mathrm{R,D}})]}^{\Phi^{-1}(1)} p(\gamma_{\mathrm{A,D}})d\gamma_{\mathrm{A,D}} \int_{\Phi^{-1}[1+\Lambda(p_u,\gamma_{\mathrm{V}},\gamma_{\mathrm{R,D}})]-\gamma_{\mathrm{A,D}}}^{\infty} p(\gamma_{\mathrm{B,D}})d\gamma_{\mathrm{B,D}}$$
$$+ \int_{\Phi^{-1}(0)}^{\Phi^{-1}[H_b(p_u)]} p(\gamma_{\mathrm{V}})d\gamma_{\mathrm{V}} \int_{\Phi^{-1}(0)}^{\Phi^{-1}[\Upsilon(p_u,\gamma_{\mathrm{V}})]} p(\gamma_{\mathrm{R,D}})d\gamma_{\mathrm{R,D}} \int_{\Phi^{-1}(1)}^{\infty} p(\gamma_{\mathrm{A,D}})d\gamma_{\mathrm{A,D}} \int_{\Phi^{-1}[\Lambda(p_u,\gamma_{\mathrm{V}},\gamma_{\mathrm{R,D}})]}^{\infty} p(\gamma_{\mathrm{B,D}})d\gamma_{\mathrm{B,D}}. \quad \text{(L.4)}$$